University of Nevada, Reno

Effects of Electrode Surface Morphology on the Transduction of Ionic Polymer-Metal Composites

A dissertation submitted in partial fulfillment of the
requirements for the degree of

Doctor of Philosophy

in

Materials Science and Engineering

by

Viljar Palmre

Dr. Kwang J. Kim and Dr. Qizhen Li/Dissertation Advisors

August, 2013

University of Nevada, Reno
Statewide • Worldwide

THE GRADUATE SCHOOL

We recommend that the dissertation
prepared under our supervision by

VILJAR PALMRE

entitled

Effects of Electrode Surface Morphology on the Transduction of Ionic Polymer-Metal Composites

be accepted in partial fulfillment of the
requirements for the degree of

DOCTOR OF PHILOSOPHY

Kwang J. Kim, Ph.D., Advisor

Qizhen Li, Ph.D., Committee Member

Dev Chidambaram, Ph.D., Committee Member

Dhanesh Chandra, Ph.D., Committee Member

Kam K. Leang, Ph.D., Graduate School Representative

Marsha H. Read, Ph. D., Dean, Graduate School

August, 2013

Abstract

Ionic polymer-metal composites (IPMCs) are innovative smart materials that exhibit electromechanical and mechanoelectrical transduction (conversion of electrical input into mechanical deformation and *vice versa*). Due to low driving voltage (< 5 V) and ability to operate in aqueous environment, IPMCs are attractive for developing soft actuators and sensors for underwater robots and medical devices. This dissertation focuses on investigating the effects of electrode surface morphology in the transduction of Pt and Pd-Pt electrodes-based IPMCs, with the aim to improve the electrode surface design and thereby enhance the transduction performance of the material. Firstly, the synthesis techniques are developed to control and manipulate the surface structure of the mentioned electrodes through the electroless plating process. Using these techniques, IPMCs with different electrode surface structures are fabricated. The changes in the electrode surface morphology and the resulting effects on the material's electromechanical, mechanoelectrical, electrochemical and mechanical properties area examined and analyzed. This study shows that increasing the impregnation-reduction cycles under appropriate conditions leads to the formation and growth of platinum nanoparticles with sharp tips and edges – called Pt nanothorn assemblies – at the polymer-electrode interface. IPMCs designed with such nanostructured Pt electrodes are first to be reported. The experiments demonstrate that the formation and growth of Pt nanothorn assemblies at the electrode interface increases considerably the total transported charge during the transduction, thereby increasing significantly the displacement and blocking force output of IPMC. The improvement of the mentioned electromechanical properties was 3–5 times, depending on the input voltage and frequency used. Also, the peak mechanoelectrically induced voltage increased somewhat, although the overall effect of the surface structure was relatively low compared to the electromechanical transduction.

The Pd-Pt electrodes-based composite systems are introduced due to their unique highly capacitive palladium inner surface layer. It is shown that by controlling the impregnation time in Pd complex solution during the electroless plating process leads to changes in the amount and distribution of porous palladium at the inner surface of the polymer membrane, which greatly affects the IPMC transduction. The results show that increasing the dispersion of Pd particulates in the polymer matrix increases noticeably the total transported charge and the resulting electromechanical output of IPMC. A three-fold increase in both displacement and peak blocking force was achieved by varying the impregnation time accordingly. Also, noticeable effect on the induced voltage amplitude was observed.

Dedication

To my wife, Kaili,

and son, Robert.

Acknowledgements

I would like to express my sincere appreciation to my advisors, Dr. Kwang Kim and Dr. Qizhen Li, for their guidance and advice throughout my graduate studies. This research would not have been possible without their continued support and guidance. I also thank Drs. Leang, Chidambaram and Chandra for their valuable advice and for serving in my dissertation committee.

I would like to thank David Pugal for insightful discussions regarding IPMC research, and also Drs. Leang and Sungjun Kim for their input. I appreciate Drs. Chien and Chandra for providing XRD analysis of Pd-Pt IPMC samples. I am grateful to Dr. Alvo Aabloo from the University of Tartu for introducing me to Dr. Kim a few years ago. I also want to thank my current and former lab mates for good discussions and great time we spent together at the UNR: MD Bhuiya, Kuok Cheng, Jiyeon Park, Youngsoo Jung, Johnson Wong, and Dr. Il-Seok Park.

I gratefully acknowledge the partial financial support from the US Office of Naval Research and the US National Science Foundation.

Lastly, but not least, I would like to give special thanks to my wife Kaili and son Robert for their love, unwavering support, encouragement and patience. I also thank the rest of my family for their support.

Contents

List of Tables

List of Figures

Nomenclature

Abbreviations

CV	Cyclic voltammetry
CDC	Carbide-derived carbon
EAP	Electroactive polymer
EDL	Electric double-layer
EDS	Energy-dispersive X-ray spectroscopy
EIS	Electrochemical impedance spectroscopy
FEM	Finite element method
IL	Ionic liquid
IPMC	Ionic polymer-metal composite
SEM	Scanning electron microscopy
SWNT	Single-walled carbon nanotube
XRD	X-ray diffraction

Greek letters

μ	Cation mobility, [$m^2/(V\cdot s)$]
δ	Tip displacement of IPMC, [mm]
ε	Absolute dielectric permittivity, [F/m]

ε_b Bending strain, [%]

ε_f Flexural strain, [mm/mm]

ρ Charge density, [C/m^3]

ρ_p Density of polymer, [kg/m^3]

σ Electric conductivity, [S/m]

σ_f Flexural stress, [MPa]

φ Electric potential in polymer, [V]

ψ_s Surface electric potential, [V]

Roman letters

C Capacitance, [mF/cm^2]

C Cation concentration, [mol/cm^3]

C_0 Initial cation/anion concentration, [mol/cm^3]

C_a Anion concentration, [mol/cm^3]

C_d Differential capacitance, [mF/cm^2]

D Diffusion constant, [m^2/s]

dV Volumetric strain, [m^3/m^3]

E_f Flexural modulus, [MPa]

F Faraday constant, [C/mol]

$\boldsymbol{F}$ Body force vector, [N/m^3]

f Frequency of electric potential, [Hz]

G Linear force coupling coefficient, [N m/mol]

H Quadratic force coupling coefficient, [N m^4/mol^2]

h Thickness of IPMC, [mm]

I Electric current, [A]

j Electric current density, [mA/cm^2]

L Free length of IPMC beam, [mm]

L_s Support span in 3-point bending test, [mm]

M Load in 3-point bending test, [N]

P Solvent pressure, [Pa]

Q Transported charge, [C]

q_s Surface charge density, [C/m^2]

R The gas constant, [J/(K mol)]

T absolute temperature, [K]

$\boldsymbol{u}$ Displacement vector, [m]

V Electric potential, [V]

V_{ind} Induced voltage, [mV]

w Width of IPMC, [mm]

z Charge number

Z'' Imaginary part of impedance, [Ω cm^2]

Chapter 1

Introduction

Ionic polymer-metal composites (IPMCs) are type of electroactive polymers (EAPs) that have received considerable research attention over the past decade. A typical IPMC consists of a thin water solvated ionomer membrane plated on both sides with platinum electrodes [1]. When a voltage is applied across the electrodes, an IPMC exhibits a large bending deformation [2-4]. Conversely, an imposed deformation on the material can generate voltage [5]. These phenomena are called electromechanical and mechanoelectrical transduction, respectively, and make IPMC applicable both as actuator and sensor. Other notable advantages of IPMCs are soft and flexible structure, low driving voltage (< 4 V), easy miniaturization and ability to operate in aqueous environment. These features make IPMCs particularly attractive for underwater biomimetic robotics, and biomedical and human affinity applications [6-11].

Among the variety of available metallic and non-metallic electrode materials, the noble metals such as Pt and Au still remain the ones offering one of the best electrical conductivity and electrochemical stability, making them an excellent choice for underwater robotic applications where fast actuation responses are required. However, while a number of studies have investigated the electric resistance effects and reliability of these electrodes, the effects of electrode surface structure have been largely neglected. There exists a very limited understanding of how to manipulate and control the surface structure of different noble metal electrodes, and how the electrode surface profile would affect the electromechanical and mechanoelectrical transduction of IPMC. Tiwari has studied the energy harvesting in case of different IPMC geometries [12, 13], but yet there is no comparative study on mechanoelectrical transduction with different electrode materials and surface profiles. **Recent finite element simulations by Pugal [14] indicate that the shape of the electrode surface profile can have a significant impact on the electromechanical performance of IPMC**. The calculations show that by designing the electrode surface as a Koch fractal structure [15] can considerably increase the total transported charge during the actuation and thereby increase the bending strain of IPMC. However, the conventional platinum electrodes have rather flat and non-porous surface profile that results a limited charge accumulation at the electrode interface during the actuation process. On the contrary, the recently developed Pd-Pt electrodes-based IPMCs have a porous surface structure with a large interfacial area [16, 17]. However, the direct effect of it on the transduction performance has not been thoroughly investigated.

Hence, in this dissertation, a through experimental study is conducted to investigate the effects of electrode surface structure on the transduction of IPMC, with the aim to improve the electrode surface design and thereby enhance the transduction performance of the IPMC material. IPMCs with two different types of electrodes – Pt and Pd-Pt – are included in the study. The mentioned electrodes are fabricated on the ionic polymer membrane by the electroless plating method [2]. In case of Pd-Pt electrodes, the Pd serves as a supporting layer at the inner surface of polymer membrane to enhance the interfacial area and the Pt at outer surface serves as a highly conductive electrode layer. The surface structure of different electrodes is altered and controlled by appropriately controlling the synthesis parameters and conditions such impregnation time, concentrations and plating cycles. The performances of the IPMCs prepared with different electrodes and surface profiles are comparatively analyzed in terms of electromechanical, mechanoelectrical, electrochemical and mechanical characteristics.

1.1 Research goal and objectives

This dissertation focuses on investigating the effects of electrode surface morphology on the transduction of Pt and Pd-Pt electrodes-based IPMCs. The goal of this research is twofold. Firstly, identify the relations between the electrode surface structure and the transduction behavior of IPMC material. Secondly, improve and optimize the electrode surface design to advance the transduction performance of IPMC. These goals are achieved by completing the following main objectives:

1) Develop the techniques for tailoring the surface structure of different noble metal (Pt and Pd-Pt) electrodes, and fabricate IPMC samples with different electrode surface morphologies.

    This step involves identifying the key parameters and conditions of the electroless plating process to alter and control the surface morphology of electrodes deposited at the ionic polymer surface. A series of IPMC samples with two types of electrodes (Pt and Pd-Pt) are synthesized by carefully varying the parameters of electroless plating within each set of samples.

2) Characterize and comparatively analyze the transduction performance of the IPMCs prepared with different electrode materials and surface structures.

This step involves a thorough experimental work for determining the electromechanical, mechanoelectrical, electrochemical and mechanical characteristics of the IPMCs with different electrodes. The electromechanical properties – displacement and blocking force of the different IPMCs are analyzed in the terms of the transported charge measured during the actuation process. The transported charge and electrode interfacial area are correlated with the electromechanical output of the IPMCs to validate the theoretical results reported earlier by Pugal [14]. The electrochemical impedance spectroscopy and cyclic voltammetry are employed to examine the interfacial surface of different electrodes in terms of the double-layer capacitance. The surface profile and the dendrites at the polymer-electrode interface are examined by analyzing the cross-sections of the samples by scanning electron microscopy (SEM) and energy-dispersive X-ray spectroscopy (EDS). The flexural stress-strain measurements are conducted to investigate the impact of generated dendrites on the flexural modulus of the composite.

1.2 Contributions

This research has three major contributions. Firstly, this study helps to improve the understanding of electrode surface morphology in the electro-mechanical and mechano-electrical coupling of IPMC. The relations identified between the electrode surface characteristics and the transduction behavior of IPMC material will allow ones to optimize the electrode surface design and thereby advance the transduction performance of IPMC.

Secondly, the methods are identified and furnished for manipulating and controlling the surface morphology of different noble metal (Pt and Pd-Pt) electrodes. These techniques can be used for tailoring IPMC electrodes for optimal performance depending on the desired applications of the material.

Thirdly, a novel nanostructured Pt electrode surface design is developed that notably enhances the transduction performance of IPMC. With the appropriate control of the synthesis parameters, the platinum nanothorn assemblies with sharp tips and edges, radiating outward from the center of assembly, are created at the polymer-electrode interface, leading to improved transduction properties of IPMC material.

1.3 Organization of the Dissertation

This dissertation is organized as follows. Chapter 2 provides the background on IPMC materials. IPMC structure, transduction mechanism, suggested applications, commonly used manufacturing methods, as well as recent advances and challenges in the development of IPMC materials are discussed. Chapter 3 presents the theoretical considerations, introducing some key aspects of the recently reported finite element simulation results that led us to this study and are also validated in this work. Chapter 4 provides the experimental details including fabrication of IPMC samples with different electrode materials and surface structures, characterization methods, and experimental setups and equipment used. Chapter 5 presents the results of characterization of IPMCs based on Pt-electrodes with different surface structures. The electromechanical, mechanoelectrical, electrochemical and mechanical properties of different IPMCs are discussed and comparatively analyzed. Chapter 6 discusses and analyzes the measured characteristics of Pd-Pt electrodes-based IPMCs. Finally, conclusion and suggestions for future work are presented in Chapter 7.

Chapter 2

Background

This chapter presents the background on ionic polymer-metal composite (IPMC) materials. The IPMC structure and transduction mechanism are first described. Then, examples of suggested applications for IPMC materials are provided. Next, the current state-of-the-art IPMC manufacturing methods, as well as the recent advances and challenges in the design and development of IPMC materials are thoroughly discussed.

2.1 IPMC structure and transduction mechanism

A conceptual structure of IPMC material consisting of perfluorinated ion-exchange membrane between two platinum electrodes is illustrated in Figure 2.1. The membrane contains water and mobile cations, such as Li^+ or Na^+ that are counterbalanced by fixed anionic groups in the polymer chains (Figure 2.2). When a voltage is applied across the electrodes, the hydrated cations migrate towards the cathode, dragging water molecules along. The transport of cations and solvent causes osmotic pressure change and therefore, an expansion of the polymer near the cathode and shrinkage near the anode that in turn results in bending of the composite towards the anode [2]. The principle of mechanoelectrical transduction is a reverse of electromechanical. An imposed bending deformation on the material causes a movement of some hydrated cations towards the expanding electrode. The resulting charge imbalance can be measured as a voltage signal across the electrodes [18-21].

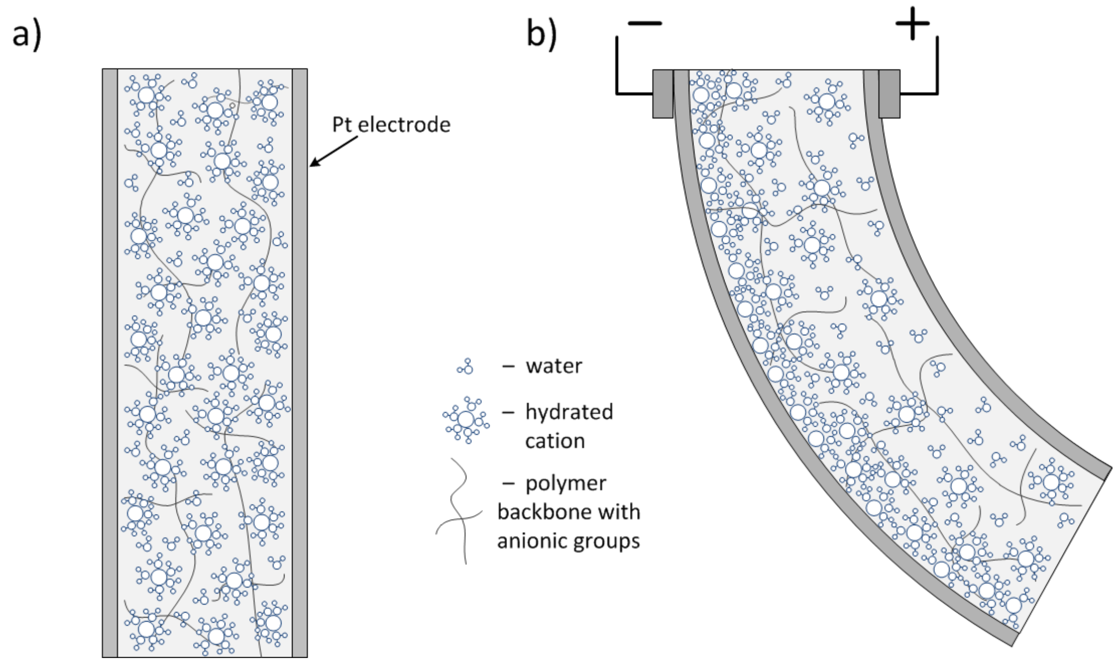

Figure 2.1: Conceptual structure of IPMC: (a) no voltage applied and (b) voltage applied.

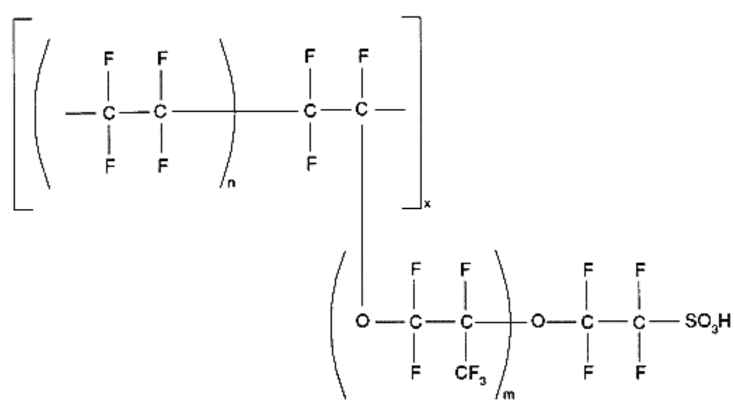

Figure 2.2: Chemical structure of Nafion® used as a membrane material for IPMCs. Reprinted from ref. [22] with permission from Elsevier.

2.2 IPMC applications

There exists an increasing demand for new transducers that are structurally simple, easily scalable, lightweight, mechanically compliant, and precisely controllable and yet require low driving voltage (Table 2.1). Actuators and sensors with such properties are highly demanded for medical, bio-robotics, space, and defense applications. IPMCs are considered one the most promising EAP materials to meet the above requirements and therefore have numerous potential applications in different engineering fields.

Table 2.1: Some important characteristics of IPMC materials.

Low driving voltage	< 5 V
Relatively large bending strain	In the range of 1%
Soft structure	Young's modulus = 0.2 GPa [14]
Lightweight	Density = 2.6 g/cm^3 [14]

Due to their lightweight and compliant structure and low driving voltage, IPMCs have been intensively researched for biomedical and human affinity applications. The specific suggested applications include artificial muscle-like actuators, cardiac-assist devices, surgical tools, tactile sensors, sheet-type braille displays, and active catheters [6, 7, 23-25]. Active catheters, for example, can be used to assist surgeons in improving safety of intravascular procedures by providing more precise manipulation and reliable approach with the force feedback compared to manual techniques [26]. Rod-shaped IPMCs with sectored electrodes that are capable of multiple degrees-of-freedom motion have been designed, and can be beneficial in such applications [27-29].

IPMC materials have gained significant attention in the field of biomimetic robotics, due to their ability to mimic the behavior of biological muscles [18, 30]. Since IPMCs can operate silently in an aqueous environment, they are particularly attractive for biomimetic underwater robotic applications. IPMC actuators have been used as propulsors in many bio-inspired underwater robotic systems to emulate the motion of fish [31, 32], jellyfish [10], tadpole [33], and manta ray [34]. Examples of other aquatic robotic systems based on IPMC actuators include hovering microswimmer [35], snake [36], and underwater walking robot [37]. IPMCs with uniquely sectored electrodes are capable of multiple degrees-of-freedom complex deformations such as twisting, and can be used to mimic the complex motions of fish fins to allow enhanced maneuverability of underwater robots [38-42].

IPMCs have been also investigated for applications in other mechatronic systems. Since they exhibit high sensitivity in voltage sensing mode IPMCs have been studied as vibration and velocity sensors [43, 44]. Dogreur and Tiwari showed that IPMCs can be also used as energy harvesters [44-46]. Examples of other suggested applications include gripping tools, metering valves, and micro-pumps [7, 47, 48].

2.3 Manufacturing methods

There are currently three commonly used manufacturing methods for fabricating IPMC materials. These are the traditional electroless plating method employed in this work, and more recently developed direct assembly process and layer-by-casting method. The following provides an overview of these fabrication methods and highlights their main advantages and limitations.

2.3.1 Traditional electroless plating method

Electroless plating (a.k.a. impregnation-reduction or chemical deposition) method is commonly used for fabrication of ionic polymer-metal composites with noble metal electrodes [2, 49]. This method can be used for a wide range of ion-exchange polymers that have ability to selectively exchange cations or anions. Nafion is one of the most commonly used commercially available cation-exchange polymer for IPMC fabrication.

Electroless plating process consists of three main stages. Firstly, the ionic polymer membrane is impregnated with desired metal cations by soaking in respective metal complex solution, such as tetraammineplatinum(II) chloride hydrate ($Pt(NH_3)_4Cl_2{\cdot}H_2O$). The metal complex cations diffuse into the polymer through ion-exchange process as illustrated in Figure 2.3. Secondly, the impregnated membrane is immersed in aqueous solution containing reducing agent such as sodium borohydride ($NaBH_4$) to reduce the metal cations contained in the polymer to metallic sate at the membrane surface. The reduction process occurs according the following reaction:

$$NaBH_4 + 4[Pt(NH_3)_4]^{2+} + 8OH^- \rightarrow 4Pt^0 + 16NH_3 + NaBO_2 + 6H_2O \tag{2.1}$$

The impregnation-reduction cycle is typically repeated 1–3 times in order to increase the thickness and electric conductivity of the electrodes. The third step is the secondary plating (or surface electroding) process to deposit additional Pt at the outer surface of the electrode to further improve the electrode surface conductivity. The membrane is

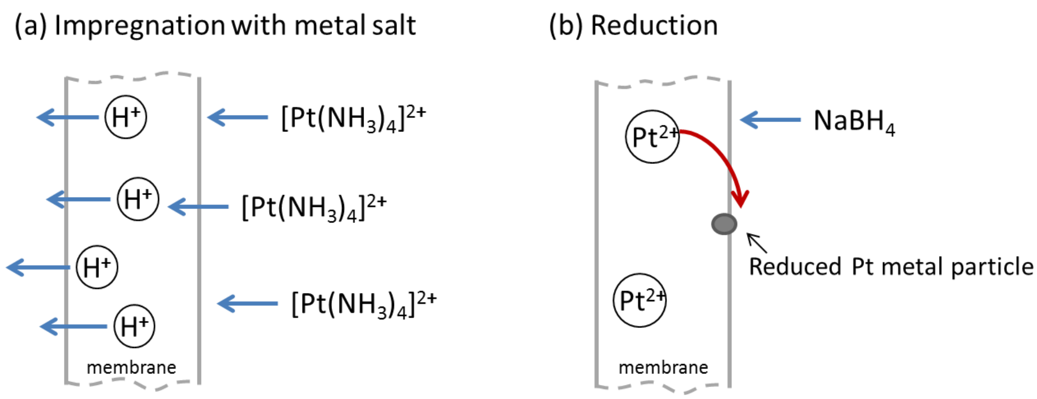

Figure 2.3: Impregnation and reduction steps in the electroless plating process.

immersed in the Pt complex solution and by using reducing agents such as hydroxylamine hydrochloride and hydrazine monohydate the platinum is deposited on the top of the initial Pt electrode layer. Lastly, desired counter ions, e.g. Li^+ or Na^+, are introduced into the polymer membrane through ion-exchange process by soaking the composite in respective metal salt (e.g. LiCl or NaCl) solution.

The described fabrication method produces the electrodes with relatively high electric conductivity. The plating conditions such as soaking time, concentrations and temperatures are critical to the outcome and determine the penetration depth and conductivity of electrodes that affect the performance of IPMC [49, 50]. The method is applicable with electrode materials that are available in a metal complex form.

2.3.2 Direct assembly method

Direct assembly method [51, 52] is used for fabrication of electrodes from various metallic and non-metallic conductive powders by physical heat-pressing. The electrodes can be applied directly either on a dry polymer membrane or solvated membrane.

Direct assembly process on dry membranes involves first dissolving the ion-exchange polymer, such as Nafion, in an ethyl alcohol solution and mixing with conductive material, e.g. RuO_2 powder. The mixture is then sonicated and stirred for 1–4 h to homogenize the dispersion of conductive particles. The obtained homogenous dispersion can be applied on the membrane surface in two ways. The first method is directly painting several layers of the mixture on both surfaces of the polymer membrane using a brush. Between each layer, the sample is dried in an oven at 130 °C for 15 min. The obtained composite is then heat-pressed at 210 °C and a pressure of 20 MPa. The heat-pressing conjugates the painted electrode layers with the membrane. The second approach consists of painting several layers of polymer-conductive powder dispersion on the Teflon reinforced glass fabric and then heat-pressing these decals on the membrane surface. The Teflon mesh is removed once the membrane is cooled down and hydrated. This approach offers more control over the electrode thickness as the decals can be weighed after the painting of each layer. The direct painting on the membrane often causes swelling and wrinkling of the polymer due to the solvents from the mixture.

The painted conductor-polymer electrodes typically have low electric conductivity, therefore additional impregnation-reduction process with Pt or electroplating of gold is required. The dry membrane can be solvated also with other electrolytes besides water, e.g. diethylene glycol or ionic liquids. However, such diluents excessively swell the membrane and cause cracks in the electrodes. Composites with low-vapor-pressure electrolytes can be laminated between two gold foils by heat-pressing to improve the electric conductivity of the electrodes.

The dry assembly may be inadequate in case of non-aqueous electrolytes as they excessively swell the polymer membrane, leading to cracking and delamination of electrodes. Also, some electrolytes may dissolve the ionic polymer in the conductive powder electrode layers. In these cases the electrolyte is first incorporated into the membrane and the direct assembly process is performed on already the solvated membrane, as shown in Figure 2.4. The main challenges with this approach are a loss of electrolyte and dimensional stability during the heat-pressing.

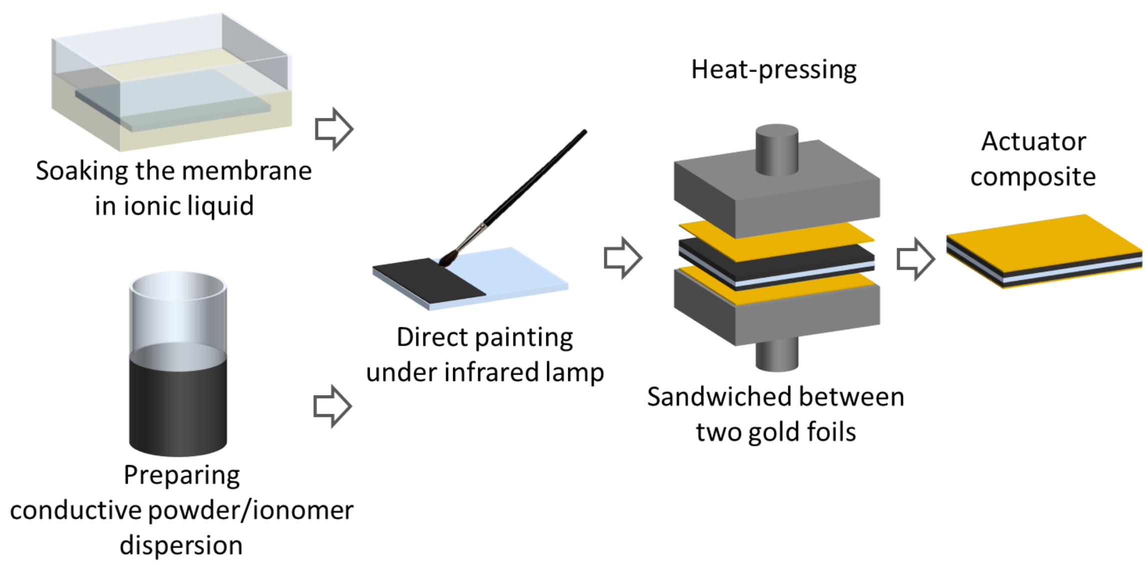

Figure 2.4: The main steps of the direct assembly process for preparing an IPMC.

2.3.3 Layer-by-layer casting method

Layer-by-layer casting method [53] is used for fabricating 'dry-type' ionic liquid based actuators by casting the constituent layers (electrode/membrane/electrode) on top of one another. The later modification of the process involves casting the electrode and membrane layers separately, and fusing the three layers together by heat-pressing step

[54]. The actuator consists of polymeric-ionic liquid gel membrane between two ionic liquid containing bucky gel electrode layers. The fabrication process consists of mixing single-walled carbon nanotubes (SWNTs), ionic liquid (IL) (e.g. 1-ethyl-3-methylimidazolium tetrafluoroborate ($EMIBF_4$)) and polyvinylidenefluoride-co-hexafluoropropylene (PVdF(HFP)) in dimethylacetamide. The suspension is grounded by ball-milling for 30 min, and then mixed with a solution of PVdF(HFP) in dimethylacetamide. After ball-milling for additional 30 min the gelatinuous mixture is sonicated for 3 h. The electrode layer is obtained by casting the mixture into aluminum mold and evaporating the solvent. The membrane layer is prepared by casting a solution of $EMIBF_4$ and PVdF(HFP) in dimethylacetamide, and evaporating the solvent. Finally, the actuator is assembled by heat-pressing the membrane layer between two bucky gel electrode layers as shown in Figure 2.5.

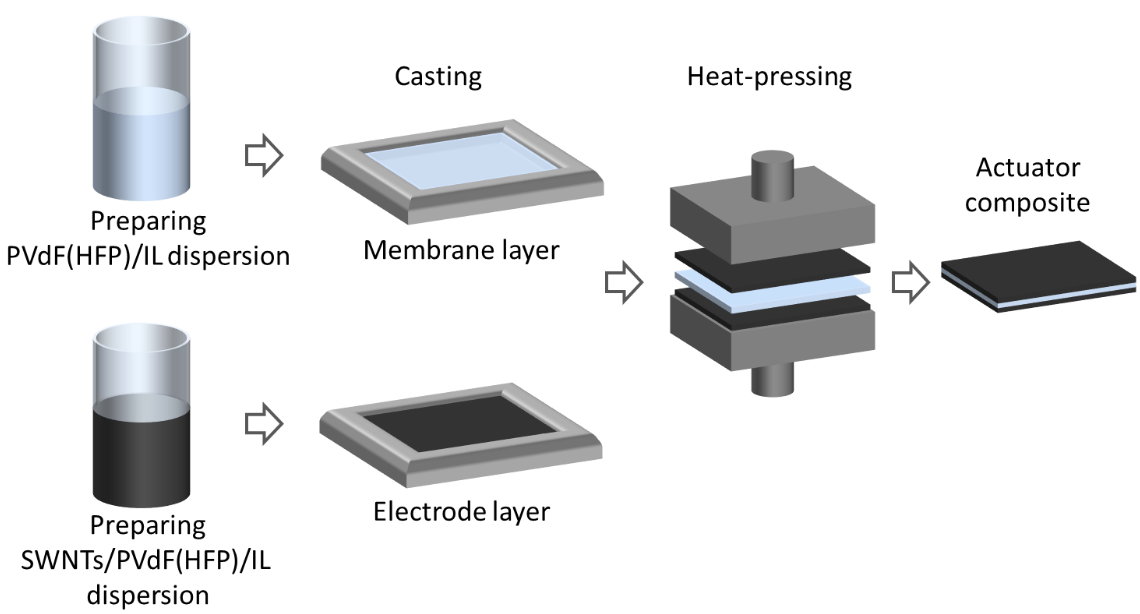

Figure 2.5: Main steps for preparing an actuator by the layer-by-layer casting method.

The described fabrication method offers good control over the thickness and uniformity of electrode layers. However, the method is applicable with electrode materials that can be dispersed in an ionic liquid. The formation of the gel has been demonstrated in case of different carbon nanotubes and carbide-derived carbons in imidazolium based ionic liquids [55-57]. In some cases the electrical conductivity of casted carbon electrodes may be insufficient and an additional gold foil layer is heat-pressed on the electrode surface [58, 59]. Also, conductive additives such as carbon black or polyaniline have been introduced in the carbon nanotube electrodes to improve the electrical conductivity [60].

2.4 Recent advances and challenges in IPMC design

Recently, a lot of effort in the design of IPMC materials has been directed towards developing the electrodes with better mechanical stability and high interfacial area while using more cost-effective materials. Electrodes are a critical part of IPMC structure since their properties affect significantly the actuation performance and cycle life of IPMC material. In the following, the recent advances and challenges in the design and development of IPMC electrodes are discussed.

The commonly used electrode materials for IPMC fabrication are platinum and gold due to their high electrochemical stability and excellent electrical conductivity [2, 49]. A relatively high cost of these materials is a concern. Also, cracking and delamination of platinum electrode from the polymer surface has been observed under prolonged cyclic deformation, leading to decreased electrode conductivity and in turn lower actuation performance [61]. Gold electrodes are more elastic, and offer better mechanical stability and higher electric conductivity [62, 63], but on the other hand, a high reactivity of the gold complex makes the electroless plating process often complicated. Also, several alternative electrode materials and their combinations have been researched. Using palladium as a supporting layer underneath the platinum layer has shown improved mechanical stability and higher transduction performance compared to the regular platinum electrodes [16, 17]. IPMCs with electrodes composed of platinum and copper have been created [64, 65], in which the reversible redox reactions upon the actuation – dissolution and reduction of Cu^{2+} ions on the inner faces of the electrodes can maintain electrical connections between the cracks in platinum layer. The main drawback of this electrode design is the formation of copper oxide. Also, silver nanopowder and nickel have been used as cost-effective electrode materials [66, 67]. However, the low electrochemical stability of these materials limits the cycle life of IPMC.

From the aforementioned electrode materials, the noble metals are a preferred choice for IPMC fabrication due to their high electrical conductivity and electrochemical stability, and availability in cation complex form that can be effectively used with the electroless plating method as described in the previous section.

Recently, with the invention of layer-by-layer casting and direct assembly fabrication methods (described in Section 2.3), also various non-metallic conductive powders have gained interest as electrode materials for IPMCs. For instance, ruthenium(IV) oxide powders [51, 68], carbon nanotubes [53, 54, 69, 70], highly porous amorphous and carbide-derived carbons (CDCs) [56, 71-73], and carbon aerogel powders [74, 75] have been investigated in actuator electrodes. The powder materials can be assembled into electrodes by direct assembly or layer-by-layer casting method as described in the previous section. Compared to the noble metals, the conductive powders are less expensive and have a large specific surface area. For instance, the specific surface area of carbon nanotubes can be up to 1000 m^2/g, whereas the highly porous carbide-derived carbons range from 1000 to 2000 m^2/g. CDCs are also unique due to their precisely controllable pore size that allows fine-tuning the pore dimensions according to electrolyte properties [76]. However, the mentioned powder materials have generally a relatively low electric conductivity. Therefore, the electrode surface is covered additionally with a conductive gold foil layer [51, 58]. The added gold layer makes the manufacturing often more complicated and causes problems due to the delamination under cyclic deformation [77]. The porous carbon materials, namely, activated carbons and carbide-derived carbons prepared at low chlorination temperatures also tend to have poor electrical conductivity within the electrode cross-section [72]. This results in a slow electrical double-layer charging and a slow electromechanical response of an actuator. Also, it has been noted that activated carbons, despite having a large specific surface area, exhibit a limited capacitance due to their low mesoporosity and resulting poor electrolyte accessibility [78, 79].

Due to the effort put into the design and development of IPMC materials, there exists a reasonable understanding of the processes behind the phenomenon. Several studies have indicated that the charge accumulation in the vicinity of electrodes is the key to producing a high strain and force output of IPMC [14, 68, 77, 80, 81]. Therefore, designing the electrodes with high specific surface area is gaining more interest in the development of EAP materials [16, 56, 57, 60, 71, 72, 74]. Promising electrode materials for this purpose are the aforementioned highly porous carbons and carbon nanotubes. However, there are still challenges associated with the use of these materials such as insufficient electric conductivity and limited electrolyte diffusion in the carbon electrodes that need to be solved. Also, it is important to note that the powder materials require a direct assembly by heat-pressing and therefore are mainly suited for fabricating ‘dry-type’ actuators based on non-volatile electrolytes such as ionic liquids [77, 82]. However, the main drawback with using the ionic liquids as electrolytes is the lower response speed compared to the water solvated membranes [83].

Despite the aforementioned advances, the water-based IPMCs manufactured by electroless plating of noble metals still offer one of the fastest and largest strain responses, and ability to be operated in aqueous environment, which makes them excellent candidates for underwater robotics. Compared to the conductive powders, the noble metal electrodes have higher electric conductivity and the electrode surface is non-porous, thus allowing almost immediate surface charging and accumulation of electrolyte that ensures a fast actuation response. Interestingly, the noble metal electrodes have received very limited attention in engineering the electrode surface design. There have been a few attempts to increase the interfacial surface of such electrodes, tough. Noh *et al.* [84] used an etched high surface area aluminum foil as a template that was pressed on the Nafion membrane. After removing the foil the replicated membrane was plated with Pt electrodes to form an IPMC, which showed improved capacitance and bending performance. However, the effect was relatively minor, which can be related to rather macroscopic changes in the electrode surface profile. Onishi *et al.* [85] developed gold electrodes with a fractal-like surface structure on the Flemion membrane through electroless plating that showed increased capacitance and improved displacement range. Aureli *et al.* [86] modeled the effect of electrode surface roughness on the impedance and found that the charge storage scales linearly with the surface roughness of IPMC. Also, other materials such as carbon nanotubes and TiO_2 have been incorporated in the electrode layers or in polymer membrane to increase the interfacial area of Pt electrodes [87, 88]. However, in some cases the issue with this approach is that the incorporated particulates inhibit the electrolyte diffusion, leading to lower actuation response.

Chapter 3

Theoretical considerations

A considerable effort has been put into modeling the transduction of IPMC material [81]. However, most physics-based models use flat electrode approximation in calculations and compensate the effect of high surface area of the electrodes by increasing both diffusion constant and dielectric permittivity values. While this approach provides the results that match with the experimentally measured values, it does not fundamentally capture the effect of electrode surface morphology. For instance, one characteristic of palladium based IPMC electrodes is the porous surface structure that results a large surface area at the polymer-electrode interface [16]. However, the direct effect of it on the transduction performance has not been fully investigated. Recently, Pugal proposed physics-based electromechanical and mechanoelectrical transduction models that take into account the surface structure (shape) of the electrodes [14]. The Koch fractal geometry was implemented in the model to mathematically describe the surface of IPMC electrodes. In the following, the key aspects of Pugal's electromechanical and mechanoelectrical transduction model and FEM simulation results with fractal electrodes are introduced. The described theoretical results were partly a motivation for this research and their experimental validation was one of the objectives of this dissertation.

3.1 Electromechanical transduction model

According to the physics-based electromechanical transduction model of IPMC proposed by Pugal [14, 81, 89, 90], the diffusion and migration of cations in the polymer due to an applied electric field is described by the Nernst-Planck equation:

$$\frac{\partial C}{\partial t} + \nabla \cdot (-D\nabla C - z\mu FC\nabla \phi) = 0\,, \tag{3.1}$$

where C is the cation concentration, D the diffusion constant, F the Faraday constant, z the charge number, φ the electric potential, and μ the mobility of cations in the polymer. The mobility μ is expressed as $\mu = D / (RT)$, where R is the universal gas constant and T is absolute temperature. As a result of ion migration in the polymer, a positive charge accumulates near the cathode and negative spatial charge near the anode. The formation of voltage due to imposed electric field and local charge densities are described by the Poisson's equation:

$$-\nabla^2 \phi = \frac{\rho}{\varepsilon}\,, \tag{3.2}$$

where ε is absolute dielectric constant, and ρ is the charge density and is defined as

$$\rho = F(C - C_a)\,, \tag{3.3}$$

with C_a being anion concentration. The force F per unit volume due to the formed charge density near the electrodes is expressed as

$$\vec{F} = (G\rho + H\rho^2)\hat{x}\,, \tag{3.4}$$

where *G* and *H* are constants. The body force is related to the displacement in time using the Newton’s Second Law

$$\rho_p \frac{\partial^2 \vec{u}}{\partial t^2} - \nabla \cdot c \nabla \vec{u} = \vec{F} \,, \tag{3.5}$$

where ρ_p is the density of the material, *c* is the Navier constant and *u* is the displacement vector. The model includes the effect of current densities and potentials in the electrodes using the differential form of the Ohm’s law:

$$\sigma \nabla V = -j \,, \tag{3.6}$$

where σ is the electric conductivity of electrodes, *V* is the electric potential and *j* is the current density in the electrodes.

It is important to note that most physics based models of IPMC use flat electrodes in calculations and therefore do not capture the effects of electrode surface properties. The described model by Pugal [14, 89] takes into account the surface structure (shape) and interfacial area of electrodes by designing the 2D polymer-electrode interface as a Koch fractal structure. The classic Koch fractal algorithm is based on dividing a line segment into three and replacing the middle segment by two sides of equilateral triangle. This procedure is recursively repeated for each of new segments. The generated fractals can be unidirectional or random directional – 50% chance for each triangle to be constructed on top or bottom of the segment. The generation of unidirectional and random directional fractal electrode surfaces (generations noted as $gen_1 \ldots gen_3$ based on the fractal depth $1 \ldots n$) is illustrated in Figure 3.1. Due to the complicated geometry of gen_2 and gen_3 fractals, the domain width for the calculations was chosen very narrow – only 40 µm.

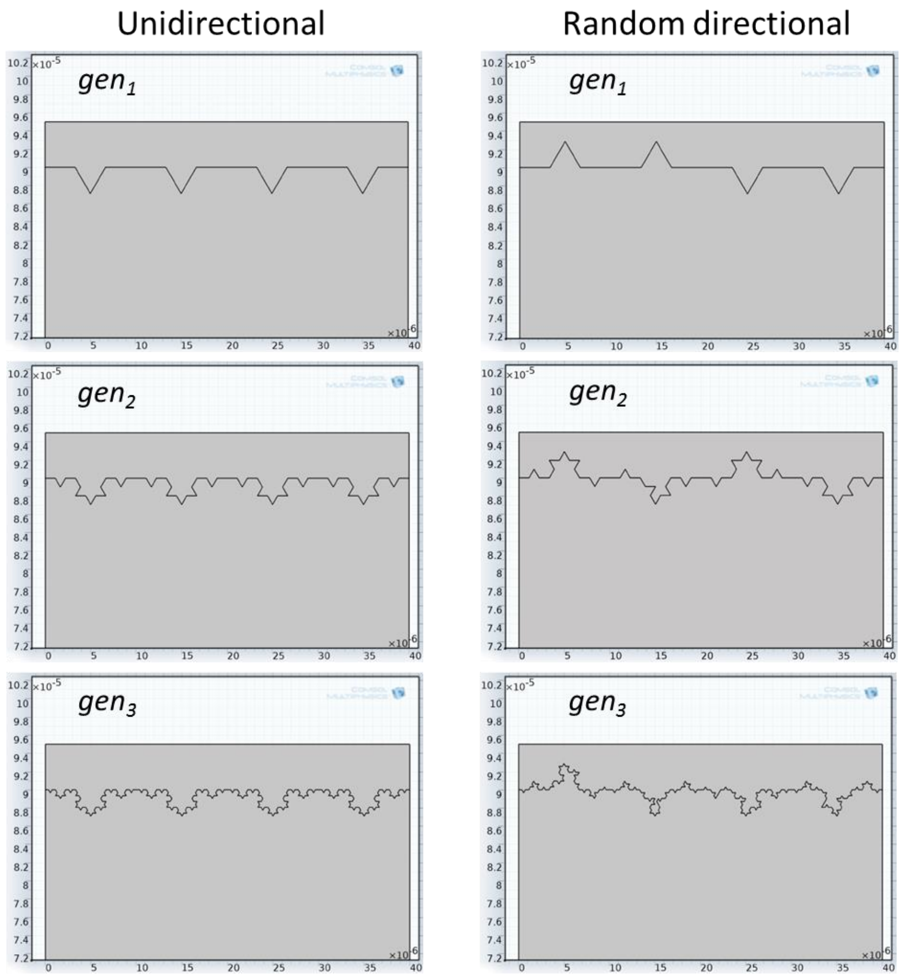

Figure 3.1: Unidirectional and random directional fractal electrodes used in the simulations (scale units in m) (from ref. [89]).

Figure 3.2 shows the calculated transported charge in case of electromechanical transduction with an applied voltage of 1 V for unidirectional and random directional fractal electrodes, compared to the flat electrodes. It can be seen that the transported charge in case of fractal electrodes is considerably higher compared to the flat electrodes and increases with the generation depth of fractals. Due to the complicated geometry of the electrodes and resulting computational cost, the body force and displacement were not considered. However, as discussed above (Eqs. 3.1–3.5), higher charge density at the electrodes results in a larger displacement. Thus, the simulations by Pugal indicate that increasing the electrode interfacial surface area by generating fractals (or dendrites) can improve the electromechanical performance of IPMC. More details were reported in [14].

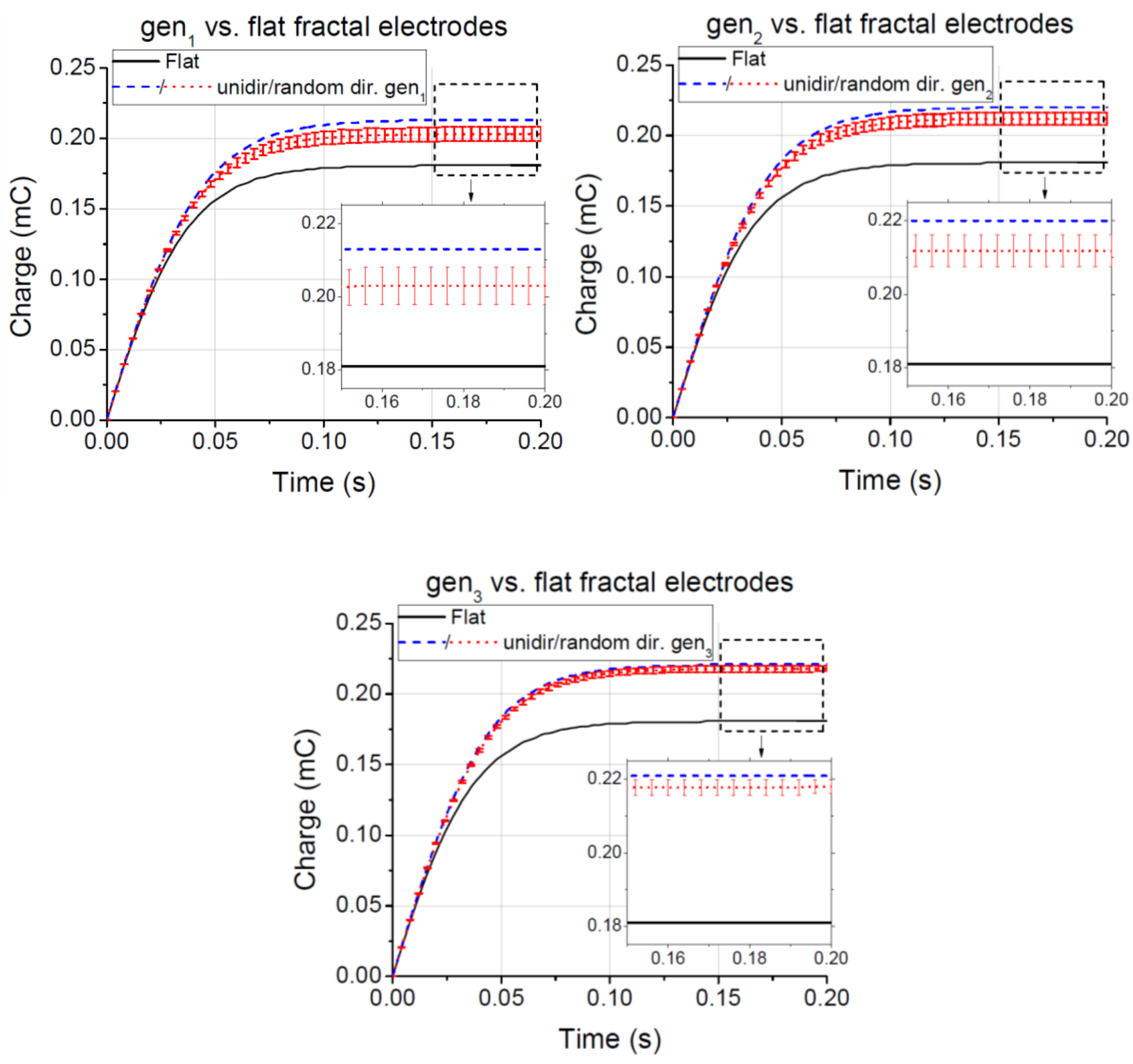

Figure 3.2: Calculated transported charge in case of *gen*$_1$…*gen*$_3$ fractal vs. flat electrodes (from ref. [89]).

3.2 Mechanoelectrical transduction model

Mechanoelectrical transduction of IPMC is basically reverse to the electromechanical. The fundamental mechanoelectrical transduction model proposed by Pugal [14] is based on the electromechanical model described in Section 3.1. The governing equations are the Nernst-Planck (Eq. 3.7), the Poisson (Eq. 3.8), the Ohm's law (3.9), and the time dependent Navier's equation (Eq. 3.10).

$$\frac{\partial C}{\partial t} + \nabla \cdot (-D\nabla C - z\mu FC\nabla\phi - \mu C\Delta V\nabla P) = 0, \tag{3.7}$$

$$-\nabla^2\phi = \frac{\rho}{\varepsilon}, \tag{3.8}$$

$$\sigma\nabla V = -j, \tag{3.9}$$

$$\rho_p \frac{\partial^2\vec{u}}{\partial t^2} - \nabla \cdot c\nabla\vec{u} = \vec{F}, \tag{3.10}$$

It should be noted that in case of mechanoelectrical transduction, the ionic current is not driven by an applied voltage but by the bending induced pressure gradient. Hence, the Nernst-Planck equation includes the pressure gradient term, where ΔV is the molar volume and P is the solvent pressure.

The described model was implemented for the same fractal electrode geometries as used in case of the electromechanical transduction (Figure 3.1). The simulations were performed with 1 s and 0.2 s ramp actuations. Figure 3.3 and 3.4 shows the induced voltage in response to the applied ramp displacements in case of flat, unidirectional and random directional fractal electrodes with different generations (gen_1 and gen_3).

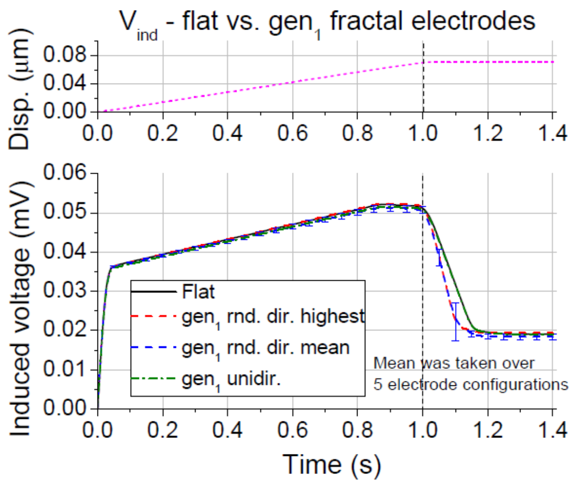

(a) 1 s ramp

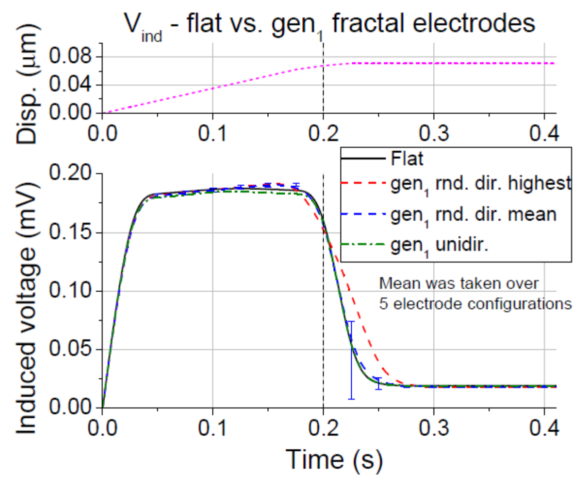

(b) 0.2 s ramp

Figure 3.3: Simulated induced voltage response in case of flat vs. gen_1 fractal electrodes (from ref. [14]).

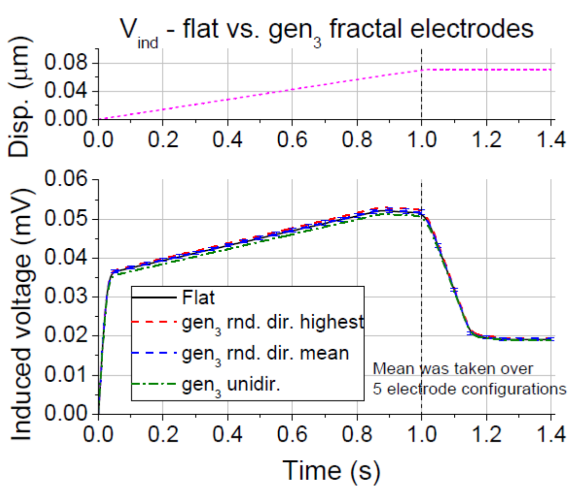

(a) 1 s ramp

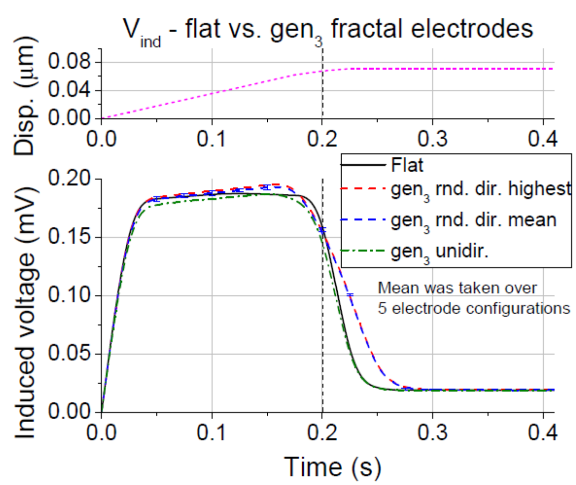

(b) 0.2 s ramp

Figure 3.4: Simulated induced voltage response in case of flat vs. gen_3 fractal electrodes (from ref. [14]).

As can be noticed, unlike in case of charge transport simulations, the induced voltages are less affected by the surface geometry of electrodes. Only slight changes in the voltage response can be observed. The reasons for a relatively weak effect of electrode surface geometry can be the following [14]. Firstly, the mechanoelectrical transduction of IPMC is a rather local phenomenon, i.e. the recorded voltage response is mainly affected by the electrode surface structure near the clamp contacts. Secondly, the voltage generation is mainly driven by a local volumetric strain, although, the effect is very low. Therefore, no significant surface charging can be expected during the deformation of IPMC.

Chapter 4

Experimental details

This chapter provides the experimental details of this research. Section 4.1 describes the procedures for preparing the IPMC samples with different types of electrodes (Pt and Pd-Pt) and different surface structures. The surface morphology of each type of electrode is altered and controlled by appropriately varying the conditions of electroless plating during the manufacturing process. Section 4.2 discusses in detail the methods and apparatus used for the characterization of electromechanical, mechanoelectrical, electrochemical and mechanical properties of the prepared IPMC samples.

4.1 Fabrication of IPMC materials

4.1.1 Chemicals and materials used

The perfluorinated sulfonic acid ionomer membrane (product of GEFC Co., Ltd) with the thickness of 0.6 mm was used as a base material for IPMC fabrication. The GEFC membrane has a similar chemical structure and properties to Nafion (Figure 2.2) and has shown one of the best performances among the ion-exchange membranes tested for

IPMC application [91]. The GEFC membrane was pretreated prior to IPMC preparation as described in the next section.

The following reagents were of analytical grade and were used as received: tetraammineplatinum(II) chloride monohydrate ($Pt(NH_3)_4Cl_2 \cdot H_2O$, 98%, Aldrich), tetraamminepalladium(II) chloride monohydrate ($Pd(NH_3)_4Cl_2 \cdot H_2O$, 98%, Aldrich), sodium borohydride ($NaBH_4$, 98%, Sigma), hydroxylamine hydrochloride ($H_2NOHHCl$, 98%, Sigma), hydrazine monohydrate ($H_2NNH_2 \cdot H_2O$, 98%, Sigma), lithium chloride (LiCl, 99%, Sigma), hydrogen peroxide (H_2O_2, 50 wt.%, Sigma), sulfuric acid (98%, Sigma), ammonium hydroxide (35%, EM Industries, Inc).

4.1.2 Conditioning of the membrane

The perfluorinated ion-exchange membrane was pretreated by roughening both surfaces with an emery paper (Grit #800 and #1000) to increase the polymer-electrode interfacial area and provide better physical bonding between the polymer and metal electrode layer. The both surfaces of the membrane were polished in one direction with straight movements until the membrane appeared non-transparent and uniformly matte. Thereafter, the cleaning procedure was carried out in order to remove organic and inorganic impurities contained in the membrane. These impurities are originated from the manufacturing process of the membranes. The polymer membrane was cleaned in 3 wt% hydrogen peroxide (H_2O_2) solution at 70 °C for 45 min and then in 1 M sulfuric acid (H_2SO_4) solution at the same temperature and duration. Finally, the membrane was cleaned in deionized water at 70 °C for 30 min (twice) to remove acid residues.

4.1.3 Fabrication of IPMC with Pt electrodes

First, the platinum particles were deposited on the inner surface of the membrane using an impregnation-reduction method [2, 49]. The ionic polymer was soaked in platinum salt ($Pt(NH_3)_4Cl_2 \cdot H_2O$) solution for 3–4 h to impregnate the polymer with Pt(II) complex ions. After rinsing with deionized water, the membrane was immersed in 350 ml of aqueous solution at 60 °C containing 0.2 g of reducing agent – sodium borohydride ($NaBH_4$) and 0.3 ml of ammonium hydroxide (NH_4OH) for pH adjustment. While under moderate stirring, 0.2 g of $NaBH_4$ was added in every 30 min for 2 h. During this procedure, the platinum salt in the polymer was chemically reduced to metallic form (Pt^0) at the inner surface of the membrane. Thereafter, the obtained composite was cleaned in 1 M H_2SO_4 solution for 30 min at 70 °C and then in deionized water at the same temperature and duration (twice). To increase the thickness of platinum layer and generate the dendrites as well as to grow them deeper into the polymer surface, the impregnation-reduction process was repeated several times.

As for next step, the platinum particles were deposited on the outer surface of the membrane using an electroless chemical deposition method. This step is typically implemented to further increase the electrode surface conductivity. The membrane was immersed in platinum salt ($Pt(NH_3)_4Cl_2 \cdot H_2O$) solution and while moderately stirring, small amounts of mild reducing agents such as hydrazine monohydrate ($H_2NNH_2 \cdot H_2O$) and hydroxylamine hydrochloride ($H_2NOHHCl$) were added in every 30 min for 4 h to deposit the Pt particles on the surface of the membrane. After typical cleaning procedure with sulfuric acid and deionized water, the chemical deposition process was repeated 1–2 times, depending on electrode surface conductivity.

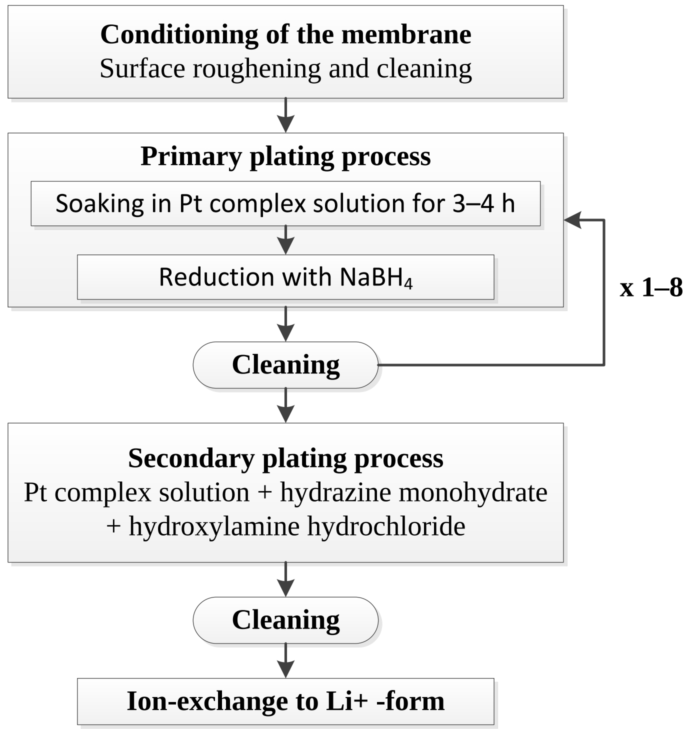

Figure 4.1: Manufacturing steps for preparing IPMC with Pt electrodes.

Using the aforementioned procedures, eight sets of Pt-IPMC samples were prepared by varying the number of impregnation-reduction cycles (referred to as primary platings) from 1 to 8. In all cases the time intervals during the impregnation-reduction process were precisely 3.5 h for impregnation in Pt complex, 2 h for reduction and 2 h for cleaning process for each plating cycle. The number of subsequent chemical deposition cycles (referred to as secondary platings) was kept constant and one plating was sufficient to reasonably equalize the electrode surface conductivity of the samples. The prepared samples were cut into 50 mm × 10 mm rectangular shape and ion-exchanged to Li^+-form by soaking in lithium chloride (1M LiCl) solution for overnight.

4.1.4 Fabrication of IPMC with Pd-Pt electrodes

In this electrode configuration, the palladium serves as a porous supporting layer at the inner surface of the polymer underneath the platinum top layer to enhance the interfacial surface area [16]. A procedure to prepare an IPMC with Pd-Pt electrodes was the following. As a first step, the palladium particles were deposited on the inner surface of the membrane using the impregnation-reduction method. The polymer was soaked in a palladium complex ($Pd(NH_3)_4Cl_2 \cdot H_2O$) solution at room temperature for 1 h to 2.5 h, depending on the desired thickness of Pd layer. After rinsing with deionized water, the membrane was immersed in 350 ml of aqueous solution containing 0.1 g of sodium borohydride ($NaBH_4$) and 0.3 ml of ammonium hydroxide (NH_4OH) at 60 °C. While under moderate stirring, 0.1 g of $NaBH_4$ was added in every 15 min for 2 h. During this process the palladium complex cations in the polymer are reduced to metallic palladium (Pd^0) at the inner surface of the membrane. Thereafter, the palladium-coated polymer membrane was cleaned in 1 M H_2SO_4 solution for 30 min at 70 °C and then in deionized water for the same temperature and duration (twice). The depth of the porous Pd layer in the membrane surface was controlled by controlling the soaking duration in Pd complex solution during the impregnation step.

As a next step, the platinum particles were deposited on the top of the palladium layer, at the outer surface of the membrane to increase the electrode surface conductivity. The membrane was immersed in platinum complex ($Pt(NH_3)_4Cl_2 \cdot H_2O$) solution and while under moderate stirring, small amounts of mild reducing agents such as hydrazine monohydrate and hydroxylamine hydrochloride were added in every 30 min for 4 h to deposit the platinum on the surface of the composite. After typical cleaning procedure with sulfuric acid and deionized water, the chemical deposition was repeated 2-4 times, depending on electrode surface conductivity.

Using the aforementioned steps, four sets of IPMC samples were prepared by varying the impregnation time from 1 h to 2.5 h in 3.8 mM Pd complex solution with 30-min increments. The Pt top layer at the outer surface of the membrane was applied by four chemical deposition cycles (secondary platings). The prepared Pd-Pt IPMC samples were cut into 50 mm × 10 mm rectangular shape and ion-exchanged to Li^+-form by soaking in lithium chloride (1 M LiCl) solution for overnight. Lithium ions are preferred due to their strong solvation by water molecules, enabling them to transport more water during the transduction. The entire manufacturing process is illustrated in Figure 4.2.

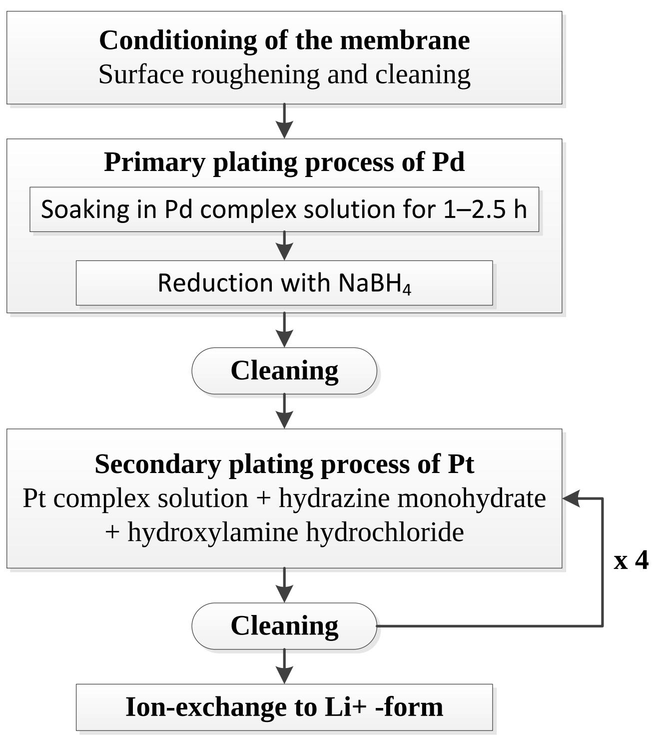

Figure 4.2: Manufacturing steps for preparing IPMC with Pd-Pt electrodes.

4.2 Characterization methods

4.2.1 Electromechanical and mechanoelectrical transduction

The electromechanical responses such as displacement and blocking force of the prepared IPMCs were measured by a laser displacement sensor (optoNCDT-1401, Micro-Epsilon) and a load cell (GSO-30, Transducer techniques) with a sample size of 50 mm × 10 mm in the test setup composed of a signal generator (FG-7002C, EZ digital), a power amplifier (LVC-608, AE Techron), a DC power supply (CPS250, Tektronix), and a DAQ (SCB-68, National Instruments), as illustrated in Figure 4.3 and 4.4. IPMC was clamped in a vertical cantilever position with a free-length of 40 mm and immersed in a transparent container filled with deionized water. The displacement measurements were conducted under ±1 to ±3AC square-wave voltages at the frequency range of 0.05 to 5 Hz. Blocking force measurements were performed at 1–3 V DC input. The voltage, current and displacement (or blocking force) responses were recorded simultaneously using National Instruments/LabView 8 data acquisition system. The performances of different IPMCs were analyzed in the terms of the total transported charge (*Q*), calculated from the measured current response according to the following equation

$$Q = \int_{t_0}^{t_1} I dt\,, \tag{4.1}$$

where I is the measured current transferred between the times t_0 and t_1. Based on the electromechanical transduction model presented in Chapter 3, the transported charge during the transduction is proportional to the bending force and deformation of IPMC.

The displacement (δ) was converted to bending strain (ε_b) according to the relation [2],

$$\varepsilon_b = \frac{2h\delta}{L^2 + \delta^2}, \tag{4.2}$$

where h is the thickness and L is the free length of IPMC.

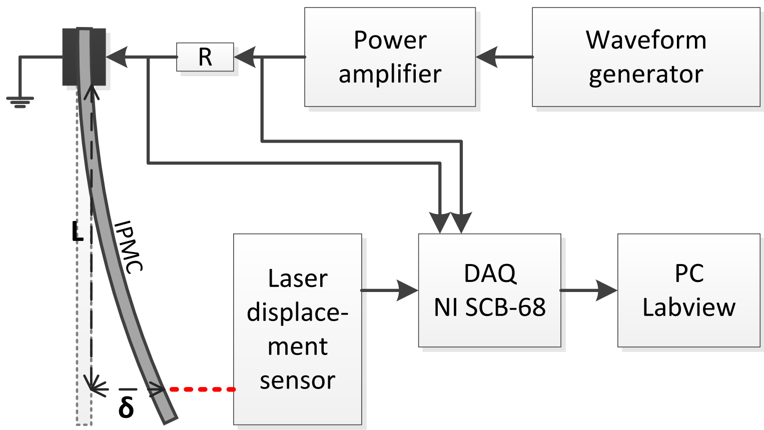

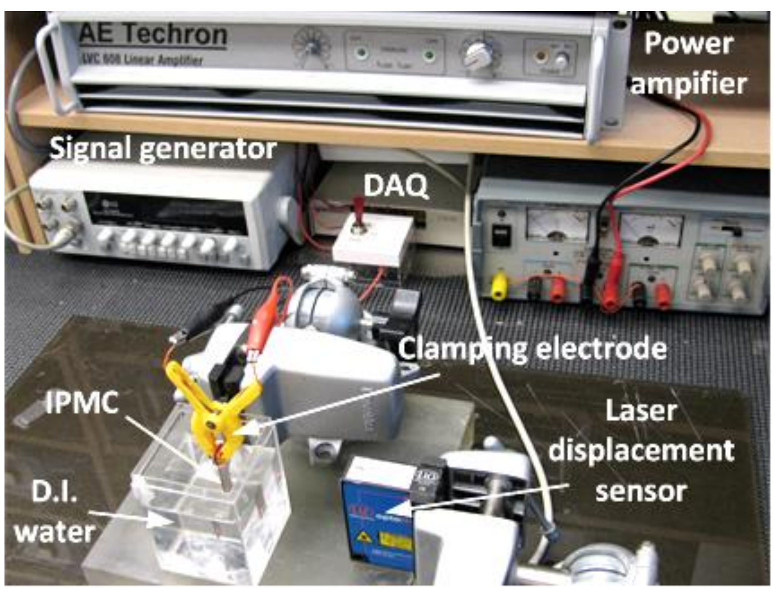

Figure 4.3: Experimental setup used for displacement measurement of IPMC.

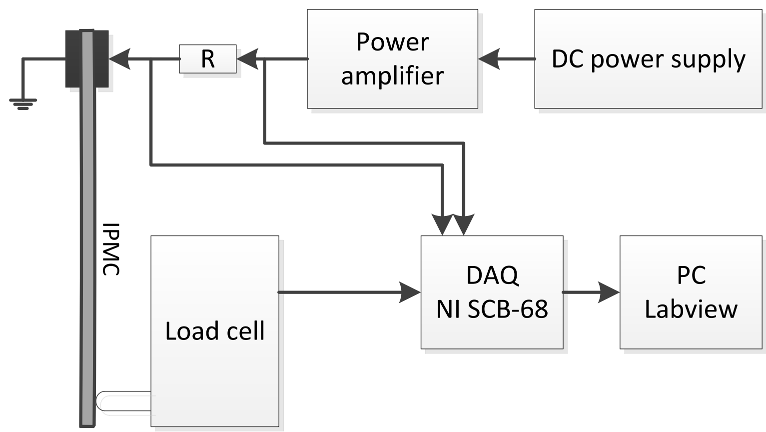

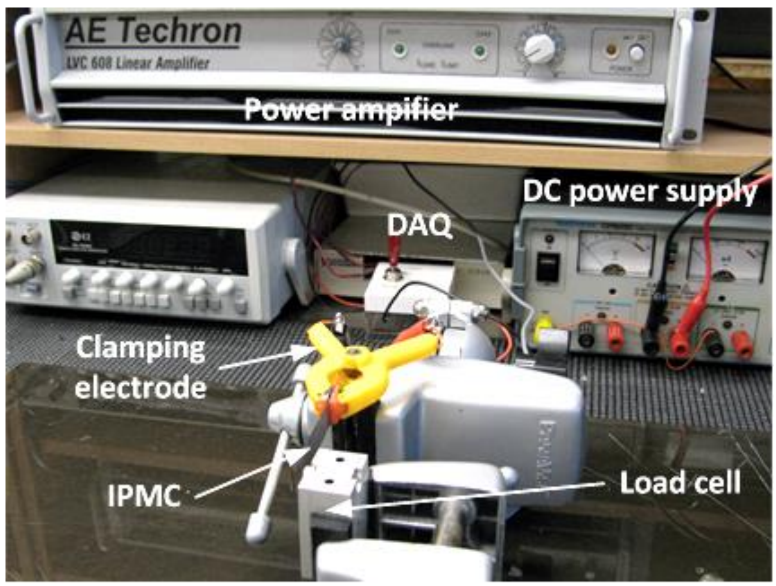

Figure 4.4: Experimental setup used for blocking force characterization of IPMC.

The mechanoelectrical transduction of the IPMC was characterized using a vibration test system composed of a vibration controller (VR-8500, Vibration Research Corporation), a power amplifier (BAA-120, TIRA), and a mechanical shaker (S-521, TIRA) as shown in Figure 4.5. The IPMC sample with a size of 50 mm × 10 mm was clamped in vertical position from one end and the shaker was used to apply a sinusoidal displacement to other end of IPMC. The generated voltage from the IPMC was measured at the clamp contacts. Since the induced voltage is in the order of millivolt, a sinusoidal displacement was applied in order to obtain cleaner and readily observable output signal. The output signal from IPMC was amplified through the custom made signal amplifier and recorded using a National Instruments USB-6008 and Labview data acquisition system. The laser displacement sensor (optoNCDT-1401, Micro-Epsilon) was used for monitoring the applied displacement at the IPMC tip (Figure 4.5).

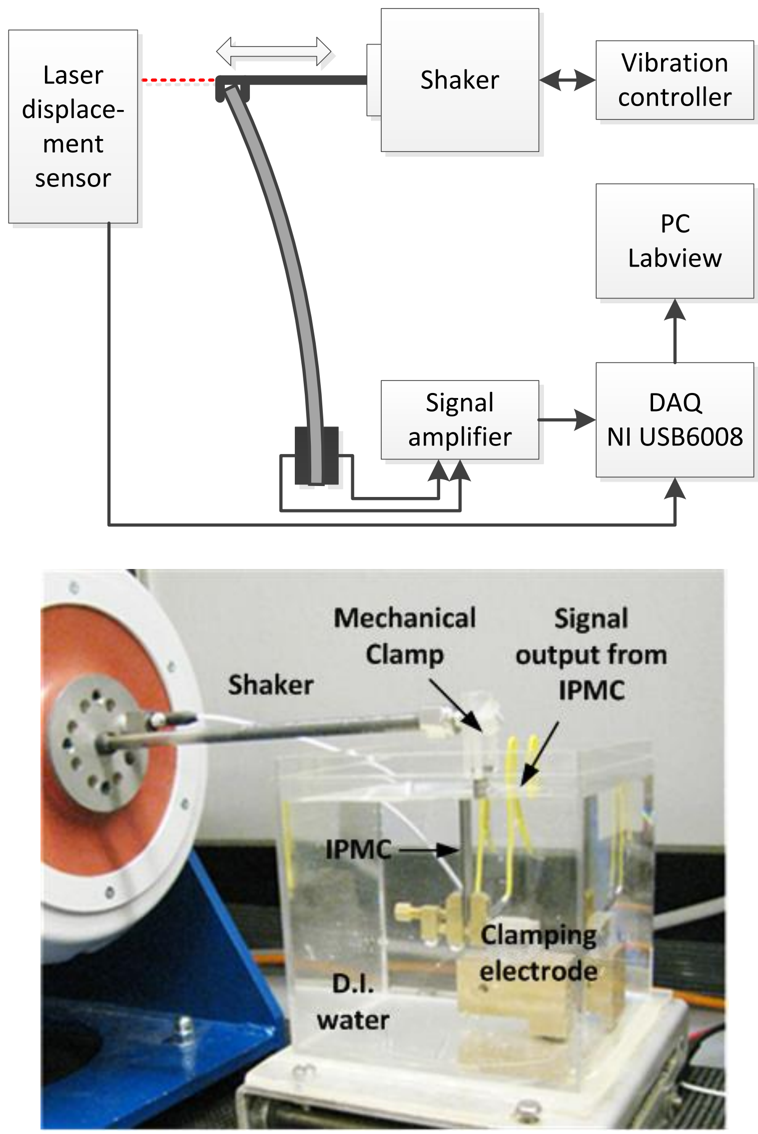

Figure 4.5: Measurement setup used for mechanoelectrical characterization.

4.2.2 Electrochemical properties

Cyclic voltammetry (CV) and electrochemical impedance spectroscopy (EIS) were employed to evaluate the interfacial surface of the IPMC electrodes in terms of capacitance. Cyclic voltammetry is commonly used technique for measuring the capacitance of electrochemical systems such as electrochemical double-layer capacitors. In this measurement technique the voltage of the electrochemical cell is swept between two vertex potentials at a fixed rate for a number of cycles while measuring the current response of the system. The CV measurements were conducted using a Radiometer Analytical PGZ-402 potentiostat in a two-electrode cell configuration in a potential range of -0.5 to 0.5 V at the scan rate of 50 mV/s. With no faradaic contribution, the current response is purely capacitive and can be expressed as

$$I = \frac{dQ}{dt} = C\frac{dV}{dt}, \tag{4.3}$$

where I is the current, C is the capacitance and dV/dt is the potential scan rate. The double-layer capacitance can be determined from the cyclic voltammograms according to the equation [92, 93]:

$$C = \frac{\left|j^{+}\right| + \left|j^{-}\right|}{2\,dV/dt}, \tag{4.4}$$

where j^+ and j^- are the polarization current densities at 0 V.

EIS is a commonly used for characterization of electrochemical cells with capacitive and resistive components. EIS measures the impedance of the system in response to an applied AC voltage over a range of frequencies and provides insight about the processes such as ionic diffusion, double-layer charging, and faradic reactions. The EIS (differential capacitance) measurements for IPMCs were performed in a frequency range of 0.1 Hz to 100 kHz with an AC perturbation voltage of 10 mV using a Radiometer Analytical PGZ-402 potentiostat.

Electrode surface conductivity measurements

Electrode conductivities of the samples were determined using a four-point probe method. This technique uses two outer probes for applying current and two inner probes for sensing the voltage. The advantage of using four probes is that it eliminates the resistance contribution of electrical wiring and probe contact resistances.

4.2.3 Surface analysis and mechanical properties

Scanning electron microscopy (SEM) was employed to investigate the cross-sectional morphology of IPMCs and evaluate the depth and density of the dendrites in the polymer surface. The SEM micrographs were obtained using a Hitachi S-4200 microscope in secondary electron image mode with accelerating voltages of 5–15 kV. The samples were quick-frozen in liquid nitrogen and fractured just before SEM observations to obtain clean cross-section cut. Energy dispersive X-ray (EDS) detector was used for chemical line-scan analysis to observe the distribution of deposited metal particles in the cross-section of IPMC.

The flexural modulus measurements were performed in order to study the impact of electrode thickness and surface structure on the flexural stiffness of IPMC material. It should be noted that the flexural stiffness can strongly affect the electromechanical performance of IPMC, especially the displacement. The flexural moduli of the samples were measured in three-point bending mode by using universal testing machine (Instron 5565, USA). The test setup is shown in Figure 4.6.

Figure 4.6: The three-point bending test setup used for measuring the flexural modulus of IPMC.

Chapter 5

Characterization of IPMCs with Pt electrodes

This chapter discusses the effects of electrode surface morphology in the transduction of platinum electrodes based IPMCs. Eight sets of Pt-IPMCs with different electrode surface structures were prepared by varying the number of impregnation-reduction cycles (primary platings) in the electroless plating process. The number of subsequent chemical deposition cycles (secondary platings) was kept constant and one plating was sufficient to reasonably equalize the electrode surface conductivity of the samples. The notation of the prepared IPMCs and applied platings are listed in Table 5.1. The chapter discusses the electromechanical, mechanoelectrical, electrochemical, and mechanical characteristics of the Pt-IPMCs with different electrode surface structures.

Table 5.1: Notation of Pt-IPMC samples used in the study.

Notation	No. of primary platings	No. of secondary platings	Electrode surface resistance (Ω/cm)
Pt(1)	1	1	4.8 ±0.5
Pt(2)	2	1	3.5 ±0.4
Pt(3)	3	1	1.8 ±0.2
Pt(4)	4	1	1.1 ±0.1
Pt(5)	5	1	0.9 ±0.1
Pt(6)	6	1	0.6 ±0.1
Pt(7)	7	1	0.6 ±0.1
Pt(8)	8	1	0.5 ±0.1

5.1 Electrode surface morphology

Figure 5.1 shows the SEM cross-sectional images of Pt-IPMC samples with different electrode surface morphologies. The micrographs were taken at 1k magnification from one side of the cross-section, and show the deposited Pt electrode layer at the surface of the polymer membrane in case of each sample. It can be seen that the electrode layer grows in thickness with increasing the number of platings from 1 to 8 (samples Pt(1)…Pt(8)). Also, noticeable changes in the electrode surface shape (profile) occur. The Pt(1) sample has a rather uniform and flat electrode layer, while the samples with higher number of platings exhibit some large bumps at the inner surface of the electrode. It should be noted that the uneven and rough regions at the polymer area are due to fracturing the samples in liquid nitrogen prior to SEM observations.

More details at the electrode surface can be seen in the SEM micrographs taken at 30k magnification (Figure 5.2). As can be observed, the electrode interface is composed of small Pt nanoparticles that gradually become larger as the number of plating cycles is increased. Starting from 5th plating (Pt(5)), the platinum particles with multiple sharp tips and edges are formed that become larger and more developed with further increment of plating cycles. The IPMC prepared with eight platings (Pt(8)) shows already very large Pt structures with sophisticated geometries at the electrode interface. There are very few reports concerning Pt nanoparticles with sharp tips and edges [94]. Tian *et al.* have synthesized similar nanostructures – called Pt nanothorn assemblies – on a glassy carbon substrate using electrodeposition method [95]. According to their study the nanothorn has single crystalline face-centered cubic structure and the growth is along [111] direction.

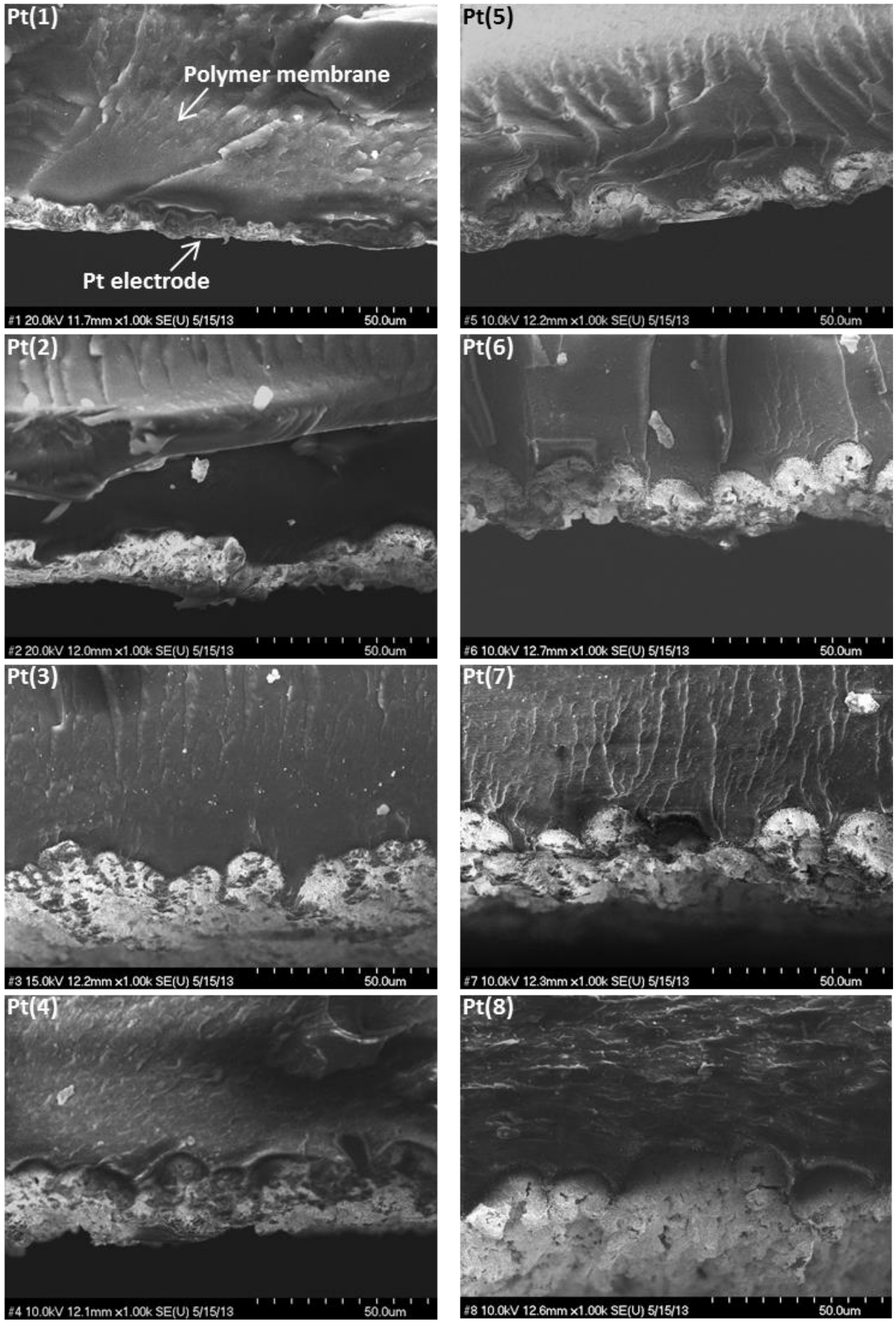

Figure 5.1: SEM cross-sectional migrographs of Pt-IPMCs with different electrode surface structures at 1k magnification.

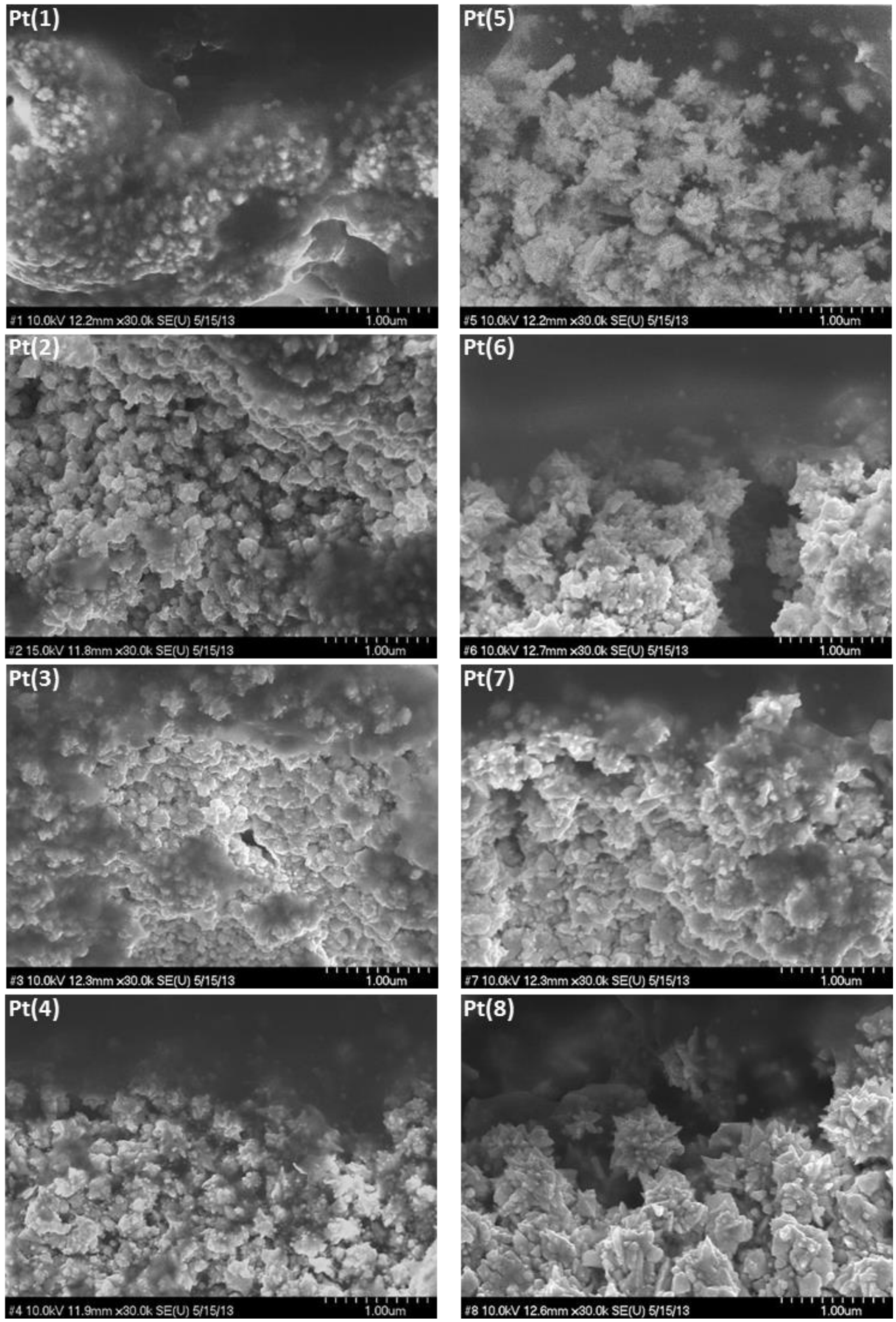

Figure 5.2: SEM cross-sectional migrographs of Pt-IPMCs with different electrode surface structures at 30k magnification.

The mechanism of formation of Pt nanothorn assemblies is not well understood. However, the dendritic crystal structures generally form due to growth instabilities when the growth rate is limited by the rate of diffusion of atoms to the surface [96]. There also has to be a concentration gradient from a solution to the equilibrium at the interface. Deposited metal particles by nature contain surface defects and imperfections such as bumps and tips. A corner or tip on the deposited particle results in a steeper concentration gradient and thereby increases the diffusion rate, leading to a faster growth of the structure at the tip and eventually formation of peak [96]. The growth of Pt nanothorn assembly with consecutive impregnation-reduction cycles is illustrated in Figure 5.3.

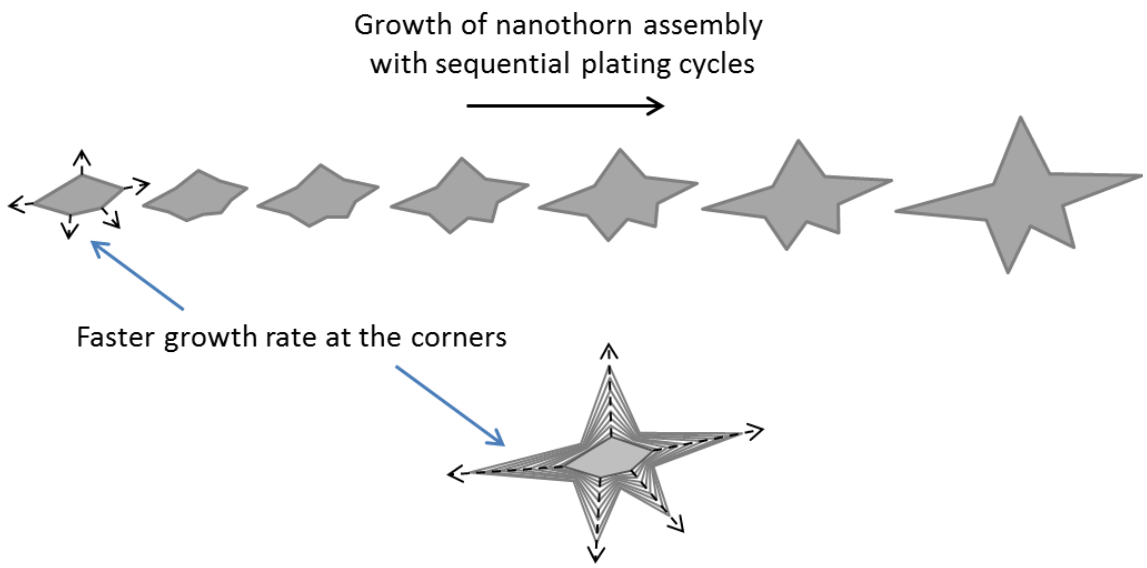

Figure 5.3: Schematic illustration of the growth of Pt nanothorn assembly with consecutive primary plating cycles. Arrows indicate faster growth rate at the tips.

Figure 5.4 shows the individual as-synthesized Pt nanothorn assemblies at the polymer-electrode interface at higher magnification. It is clear that these nanostructured Pt assemblies result significantly higher interfacial surface area compared to the regular flat-surfaced Pt electrodes which, according to the theory presented in Chapter 3, should lead to higher total transported charge during the transduction process of IPMC. To the best of our knowledge, such nanostructured Pt assemblies synthesized through impregnation-reduction method at the polymer-electrode interface have not been reported before or considered for use in IPMC application.

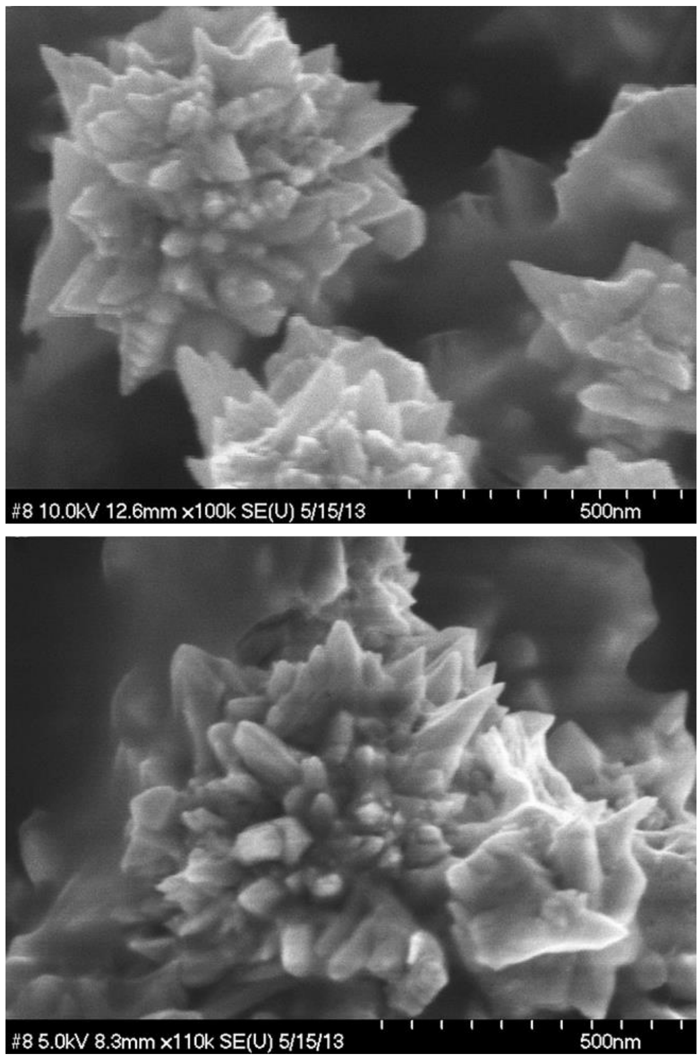

Figure 5.4: SEM cross-sectional images of Pt(8) sample at 100k and 110k magnification showing Pt nanothorn assemblies at the electrode interface at different locations.

5.1.1 Flexural modulus

Figure 5.5 presents the flexural stress-strain curves for the Pt-IPMC samples measured at a strain rate of 0.1 mm/mm/min in a three-point bending configuration. The flexural stress σ_f and flexural strain ε_f for a rectangular beam in three-point bending mode were calculated as follows [97]:

$$\sigma_f = \frac{3ML_s}{2wh^2}, \tag{5.1}$$

$$\varepsilon_f = \frac{6Dh}{L_s^2}, \tag{5.2}$$

where M is the applied load, L_s – the support span, w – the width of the beam, h – the thickness of the beam, and D – the deflection of IPMC. The flexural modulus E_f of IPMC was determined from the slope of the initial linear portion of the stress-strain curve:

$$E_f = \frac{\Delta\sigma_f}{\Delta\varepsilon_f} \tag{5.3}$$

As can be observed in Figure 5.5, the addition of primary platings increases the flexural modulus of IPMC samples. This can be expected since the electrode layers grow deeper into the polymer membrane surface. It should be noted that the flexural stiffness can strongly affect the electromechanical performance of IPMC, especially the displacement. Generally, higher stiffness leads to a lower displacement range. For the IPMC samples under study the variation of flexural modulus is rather noticeable, ranging from 126–189 MPa. Therefore, it is likely that at certain point the increasing mechanical stiffness will start to limit the displacement performance of the samples.

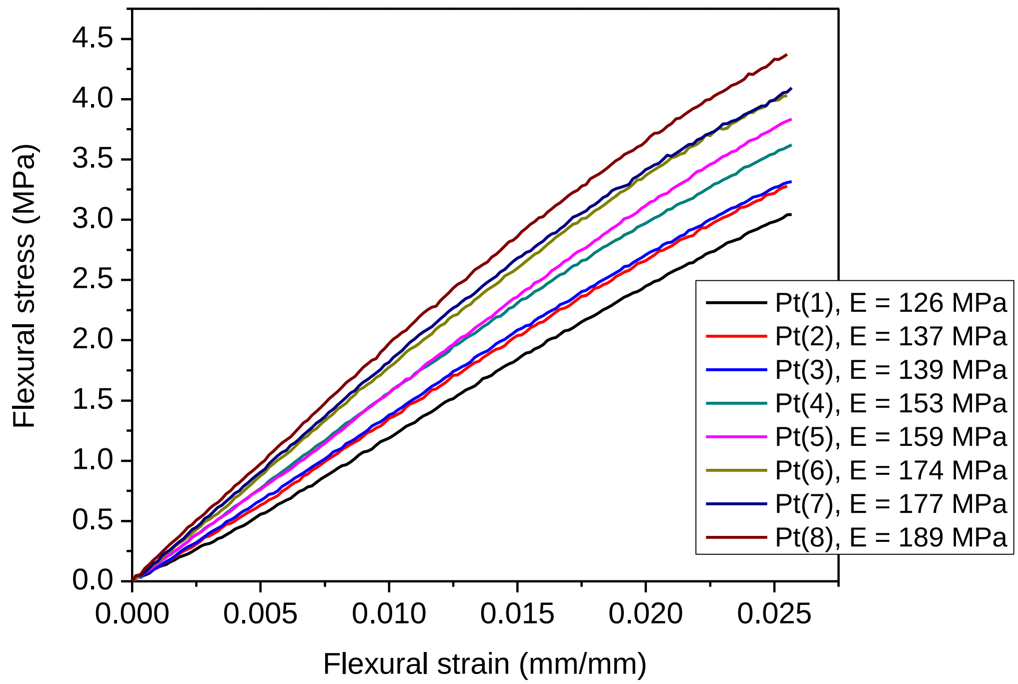

Figure 5.5: Flexural stress-strain diagrams for Pt-IPMCs with different electrode structures and respective flexural modulus values, measured in a 3-point bending mode.

5.1.2 Interfacial capacitance

The IPMCs with different electrode surface structures were evaluated in terms of the electric double-layer capacitance, which directly describes the electrode interfacial area and its effectiveness to accommodate charges at the electrode/electrolyte boundary. The electric double-layer with the differential capacitance, C_d, is defined as [98, 99]

$$C_d = \frac{dq_s}{d\psi_s}, \tag{5.4}$$

where q_s and ψ_s are the surface charge density and the surface electric potential, respectively. The differential double-layer capacitance for IPMC was determined from EIS measurements according to the following equation [100-102],

$$C_d = \frac{-1}{2\pi f Z''}, \tag{5.5}$$

where f is the frequency of applied electric potential signal and Z'' is the imaginary part of the impedance. IPMC is considered as a circuit consisting of a capacitor and resistor in series [103, 104]. Equation (5.5) is commonly used for determining the differential capacitance for IPMCs and electrochemical double-layer capacitors (EDLCs) from EIS measurements [100-102, 105]. It should be noted that IPMC is analogous electrochemical system to EDLC when operated at lower voltage range (< 1.5 V).

Figure 5.6 shows the frequency dependence of the differential capacitance for Pt-IPMCs obtained from EIS measurements in the frequency range of 0.1–100 Hz with an AC perturbation voltage of 10 mV and DC bias of 0.1 V in two-electrode cell. This data

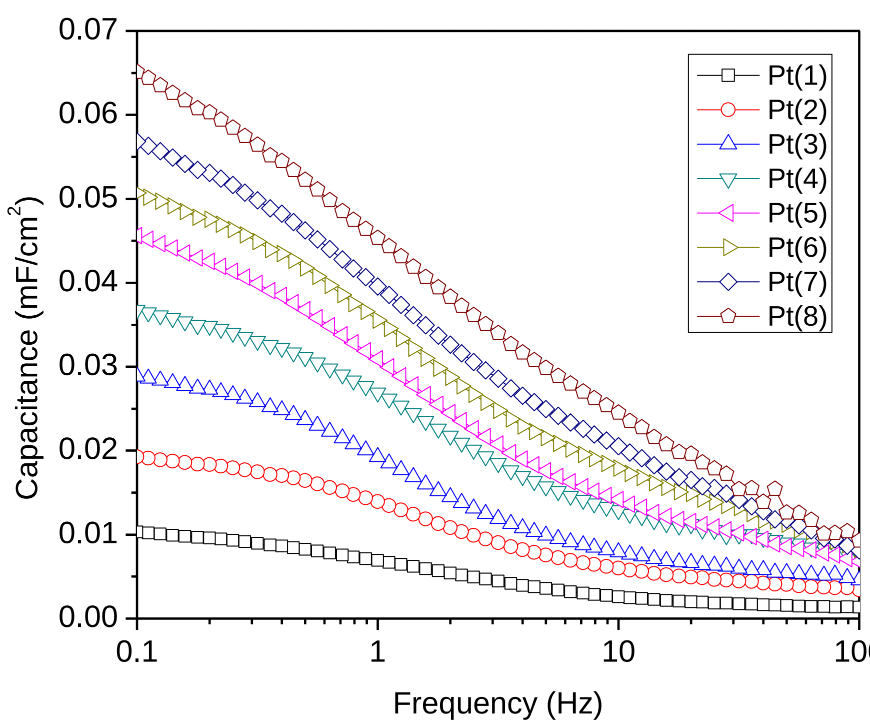

Figure 5.6: Frequency dependence of differential capacitance for Pt-IPMCs with different electrode surface morphologies from EIS measurements at DC bias of 0.1 V.

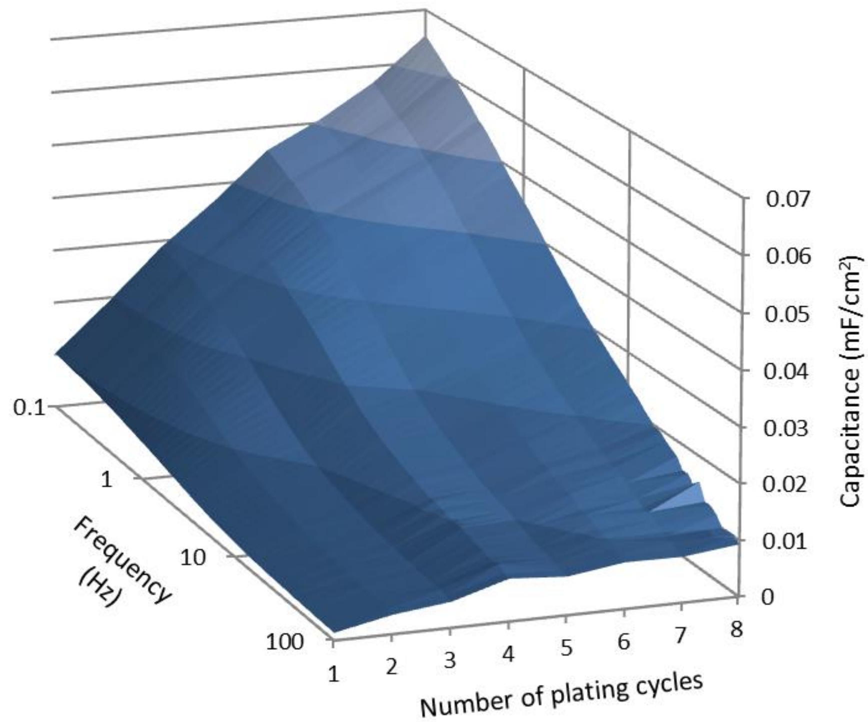

Figure 5.7: An alternative representation of the data in Figure 5.6. The capacitance of Pt-IPMCs as a function of frequency and plating cycles.

is also represented in Figure 5.7 as a contour plot of the capacitance with respect to the frequency and number of plating cycles. The measured data shows that increasing the primary plating cycles and thereby developing nanothorn assemblies at the electrode interface leads to a notable increase in the double-layer capacitance of IPMC at the lower frequencies (f < 10 Hz), indicating an enlarged interfacial surface area of nanostructured electrodes. A higher charge accumulation in case of more developed surface geometry is in accordance with the fractal electrode simulations presented in Chapter 3.

The charging-discharging capacitance of Pt-IPMCs with different electrode surface structures was determined using cyclic voltammetry in a potential range of -0.5 to 0.5 V at the scan rate of 50 mV/s in two-electrode cell (Figure 5.8). The measured cyclic

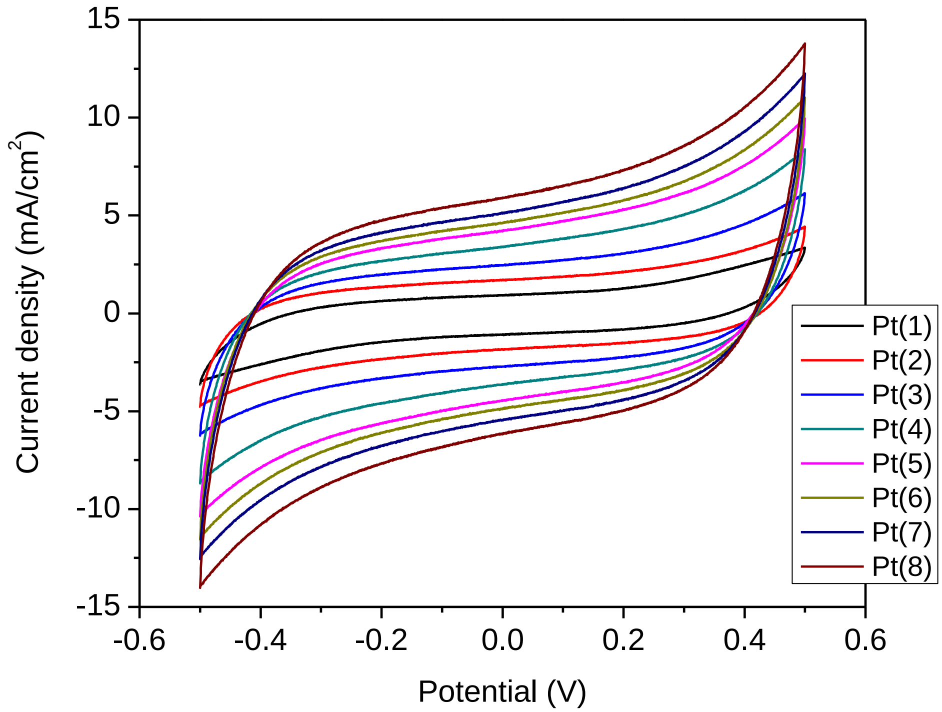

Figure 5.8: Cyclic voltammograms of Pt-IPMCs with different electrode surface structures measured at a potential scan rate of 50 mV/s.

voltammograms indicate non-faradaic capacitive current behavior. It can be seen that increasing the number of primary platings leads to a considerably higher current densities during the charging and discharging, which can be expected as more charges are involved in the double-layer formation due to the larger interfacial surface area of electrodes.

The charging-discharging capacitance values were determined from the measured cyclic voltammograms according to the equation (4.3) and were plotted against the number of plating cycles as shown in Figure 5.9. The capacitance at 0 plating corresponds to a bare membrane with no Pt plating on the surface. As can be seen, there is a steady and almost linear increase in the capacitance with the increment of plating cycles. The improvement in the capacitance is six times (0.02 mF/cm^2 to 0.121 mF/cm^2)

with increasing the plating cycles from 1 to 8. The obtained results are consistent with EIS measurements as well as with the SEM data discussed earlier in Section 5.1. Based on the model (see Chapter 3), a higher charge density at the electrodes leads to a higher electromechanical performance of IPMC. The data demonstrates that a careful control of the synthesis parameters of the impregnation-reduction process allows good control over the interfacial area of Pt electrodes. Oguro *et al.* [85] observed a similar systematic increase in the capacitance with the plating cycles in case of Au electroded Flemion membrane-based IPMCs due to the growth of fractal-like dendrites. While their capacitance values are fairly close to our Pt-IPMCs, the direct comparison of the data is difficult due to very different composite systems and experimental conditions involved.

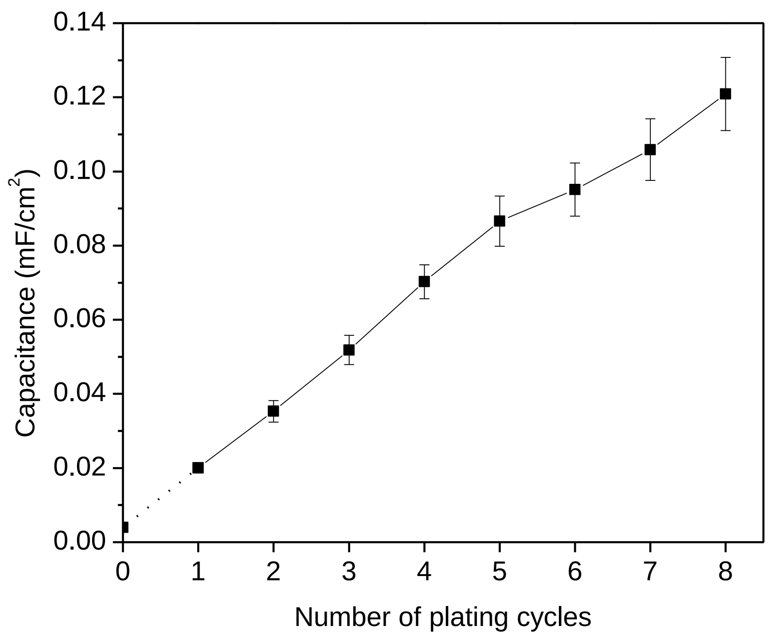

Figure 5.9: Charging-discharging capacitance of Pt-IPMC samples versus the number of primary plating cycles.

5.2 Electromechanical transduction

The electromechanical performances of the IPMCs with different Pt electrode surface structures were characterized at 1 to 3 V DC and ±1 to ±3 AC square-wave inputs at the frequency range of 0.05 to 5 Hz. Although the IPMCs of this type are typically operated at input voltages between 2–4 V, a lower voltage (1 V) was used in order to avoid electrochemical processes (i.e. electrolysis of water) – the lost current, to allow more exact comparison of the results in terms of the transported charge.

5.2.1 Actuation performance

Figure 5.10 shows the measured voltage, current, transported charge and corresponding displacement in time for Pt-IPMCs at ±1 V AC square-wave input at 0.1 Hz. It can be seen that the current as well as the transported charge and displacement are the lowest in case of Pt(1) sample and increase significantly with the number of plating cycles. The peak displacement of Pt(3) sample is already three-fold compared to that of Pt(1). However, it can be noticed that after the 4th plating, while there is still a noticeable increase in the transported charge with the number of plating cycles, the increment in the displacement response slows down and is relatively minor (see Figure 5.11). The reason may be that the generated bending force at 1 V may be too low to overcome the increasing flexural stiffness of the samples with higher number of platings. Overall, the measurements show that repetitive impregnation-reduction of Pt leads to a higher transported charge during the actuation that in turn results in a larger displacement of IPMC. This data is in good agreement with the theory presented in Ch. 3 and in ref. [14].

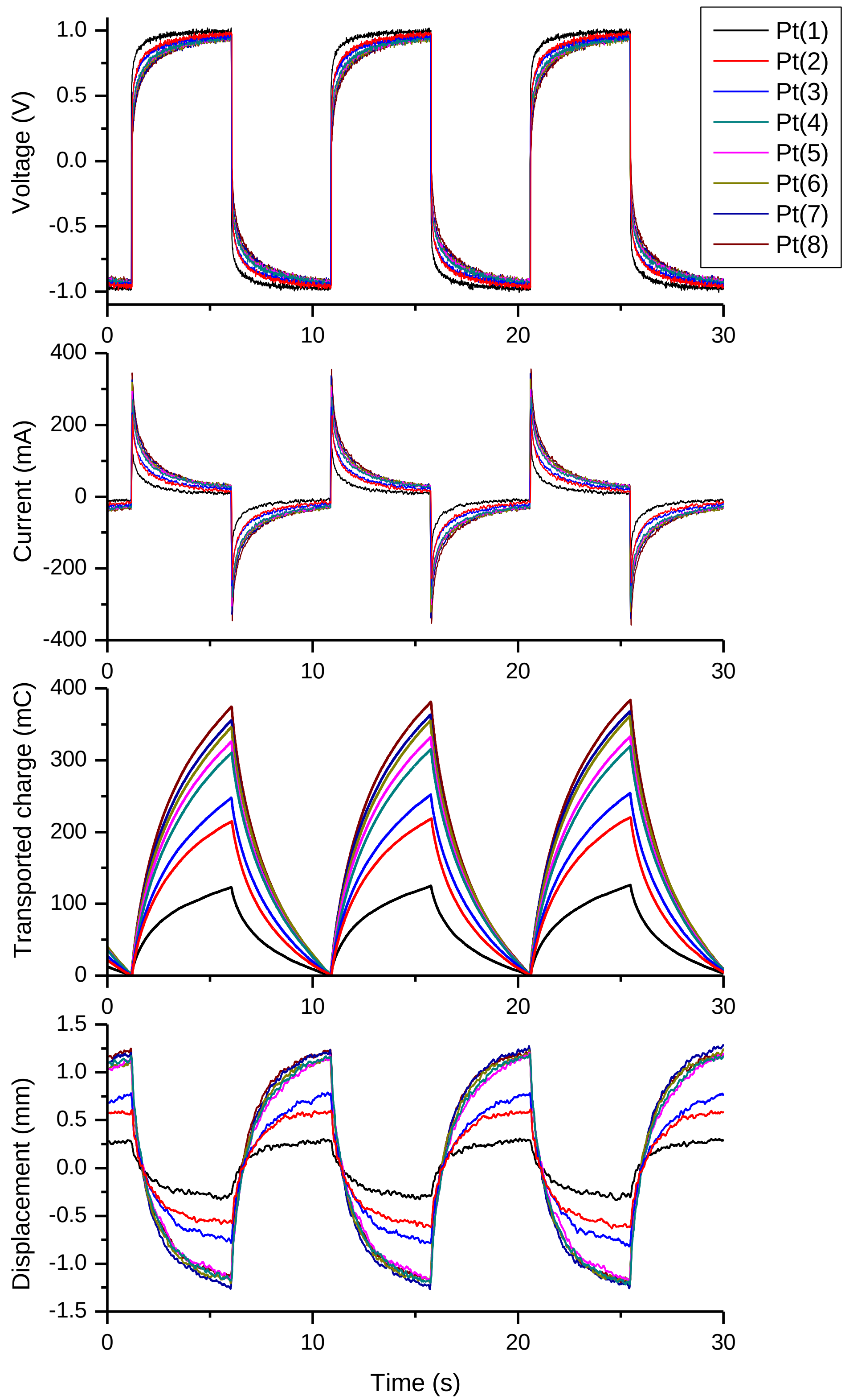

Figure 5.10: Measured voltage, current, transported charge and displacement responses at ±1 V AC square-wave at 0.1 Hz for Pt-IPMCs with different electrode surface structures.

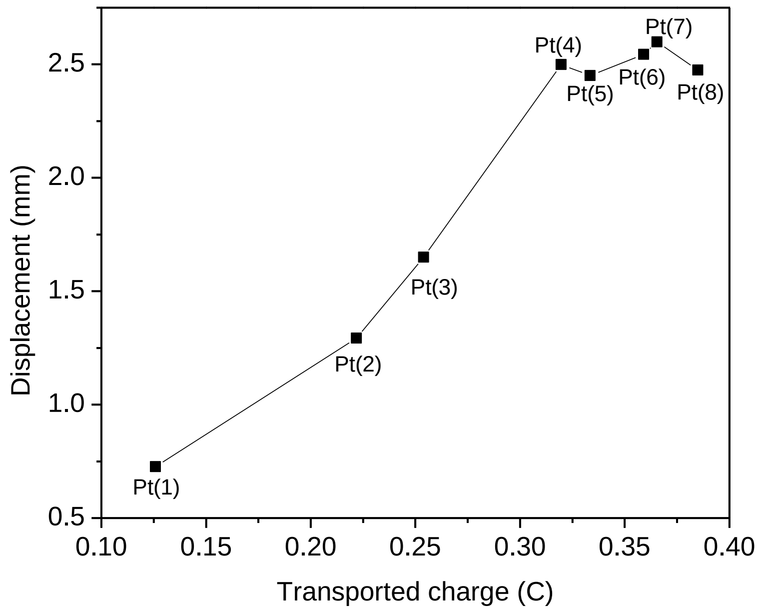

Figure 5.11: Peak-to-peak displacement versus transported charge at 0.1 Hz, ±1 V AC.

The displacement measurements were also performed at higher voltages in order to see how the transported charge correlates with the actuation performance at normal operating voltages (2–3 V). Figure 5.12 shows the measured voltage, current, transported charge and displacement responses at ±3 V AC square-wave at 0.1 Hz. As can be noticed, the differences in measured voltage and current responses as well as in charge transport and corresponding displacement are more apparent compared the measurements at ±1 V AC input (Figure 5.10). The peak currents are higher and decay at a slower rate as the number of platings is increased, indicating a higher double-layer charging due the larger interfacial surface area of electrodes. However, it should be noted that the measured current response at a given voltage also includes the charge transfer associated with faradaic processes – electrolysis of water, which does not contribute to the actuation of IPMC. Therefore, exact evaluation of the actuation performance in terms of transported

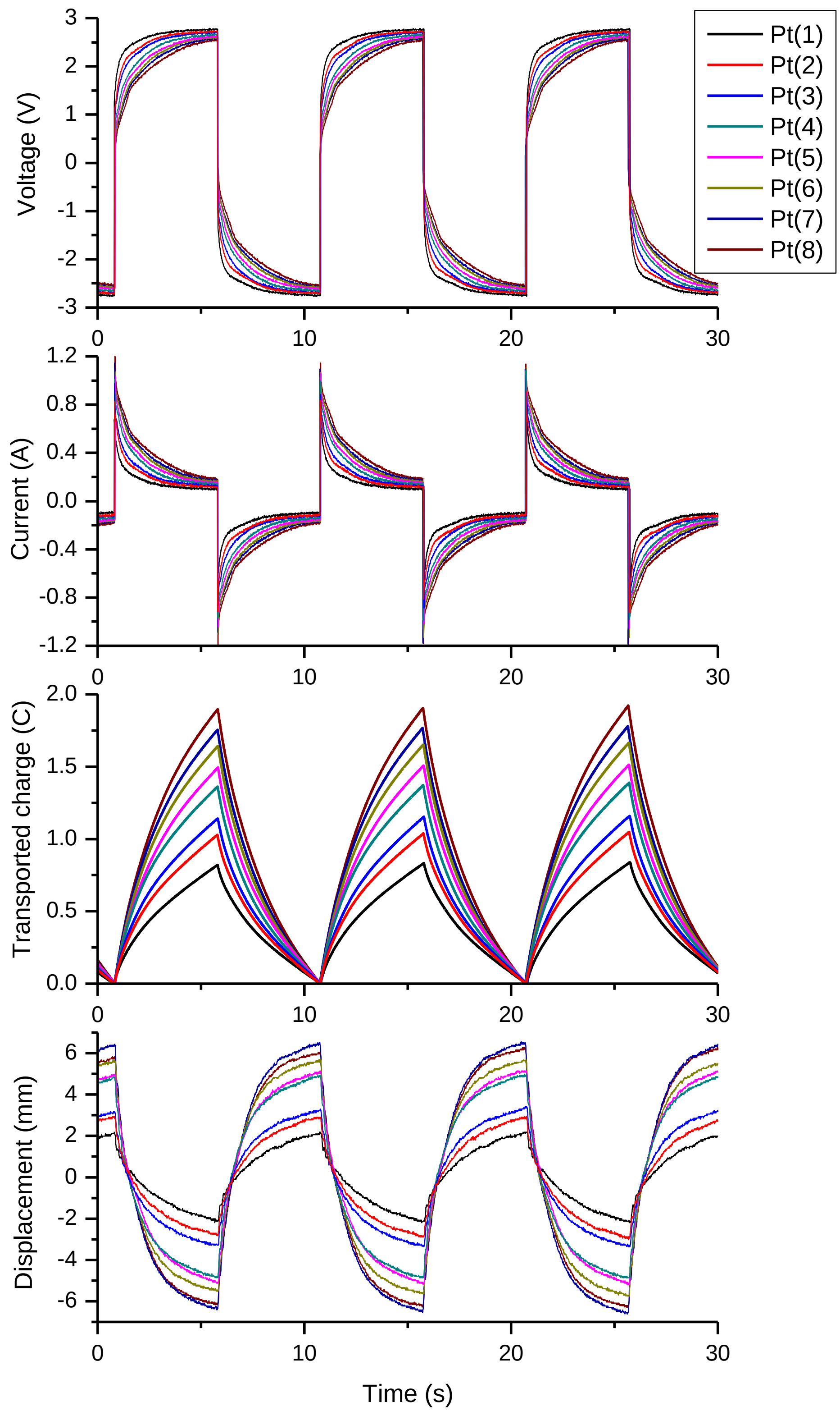

Figure 5.12: Measured voltage, current, transported charge and displacement responses at ±3 V AC square-wave at 0.1 Hz for Pt-IPMCs with different electrode surface structures.

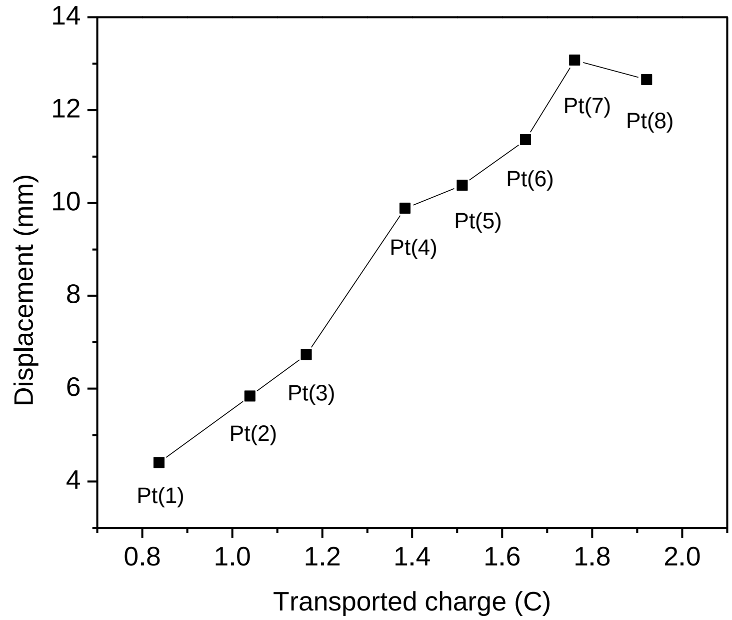

Figure 5.13: Peak-to-peak displacement versus transported charge at 0.1 Hz, ±3 AC.

charge is complicated at higher input voltages (> 1.8 V). Nonetheless, the measured current/transported charge data correlates well with the displacement response of the samples (Figure 5.13). As compared to the measurements at ±1 V AC (Figure 5.11), the differences in the transported charge and displacement are more pronounced, especially for the IPMCs with higher number of primary platings, i.e. samples Pt(4)…Pt(8). While there is a steady increment in the charge transport with the number of added platings, the displacement increases up to seventh plating, and the sample with eight platings (Pt(8)) already shows slightly less displacement than Pt(7). This is likely due to increasing flexural stiffness of the material that starts to limit the actuation performance (Figure 5.5). Overall, the data shows that increasing the number of impregnation-reduction cycles from 1 to 7 results in an improvement of displacement amplitude more than 3 times.

Figure 5.14 shows the transported charge and corresponding peak-to-peak displacement of Pt-IPMCs as a function of frequency from 0.05 to 5 Hz at ±1 AC square-wave input. The transported charge and the displacement values were calculated by taking an average over minimum of 6 actuation cycles at each measured frequency. As can be seen, the transported charge data correlates rather well with the actuation performance of IPMCs in the tested frequency range. It can be noticed that at higher frequencies (> 1 Hz) the effect of plating cycles on the transported charge and corresponding displacement response is relatively low. This is due to limited charging time at higher actuation frequency that prevents utilizing the larger interfacial area of the electrodes in case of the samples with higher number of platings.

At 0.5 Hz and below, there is a notable increase in the charge transport and displacement response with increasing the number of plating cycles from 1 to 4. However, increasing the platings from 4 to 8 results relatively minor changes in the displacement performance, i.e. the samples Pt(4)…Pt(8) all perform rather similarly in the entire frequency range. There are some noticeable changes at 0.05 Hz though. This data indicates that at 1 V input the electrolyte diffusion and interfacial charging are not fast enough to take an advantage of higher electrode surface area. As can be seen in Figure 5.14, a noticeable increase in the transported charge for samples Pt(4)…Pt(8) only occurs at the lowest actuation frequency (0.05 Hz), which also results more apparent changes in the corresponding displacement response.

The same set of measurements was also performed at ±3 V AC at 0.05–5 Hz (Figure 5.15). It can be seen that with higher input voltage the differences in the transported charge and displacement for samples Pt(4)…Pt(8) are already noticeable at 0.1 Hz.

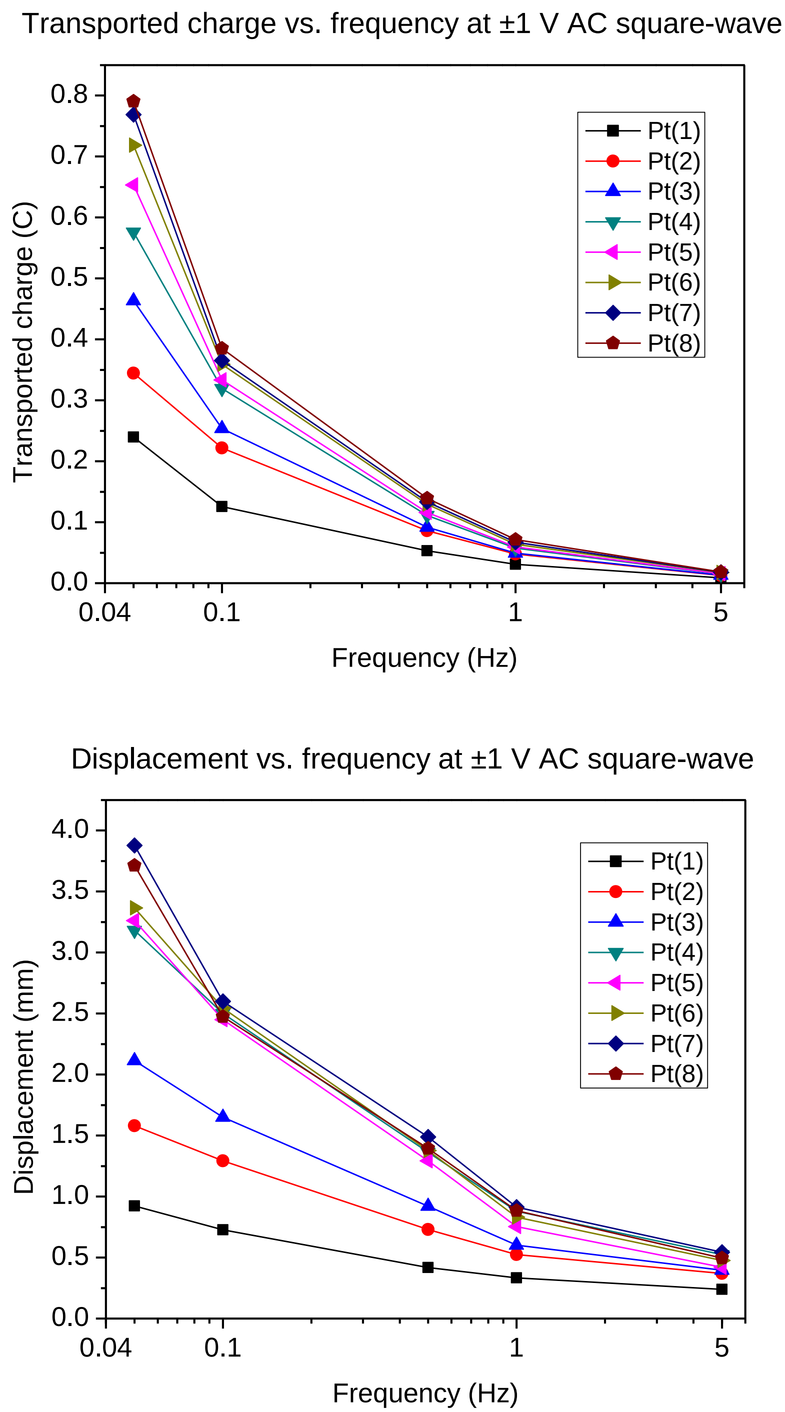

Figure 5.14: Frequency dependences of the total transported charge and corresponding displacement of Pt-IPMCs at ±1 V AC square-wave input between 0.05–5 Hz.

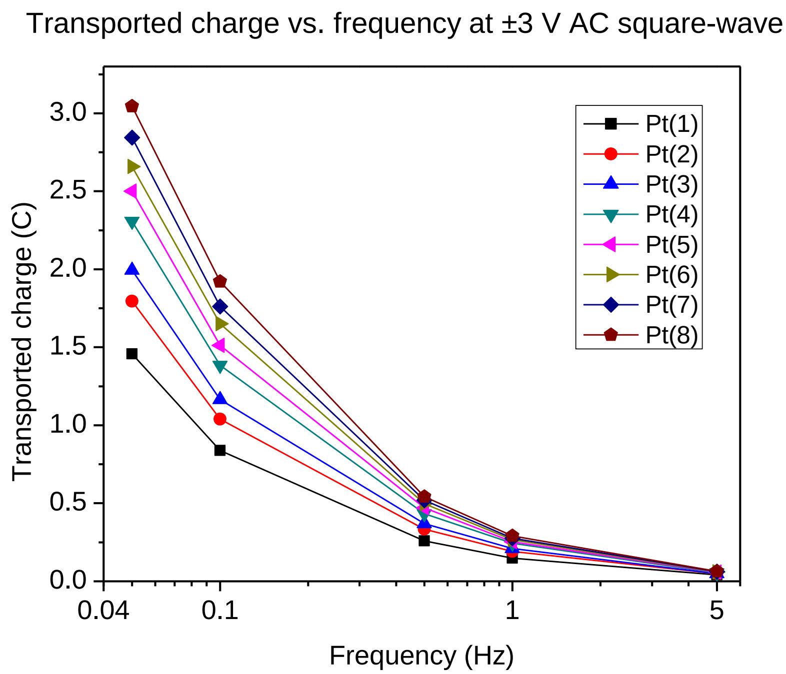

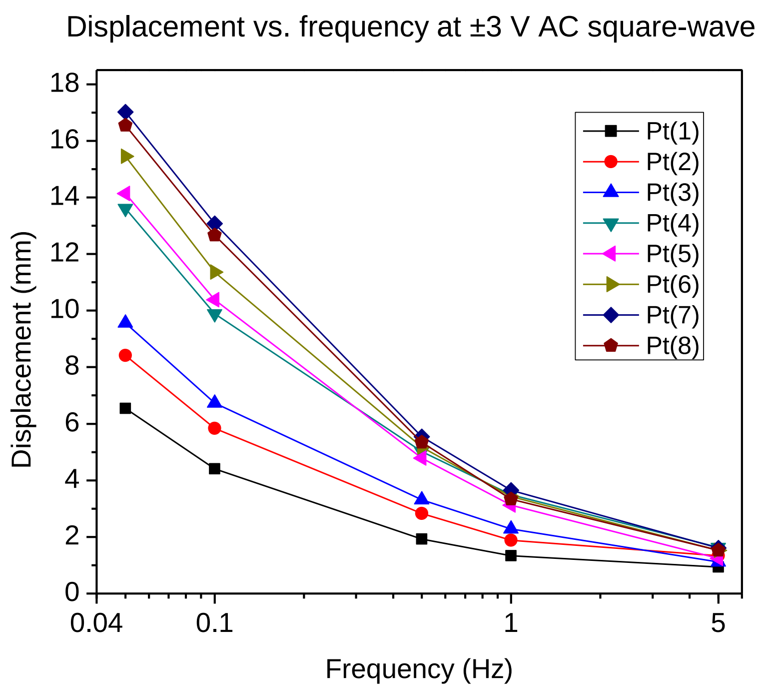

Figure 5.15: Frequency dependences of the total transported charge and corresponding displacement of Pt-IPMCs at ±3 V AC square-wave input between 0.05–5 Hz.

The actuation performances of the Pt-IPMCs with different electrode surface morphologies were also evaluated in terms of the ratio of peak bending strain to total transported charge. A higher bending strain to charge ratio indicates more effective transduction process of IPMC. The displacement was converted to bending strain according to Eq. (4.2).

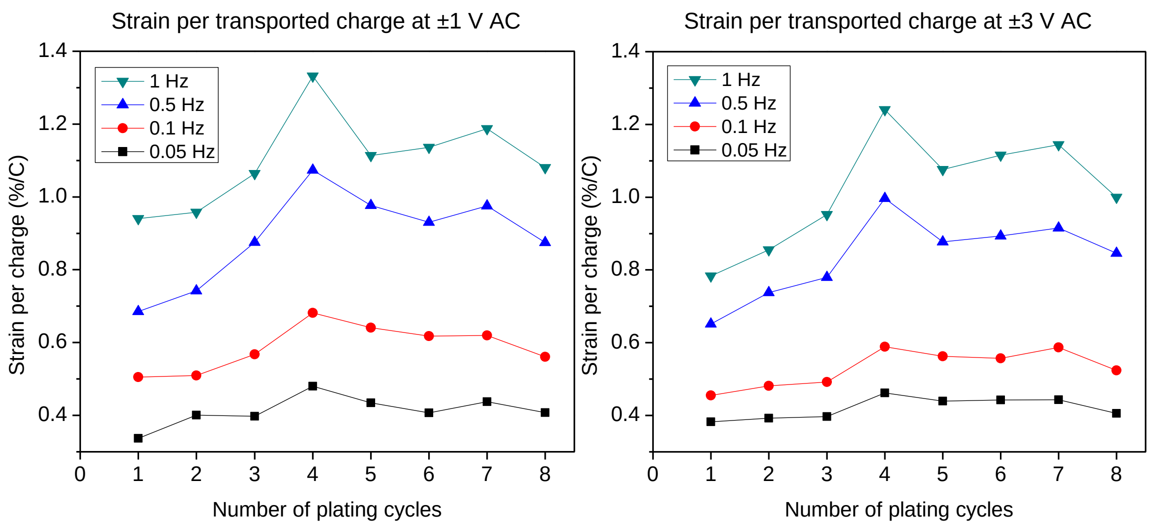

Figure 5.16: Peak bending strain per transported charge versus plating cycles for Pt-IPMCs at ±1 V and ±3 V AC square-wave input.

Figure 5.16 presents the ratio of peak bending strain to transported charge versus the number of primary platings at ±1 V AC and ±3 V AC square-wave at different frequencies. As can be seen, the strain to charge ratio increases with the increment of plating cycles, and reaches the maximum at the 4th plating (Pt(4)). Further increment of the plating cycles leads to a slight decrease in the strain to charge ratio. The slight decrease can be due the increasing flexural stiffness of the samples that IPMC has to overcome during the actuation. The increase in the strain to charge ratio is more noticeable at higher actuation frequencies.

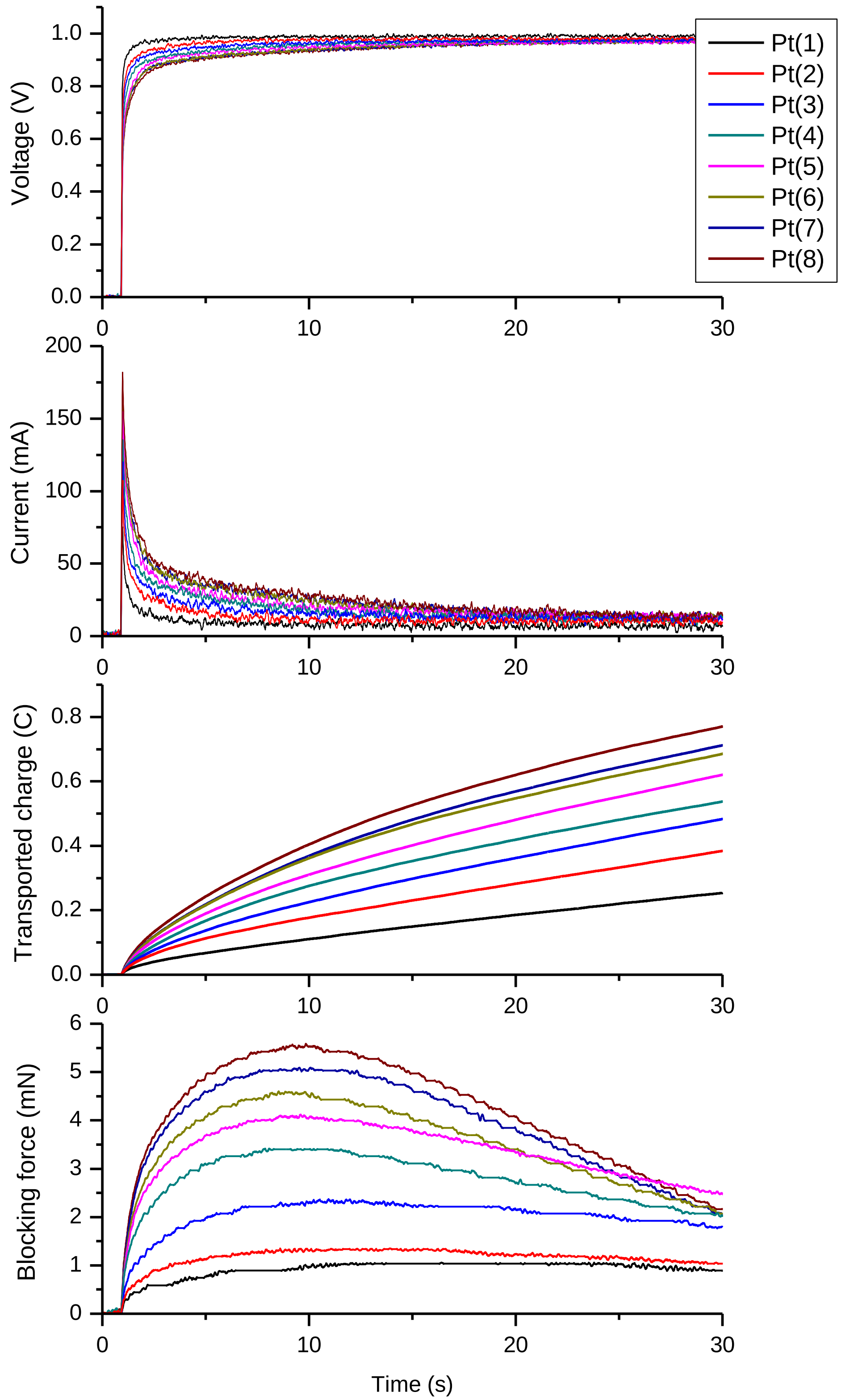

Figure 5.17: Voltage, current, transported charge and blocking force responses of IPMCs with different Pt electrode surface structures measured at 1 V DC input.

5.2.2 Blocking force performance

The blocking force performance of the Pt-IPMCs with different electrode surface morphologies was examined under 1, 2 and 3 V DC inputs. Figure 5.17 shows the measured voltage, current, transported charge and corresponding blocking force response in time for different Pt-IPMC samples at 1 V DC input. The data shows that increasing the impregnation-reduction cycles leads to a significant increase in the total transported charge and resulting blocking force performance of IPMC. These results are in accordance with the capacitance and displacement measurements discussed the previous sections. Also, it can be noticed that unlike in case of actuation measurements, the increments in the blocking force are more steady and apparent, especially in case of the samples Pt(4)…Pt(8) that showed rather minor differences in the displacement performance at 1 V (Figure 5.10). This is due to the fact the blocking force is measured at zero displacement (the IPMC beam against the fixed load cell) and therefore the result is less affected by the increasing flexural modulus (and the stiffness) of the IPMC samples (Figure 5.5).

Figure 5.18 presents the peak blocking force of the Pt-IPMCs as a function of the number of primary plating cycles at different input voltages, 1, 2 and 3 V DC. As can be observed, there is a significant increase in the blocking force output with the number of primary plating cycles, especially at the higher input voltages (2–3 V). However, the most dramatic increase in the measured force response occurs from the 2nd to 5th plating cycle. The overall improvement in the blocking force performance is more than 5 times in case of 1 V DC and more than 3 times in case of 3 V DC input.

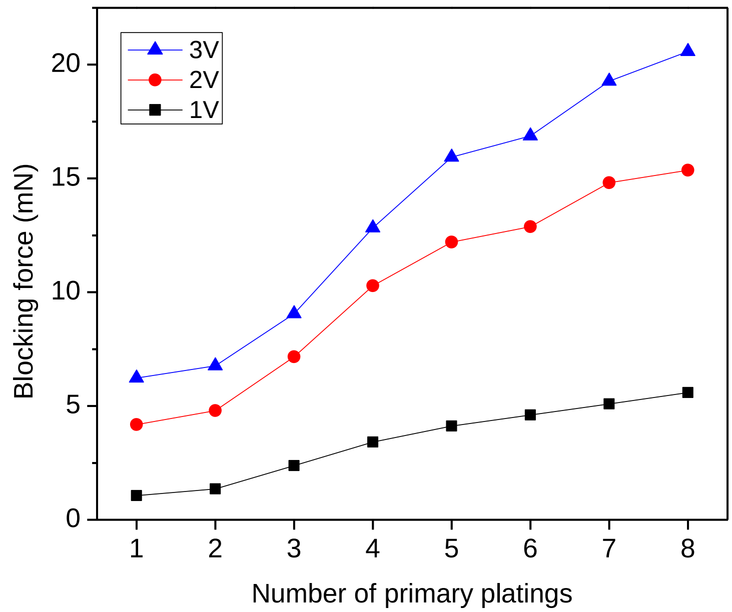

Figure 5.18: The peak blocking force versus the number of primary plating cycles of Pt-IPMCs measured at 1, 2 and 3 V DC input.

The blocking force performance of different Pt-IPMC samples was also evaluated in terms of the ratio of peak blocking force to the total transported charge (Figure 5.19). As can be seen, the ratio of blocking force to the transported charge increases significantly with the number of plating cycles. Unlike in case of the bending strain per charge plots (Figure 5.16), the increase is very steep and reaches maximum with 6–7 plating cycles. This further confirms the fact that the bending strain of IPMC is strongly affected by the flexural modulus, while the corresponding effect on the blocking force is less noticeable, since no displacement is involved. At 1 V DC the samples Pt(3)…Pt(6) exhibit somewhat higher force to charge ratio compared to the measurements at 2 and 3 V DC, which can be attributed to purely capacitive (non-faradaic) charging current at the lower voltage. The overall improvement in the blocking force to transported charge ratio is more than

2.5 times. Also, it is interesting to note that increasing the input voltage from 1 to 3 V does not affect much the force to charge ratio, i.e. the plots at different volts are fairly close. Thus, the conversion rate of electrical charge to force is roughly a constant and independent of input voltage in case of blocking force. This can be related to the fact that measurement is performed at zero displacement and therefore is not affected by the flexural stiffness of the material.

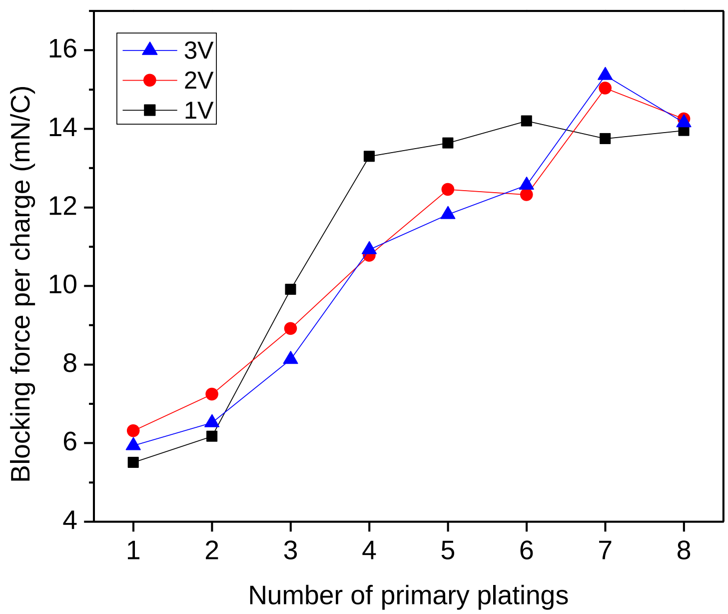

Figure 5.19: Peak blocking force to total transported charge ratio versus the number of plating cycles of Pt-IPMCs at 1, 2 and 3 V DC input.

5.3 Mechanoelectrical transduction

The mechanoelectrical transduction measurements were conducted at different actuation frequencies (1– 10 Hz) using a sinusoidal displacement with an amplitude of 10 mm. Higher frequencies were not considered due to the increasing drag in the water that causes buckling of the sample and distortions in the output signal. Also, it was observed that the electromechanical shaker is not able to maintain the constant displacement with rather high amplitude (10 mm) at the higher frequencies. Figure 5.20 shows the induced voltage in response to imposed 1, 5 and 10 Hz actuations for Pt-IPMCs with different electrode surface morphologies. As can be seen, the differences in the generated voltage in case of different IPMC samples are relatively minor and hardly distinguishable at 1 Hz actuation. The measurements at 5 and 10 Hz actuation show overall increase in the voltage amplitude and higher output voltage in case of IPMCs with higher number of primary platings. Also, it can be noticed that the induced voltage peaks are ahead of the imposed displacement peak. The delay between the displacement and voltage response decreases somewhat with the increase of actuation frequency. Interestingly, this delay is not affected by the surface morphology of electrodes, i.e. the voltage peaks in case of different samples are well aligned. These observations are consistent with the earlier study by Pugal [14]. According to the FEM simulations the induced voltage is mainly governed by a local change in the anion concentration, which is dependent on the local volumetric strain and is expressed as

$$C_a = C_0(1-dV)\,, \tag{5.6}$$

where C_0 is the initial anion concentration and dV is the volumetric strain. The effect of ionic current is very low in case of mechanoelectrical transduction. The observed shift between the actuation and voltage response can be related to the anion concentration. The simulations suggest that increasing the volumetric strain decreases the delay between the actuation and voltage signal, and increases the voltage amplitude.

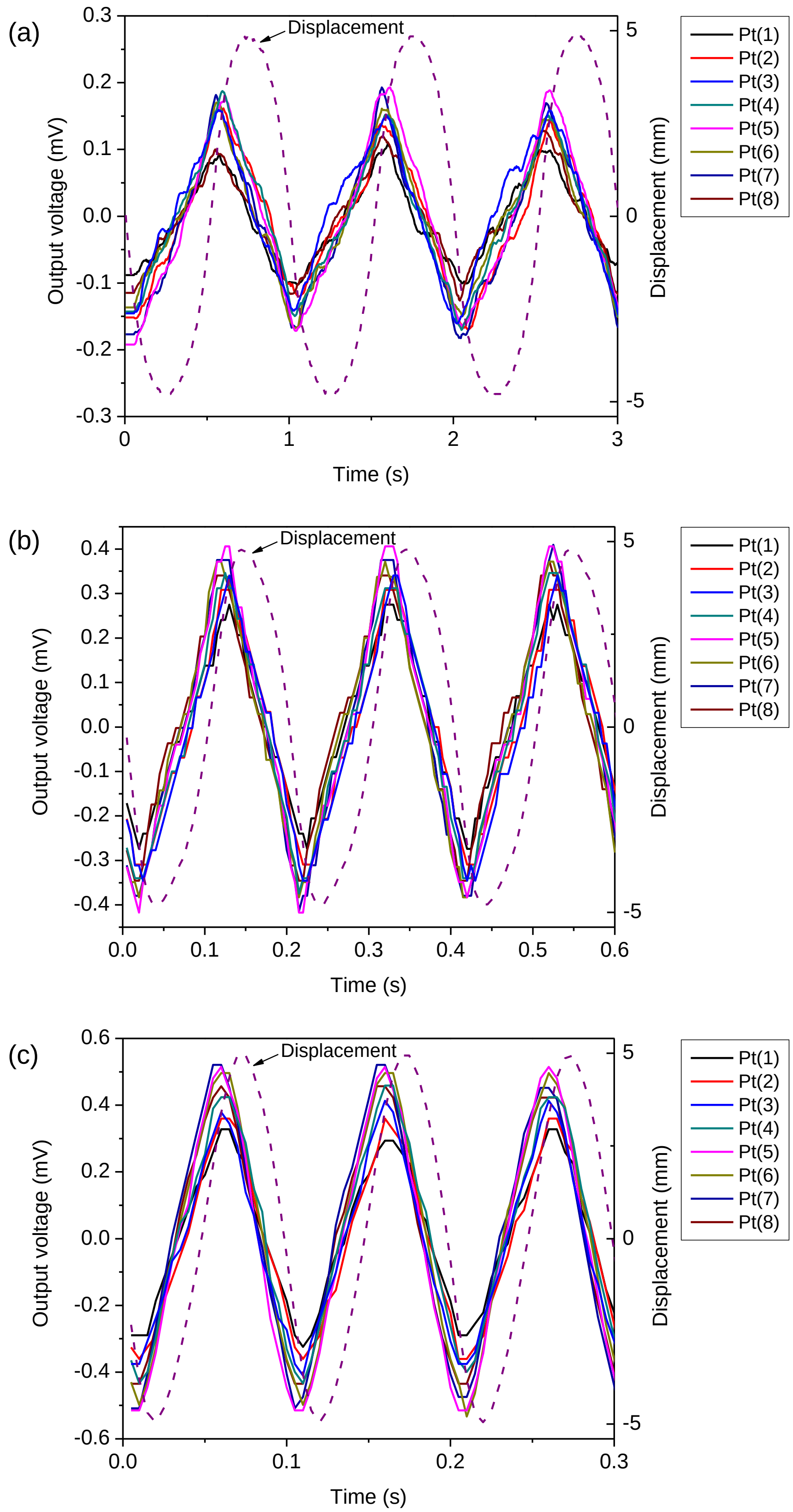

Figure 5.20: Induced voltage of Pt-IPMCs at 1 Hz (a), 5 Hz (b) and 10 Hz (c) actuation.

The differences in the transduction performance in case of different electrode surface morphologies can be observed more explicitly in Figure 5.21 that shows the induced voltage amplitude of the IPMCs versus the number of primary plating cycles at 1, 5 and 10 Hz actuation. The peak-to-peak voltage amplitude was calculated by taking an average over a minimum of 20 actuation cycles. It can be seen that the voltage amplitude increases slightly with the number of plating cycles and reaches the maximum at 5th plating (sample Pt(5)). The voltage amplitude decreases with further increment of the platings cycles (samples Pt(6)…Pt(8)). This trend is more pronounced at higher actuation frequencies. A slight decrease in the voltage amplitude can be related to the increasing flexural modulus of the samples (Figure 5.5). IPMCs with more flexible structure can bend more locally near the clamp contacts while in case of the stiffer samples the imposed deformation can be dissipated along the beam length, thus resulting less local volumetric strain near the clamp area.

Overall, compared to electromechanical transduction data discussed in the previous section, the effect of electrode surface structure on the induced voltage is relatively low. These results are in good agreement with the finite element simulation data presented in Section 3.2 and ref. [14]. As mentioned, there are two reasons for a rather low electrode surface geometry effect. Firstly, the induced voltage is a local phenomenon and mainly affected by the electrode surface structure in the vicinity of clamp contacts. Secondly, the induced voltage is mainly determined by the local volumetric strain induced changes in the anion concentration, although the magnitude of the effect is very low (in the range of millivolt). Therefore, the surface charging is very low and the electrode surface structure has relatively minor effect in the mechanoelectrical transduction process.

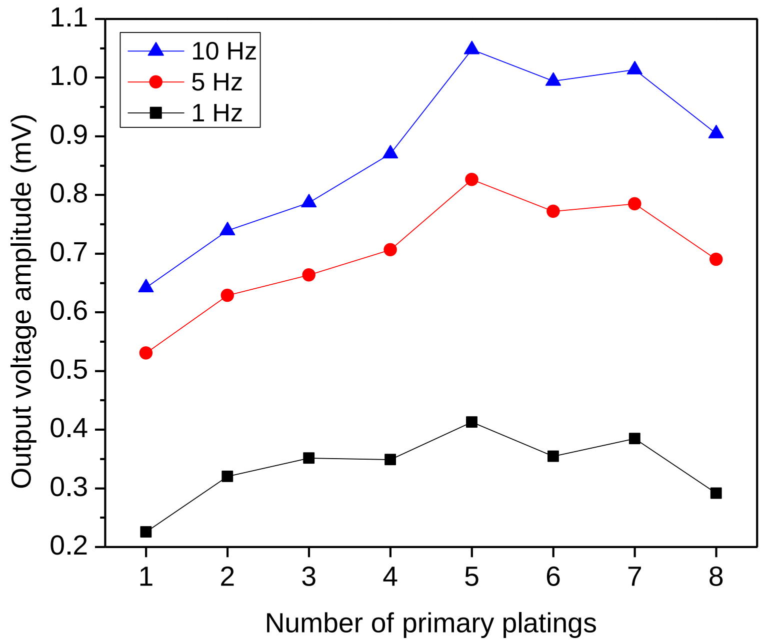

Figure 5.21: Induced voltage amplitude of Pt-IPMCs vs. the number of primary plating cycles at 1, 5 and 10 Hz imposed actuation.

5.4 Concluding remarks

IPMCs with different Pt electrode surface morphologies were synthesized by varying the impregnation-reduction cycles in the electroless plating process. It was shown that increasing the number of plating cycles under appropriate conditions results in the formation and growth of platinum nanoparticles with sharp tips and edges – called Pt nanothorn assemblies. The formation of such nanostructures at the electrode interface increased significantly the double-layer capacitance of IPMC, indicating an enlarged interfacial surface area of the electrodes. Electromechanical transduction measurements showed that increasing the plating cycles and thereby promoting the development of Pt nanothorn assemblies increases notably the total transported charge and the resulting displacement of IPMC. The displacement range improved more than 3 times (at 0.1 Hz, ±3 V AC) with increasing the plating cycles from 1 to 7. The improvement in the blocking force performance was more than 3 times at 3 V DC and more than 5 times at 1 V DC input. These observations are in good agreement with the recently reported finite element simulations (see Chapter 3). Mechanoelectrical transduction measurements at different actuation frequencies showed higher induced voltage amplitude in case of nanostructured electrodes. However, compared to the electromechanical transduction, the overall effect of the electrode surface morphology on the induced voltage is relatively low. This is consistent with the earlier theoretical prediction and can be attributed to a localized transduction phenomenon in case of induced voltage which is mainly governed by a local volumetric strain in the polymer [14]. Thus, the effect of electrode surface charging is rather low. Overall, the experiments demonstrate that the designed synthesis conditions of electroless plating produce nanostructured Pt electrodes in controllable manner and can be effectively used for tailoring the transduction performance of IPMC. The designed IPMC electrodes with the Pt nanothorn assemblies are first to be reported.

Chapter 6

Characterization of IPMCs with Pd-Pt electrodes

This chapter discusses the effects of electrode surface morphology in the transduction of Pd-Pt electrodes-based IPMCs. The amount of porous palladium at the inner surface of the polymer membrane was varied by controlling the impregnation time in Pd complex solution during electroless plating process. Four sets of IPMCs were prepared by varying the impregnation time from 60 to 150 min with 30 min increments in 3.8 mM Pd complex. The Pt top layer at the outer surface of the membrane was applied by four chemical deposition cycles (secondary platings). The notation of the prepared IPMC samples and deposited layers are listed in Table 6.1. The chapter discusses the measured electromechanical, mechanoelectrical, electrochemical and mechanical properties of the Pd-Pt IPMCs with different electrode surface structures.

Table 6.1: Pd-Pt IPMCs prepared by varying the impregnation time in Pd complex.

Notation	Impregnation time in Pd complex (min)	Pd content (wt.%)	No. of secondary platings of Pt	Electrode surface resistance (Ω/cm)
Pd(60)	60	0.4	4	1.9 ±0.2
Pd(90)	90	1.1	4	1.7 ±0.2
Pt(120)	120	2.5	4	2.1 ±0.3
Pt(150)	150	7.1	4	1.8 ±0.2

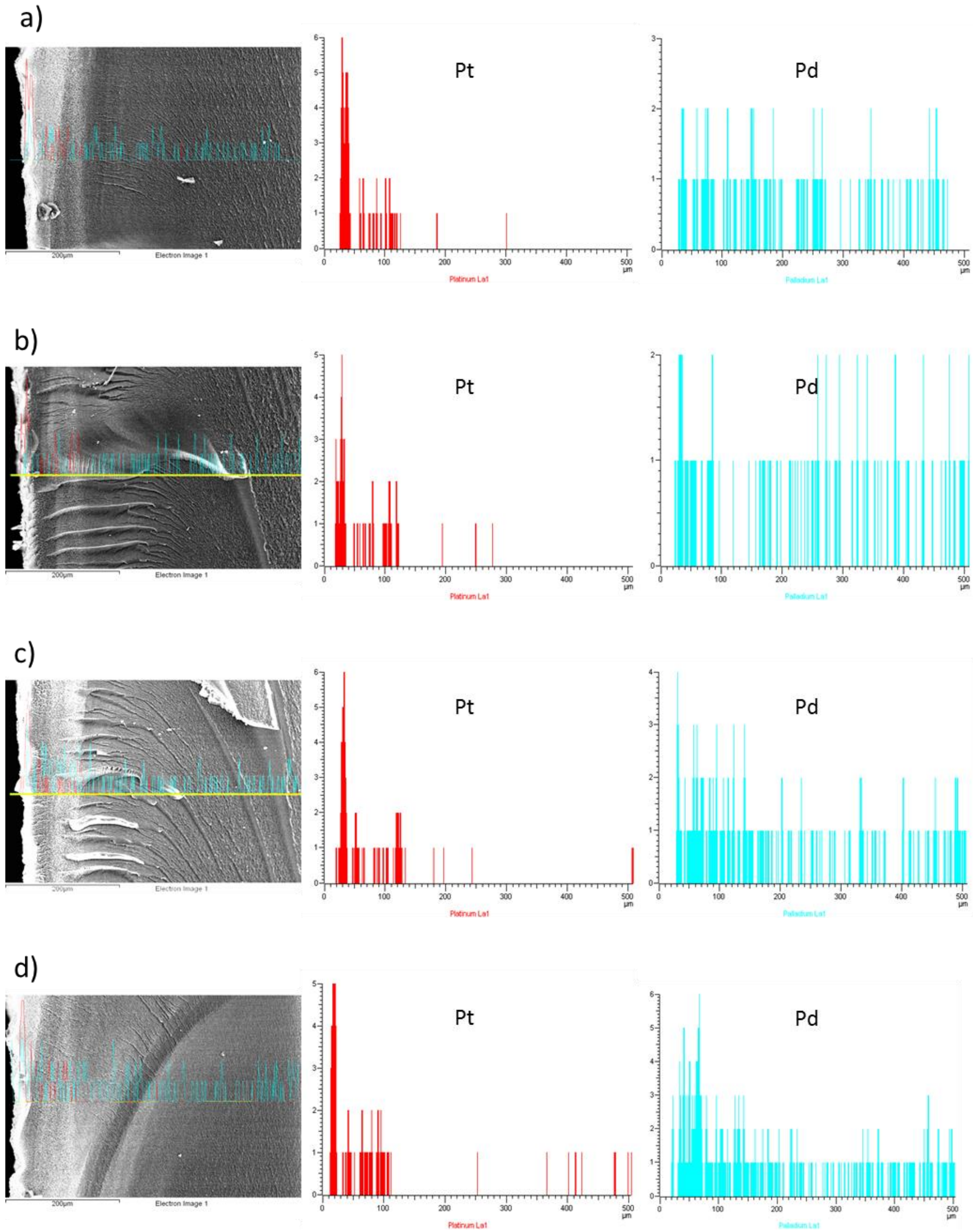

Figure 6.1: SEM cross-sectional micrographs and corresponding EDS line-scan analysis of elements Pt and Pd for different Pd-Pt IPMC samples: a) Pd(60), b) Pd(90), c) Pd(120), and d) Pd(150).

6.1 Electrode surface morphology

Figure 6.1 shows SEM micrographs and corresponding EDS line-scans for Pt and Pd element distribution along the cross-section of different IPMC samples. It can be seen that platinum is concentrated at the membrane surface with rather similar distribution profile in case of different samples (Figure 6.1 a–d), while palladium is penetrated rather deep in the polymer matrix and the distribution varies among the samples. The samples Pd(60) and Pd(90) (Figure 6.1 a, b) show the lowest intensity for Pd, whereas the Pd(150) (Figure 6.1 d) shows the highest intensity and the widest distribution of Pd in the 150-µm range from membrane surface. Thus, the data indicates that longer impregnation period in Pd complex solution results in a higher content of palladium particles in the vicinity of membrane surface, thereby increasing the interfacial surface area of electrodes.

Figure 6.2 presents the SEM cross-sectional micrographs for Pd(60) and Pd(150) samples with more details. Unlike in case of Pt-IPMCs, the Pd-Pt samples do not have distinct polymer-metal electrode interface; the Pd particles are dispersed deep in the polymer matrix with increasing gradient towards the membrane surface (called diffusion layer). A wide dispersion of Pd particles makes SEM analysis of the samples difficult. However, the following differences in case of two rather different samples – Pd(60) and Pd(150) can be observed in Figure 6.2. While both IPMCs have very similar thin and uniform compact Pt metal layer at the surface, the Pd diffusion layer in case of Pd(60) is fairly thin compared to Pd(150). The Pd(150) sample shows overall more dense distribution of Pd particles in the polymer matrix and the particles are dispersed tens of micrometers deep in the polymer with higher concentration near the membrane surface.

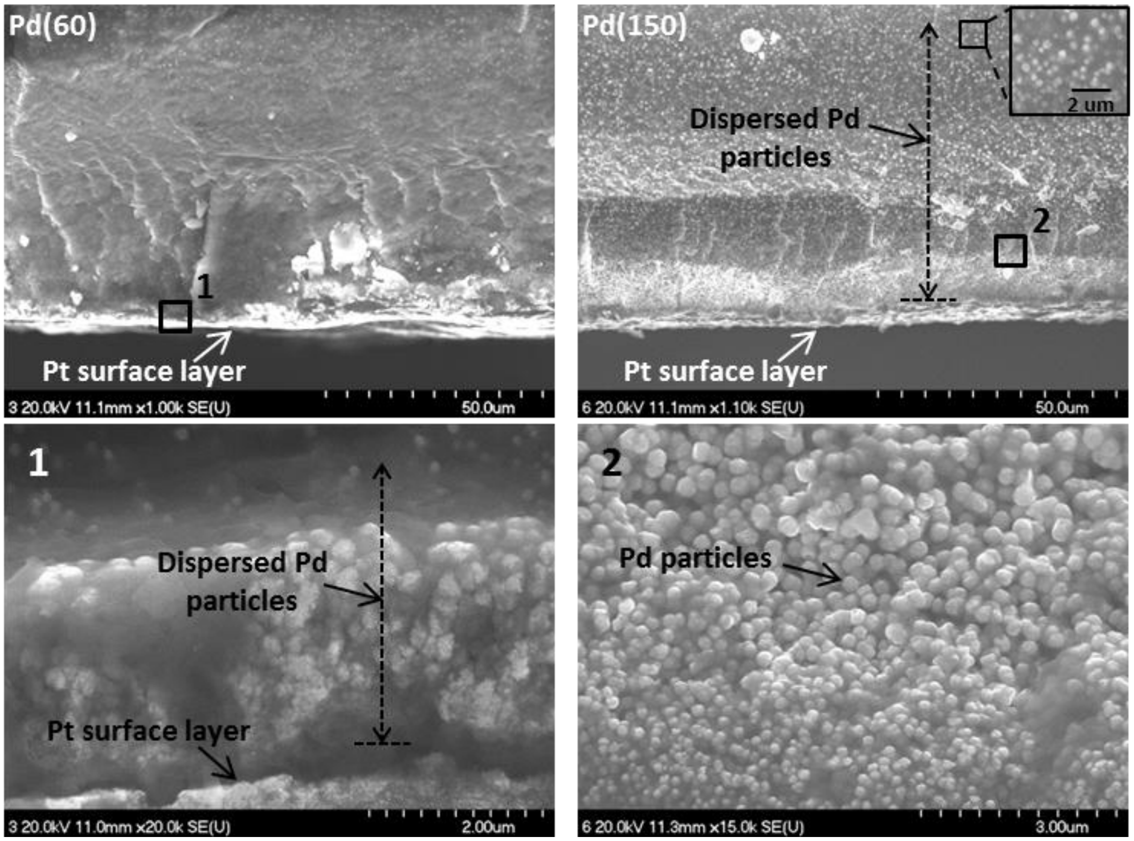

Figure 6.2: SEM cross-sectional images of Pd(60) and Pd(150) IPMC samples.

Using hydrogen containing reducing agents, such as sodium borohydride ($NaBH_4$) used in this work, raises the possibility of formation of palladium hydride during the reduction of Pd complex. Palladium can adsorb the hydrogen and form Pd hydrides even at low hydrogen pressures and temperatures [106, 107]. Therefore, X-ray diffraction (XRD) analysis was performed on the membrane surface to determine the composition of deposited Pd layer. Figure 6.3 presents the XRD pattern obtained from the membrane surface after impregnation-reduction step of palladium, prior to the deposition of Pt top layer. The XRD pattern shows the elemental form of palladium with face-centered cubic structure in the polymer surface. Thus, no palladium hydride was found. The intensities of the peaks are rather low due to the presence of ionic polymer and low relative amount

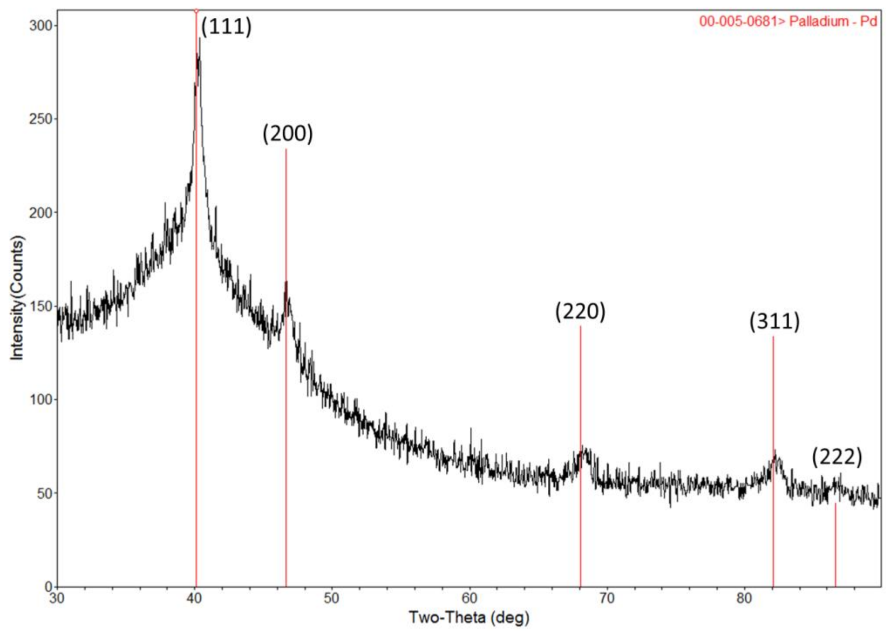

Figure 6.3: XRD pattern obtained from the membrane surface before deposition of Pt top layer, showing elemental form of Pd in the polymer surface.

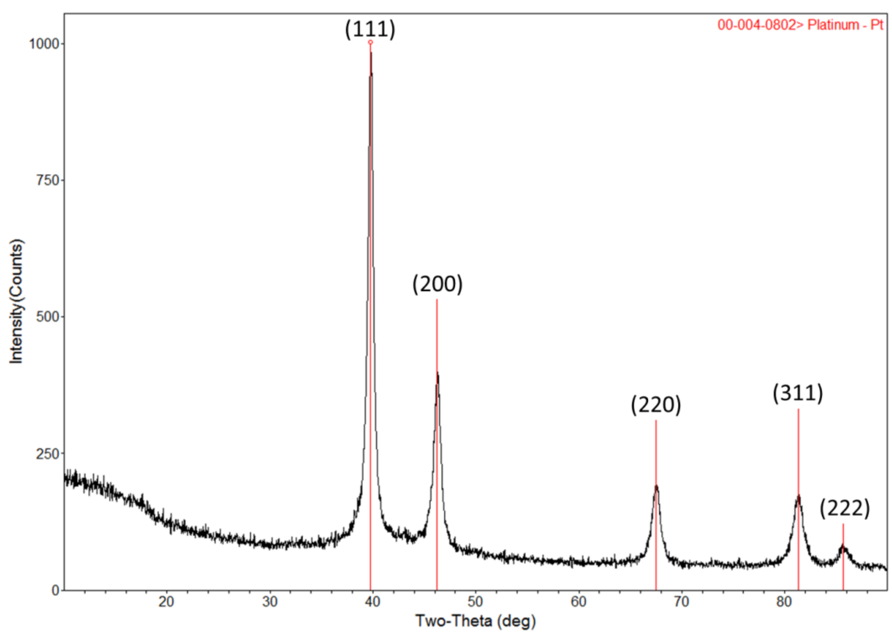

Figure 6.4: XRD pattern obtained from the membrane surface after deposition of Pt top layer on the Pd surface. Only Pt is present at top surface.

of Pd in the polymer matrix. Figure 6.4 shows the XRD pattern obtained after deposition of Pt layer on top of the Pd surface. As can be seen, only platinum is on the top surface, no Pd is present. The peak intensities area noticeably higher compared to Pd pattern, since the composite surface is purely metallic with no presence of ionic polymer.

6.1.1 Flexural modulus

Figure 6.5 shows the stress-strain diagrams of Pd-Pt IPMCs with different electrodes and corresponding values of flexural moduli measured at a strain rate of 0.1 mm/mm/min in 3-point bending mode. The flexural stress and strain for an IPMC in the three-point bending configuration were calculated as described in Section 5.1.1. It can be seen that extending the impregnation time and thereby increasing the content of palladium in the membrane surface increases the flexural modulus of IPMC. The Pd-Pt IPMC samples

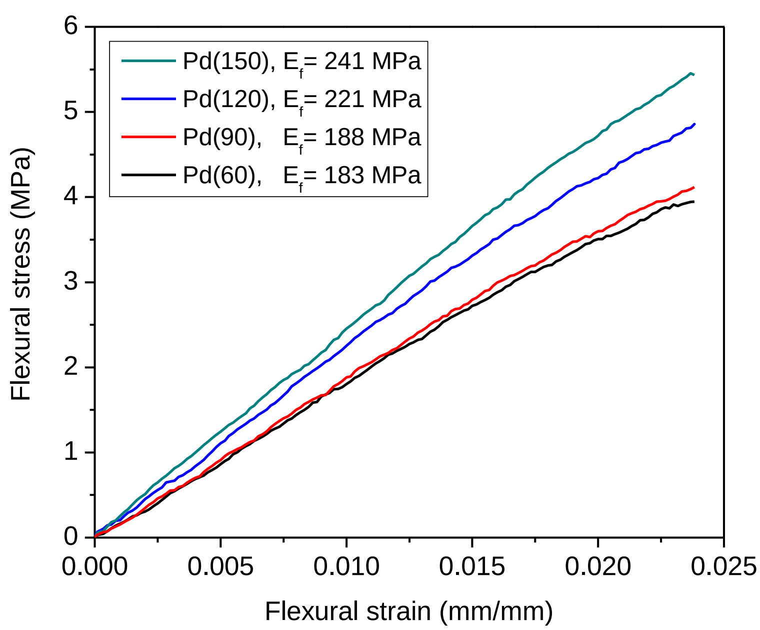

Figure 6.5: Flexural stress-strain diagrams for Pd-Pt IPMCs with different electrode structures and respective flexural modulus values, measured in 3-point bending mode.

exhibit overall higher flexural modulus compared to the Pt IPMCs (Figure 5.5). The main portion of the flexural stiffness is probably due to four secondary platings of platinum deposited on the top surface of the composite.

6.1.2 Interfacial capacitance

The double-layer capacitance of Pd-Pt IPMCs as a function of frequency was determined from EIS measurements between 0.1–100 Hz with an AC perturbation of 10 mV and DC bias of 0.1 V (Figure 6.6). The measurements show that extending the impregnation time in Pd complex solution leads to a notable increase in the capacitance of IPMC at the lower frequencies, indicating an enlarged surface area of the electrodes that provides more access to the charges for the double-layer formation. This data is consistent with the SEM-EDS results discussed in the previous section (Figure 6.1) that showed higher content of palladium in the electrodes prepared with longer impregnation period. Compared to the EIS data of Pt-IPMCs (Figure 5.6), the Pd-Pt IPMCs exhibit higher capacitance at the lower frequencies (f < 1 Hz), which is in accordance with our earlier studies and can be attributed to highly dispersed porous Pd particles in the polymer matrix [16]. The capacitance at the higher frequencies (f > 10 Hz) is rather low, indicating a diffusion limiting effect of the porous Pd inner surface layer. Interestingly, the Pd(90) sample shows only slightly higher capacitance compared to Pd(60), while the differences in the capacitance in case of other samples are very drastic. It can be noticed that also the EDS elemental distributions of Pd are very similar in case of Pd(60) and Pd(90) samples (Figure 6.1 a, b). Therefore, rather minor changes in the capacitance for these samples can be expected.

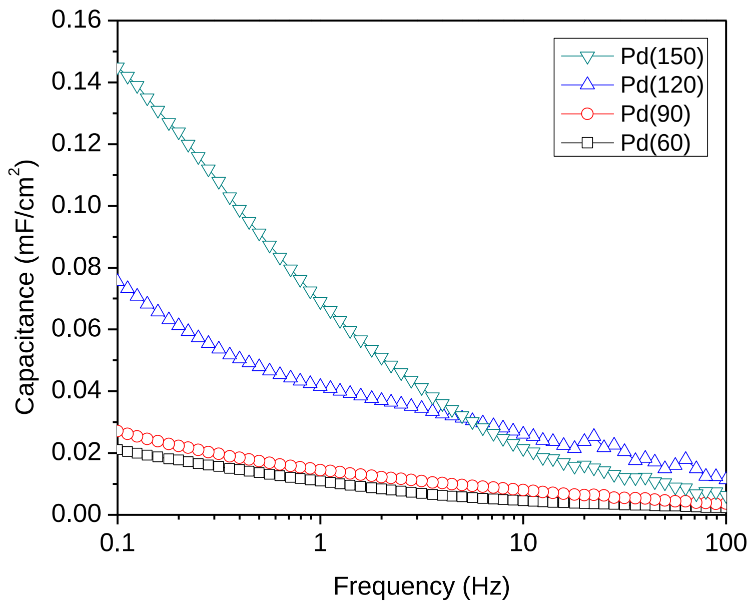

Figure 6.6: Frequency dependence of differential capacitance for Pd-Pt IPMCs with different electrode structures from EIS measurements at DC bias of 0.1 V.

The charging-discharging capacitance of Pd-Pt IPMCs with different electrodes was measured using cyclic voltammetry in a potential range of -0.5 to 0.5 V at a scan rate of 50 mV/s (Figure 6.7). The measured cyclic voltammograms indicate capacitive current behavior, no faradaic peaks are present. As can be seen, the current densities are considerably higher in case of IPMC samples prepared with longer impregnation period. The charging-discharging capacitance values determined from CV curves according to Eq. (4.4) are 0.04 mF/cm^2, 0.06 mF/cm^2, 0.12 mF/cm^2 and 0.22 mF/cm^2 for the samples Pd(60), Pd(90), Pd(120) and Pd(150), respectively. Figure 6.8 shows the capacitance values as a function of impregnation time in Pd complex solution. These results are consistent with the EIS data as well as with the SEM-EDS results discussed earlier. Thus, increasing the impregnation time in Pd complex solution during the electroless plating process has a significant effect on increasing the charge accumulation in the vicinity of electrodes. Also, it can be noticed that the CV current densities and capacitance values are overall somewhat higher compared to Pt-IPMCs (Figure 5.8 and 5.9).

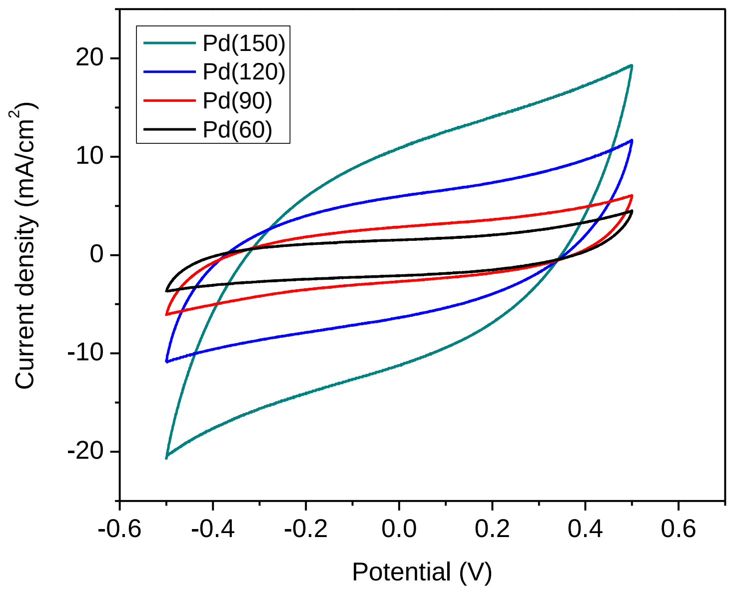

Figure 6.7: Cyclic voltammograms of Pd-Pt IPMC samples with different electrode structures measured at a potential scan rate of 50 mV/s.

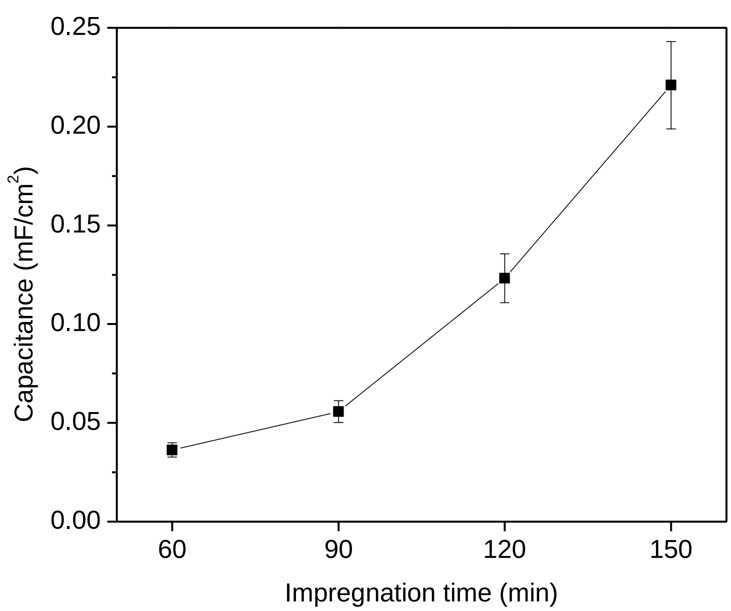

Figure 6.8: Charging-discharging capacitance of Pd-Pt IPMC samples versus the impregnation time used in the electroless plating process of palladium.

6.2 Electromechanical transduction

The electromechanical properties – the blocking force and displacement of Pd-Pt IPMCs with different electrodes were examined under 1–3 V DC and ±1–3 V AC square-wave (0.05–5 Hz) driving signals. Lower input voltages (1 V) were used in order to avoid electrochemical current (i.e. electrolysis), to allow more exact comparison of the results in terms of the transported charge monitored during the transduction process.

6.2.1 Actuation performance

Figure 6.9 shows the measured voltage, current, transported charge and corresponding displacement responses in time for Pd-Pt IPMCs at ±1 V AC square-wave at a frequency of 0.1 Hz. It can be seen that varying the impregnation duration in Pd complex has a notable impact on the charge dynamics and resulting electromechanical performance of IPMC. The current as well as the transported charge and displacement are the lowest in case of Pd(60) sample and increase noticeably for the samples prepared with longer impregnation time in Pd complex solution. The displacement amplitude of the Pd(150) sample is more than three times that of the Pd(60). Thus, the results demonstrate that increasing the impregnation time (and thereby the interfacial area of electrodes) leads to a higher charge density at the electrodes that in turn results in a larger deformation of IPMC. This data is in accordance with the capacitance measurements as well as with the finite element simulation results presented in Chapter 3 and in ref. [14].

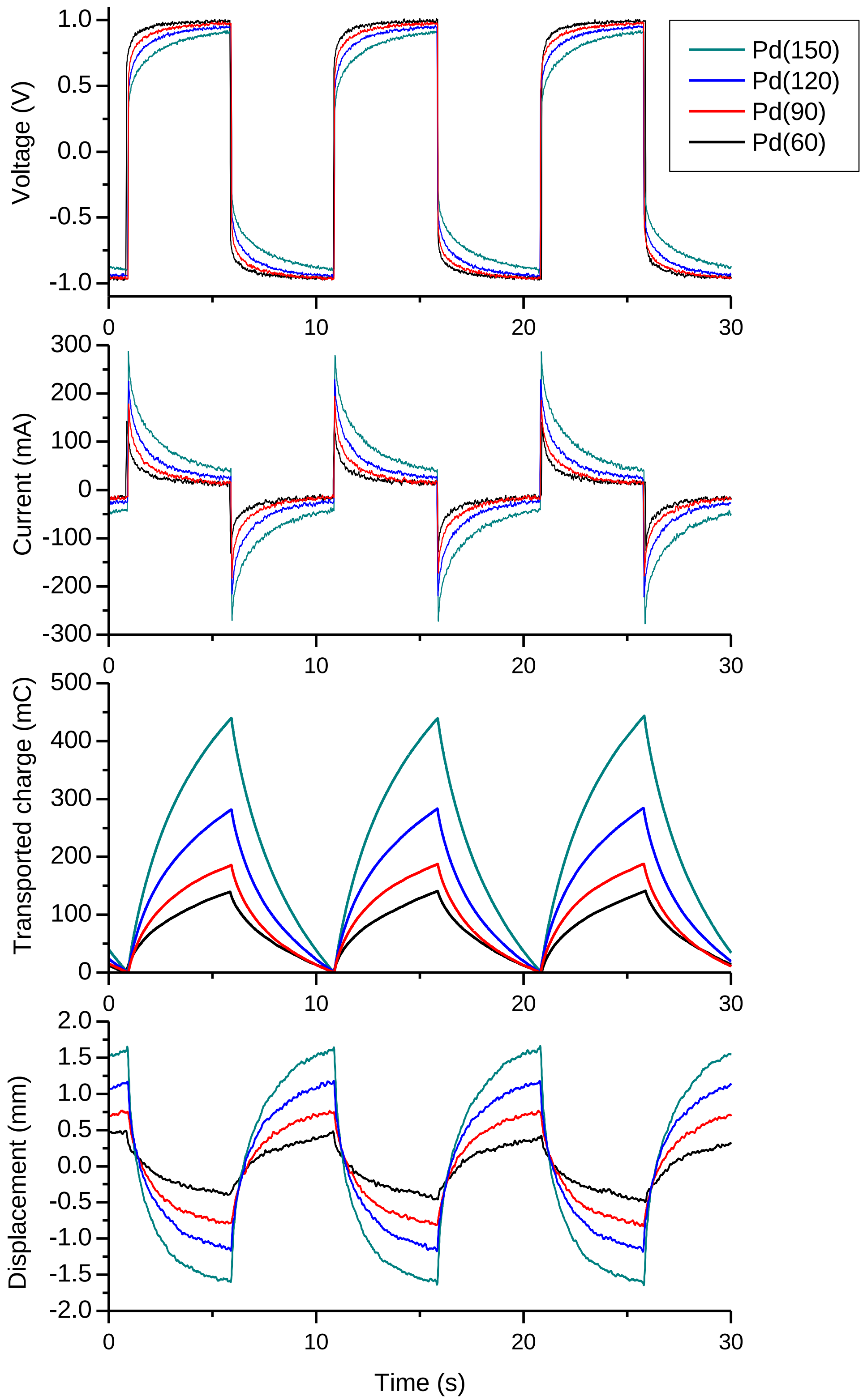

Figure 6.9: Measured voltage, current, transported charge and displacement responses at 0.1 Hz, ± 1 V square-wave for Pd-Pt IPMCs with different electrodes.

Figure 6.10 presents the measured transported charge and corresponding peak-to-peak displacement of Pd-Pt IPMCs as a function of actuation frequency from 0.05 Hz to 5Hz at ±1 AC square-wave input. As can be seen, the transported charge correlates well with the displacement response of the samples in the entire frequency range. Both the transported charge and the displacement are rather low at the higher frequencies (> 1 Hz) and increase noticeably as the frequency is lowered (< 1 Hz). This increase is much more pronounced in case of IPMCs prepared with longer impregnation time. Clearly, at higher actuation frequencies the charging time is too short and not sufficient to fully utilize the large interfacial area of electrodes, which explains relatively minor differences in the displacement amplitude in case of different samples. It can be noticed that the magnitude and shape of the frequency dependencies are rather similar to those of Pt-IPMCs discussed in the previous chapter (Figure 5.14). It is interesting to note that while our previous studies have shown Pd-Pt IPMCs over perform the Pt-IPMCs in the displacement range [16], the performances compared to the newly developed Pt-IPMCs with nanostructured electrodes are rather similar.

The same sets of measurements were also performed at ±3 V AC to examine the actuation performance of IPMCs at normal operating voltages (Figure 6.11). It can be seen that while the transported charge–displacement correlation still holds, noticeable changes in the displacement responses occurred. Unlike in case of ±1 V measurements, the displacement amplitudes of Pd(90), Pd(120) and Pd(150) samples are relatively close even at the lower frequencies. This can be related to higher flexural modulus of the samples prepared with longer impregnation time (Figure 6.5) that increases the flexural stiffness of the material and in turn can limit the actuation range of IPMC.

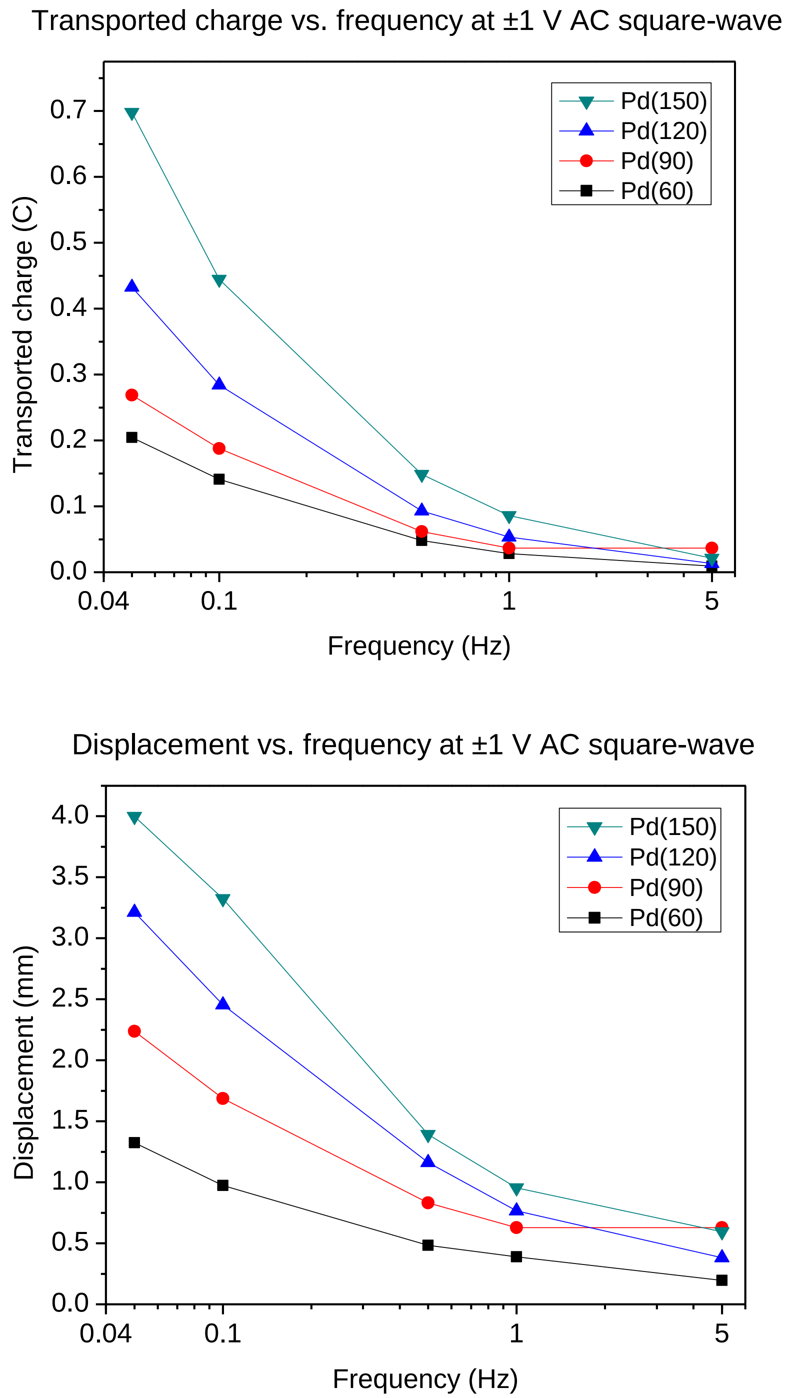

Figure 6.10: Frequency dependences of the total transported charge and corresponding displacement of Pd-Pt IPMCs at ±1 V AC square-wave input between 0.05–5 Hz.

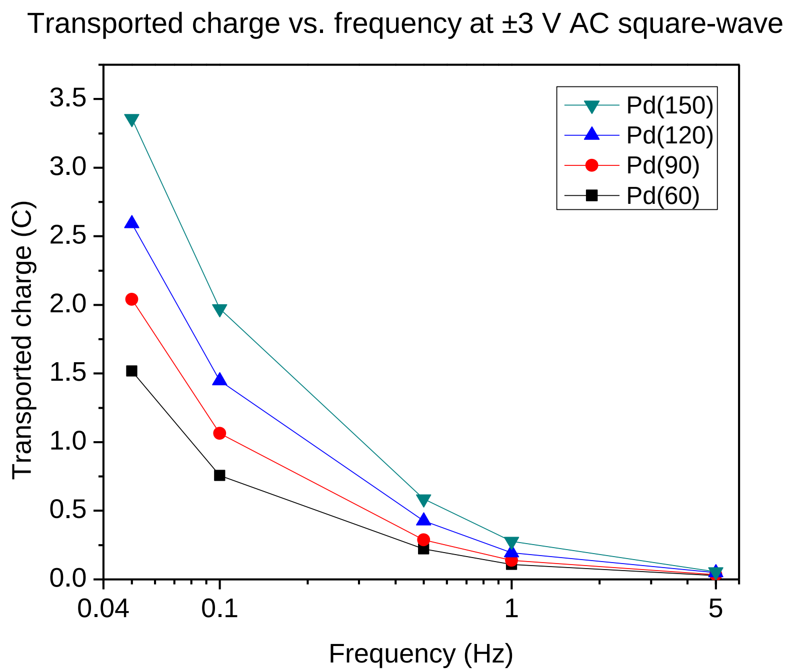

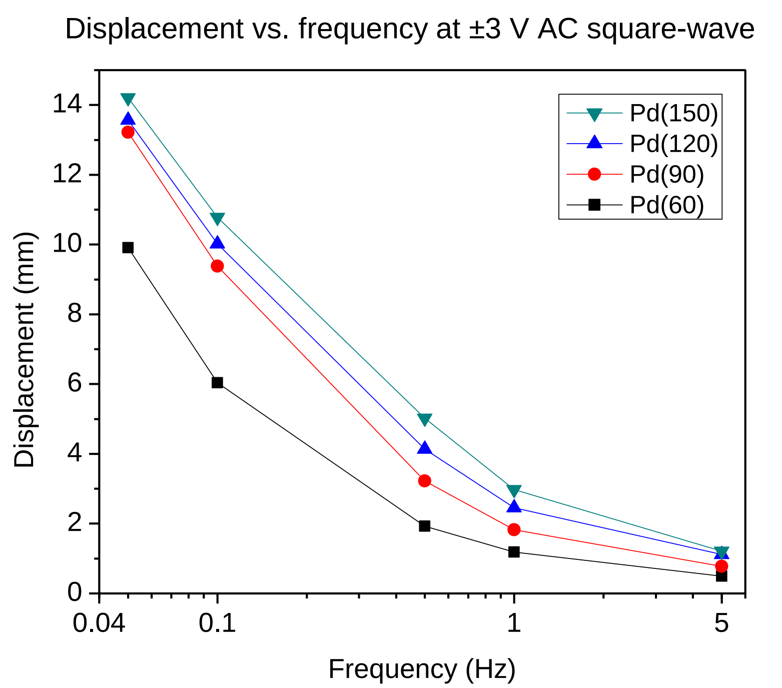

Figure 6.11: Frequency dependences of the total transported charge and corresponding displacement of Pd-Pt IPMCs at ±3 V AC square-wave input between 0.05–5 Hz.

Figure 6.12 shows the ratio of peak strain to total transported charge for Pd-Pt IPMCs as a function of impregnation time at ±1 V and ±3 V AC square-wave input at different actuation frequencies. The higher ratio indicates more efficient transduction process. The displacement was converted to bending strain according to Eq. (4.2).

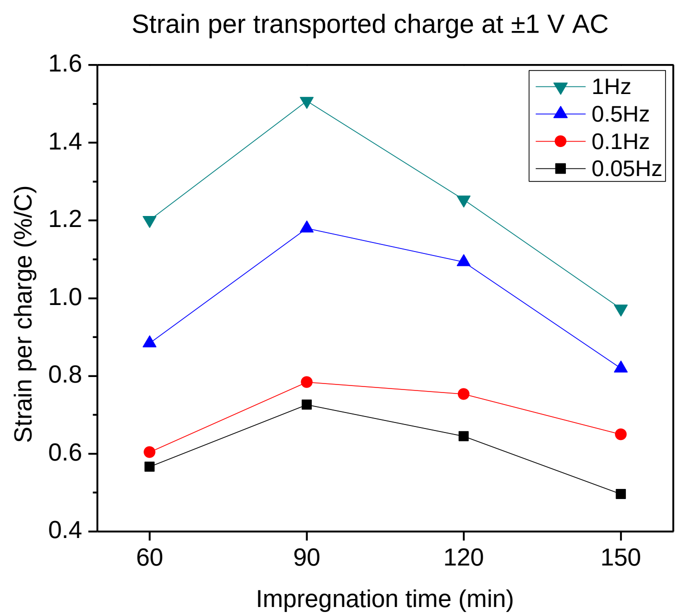

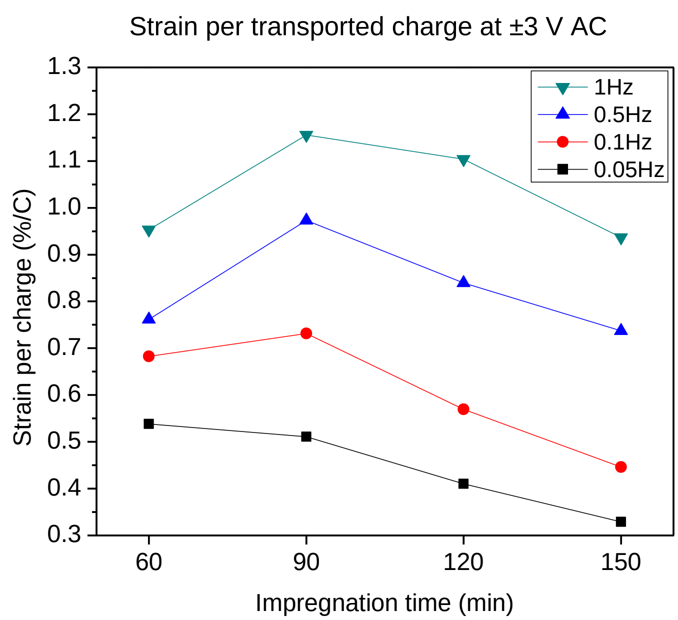

Figure 6.12: Peak strain per transported charge of Pd-Pt IPMCs versus impregnation time at ±1 V and ±3 V AC square-wave input at different frequencies.

It can be seen that increasing the impregnation duration from 60 min to 90 min increases slightly the peak strain to charge ratio. However, further increments in the impregnation time lead to a decrease in the strain to charge ratio. This can be related to the increasing flexural stiffness of the material that IPMC has to overcome during the actuation. The strain to charge ratio also increases with the actuation frequency, which can be expected since the displacement amplitude decreases with the frequency and therefore less energy is dissipated in the deformation of the material. It can be noticed that the strain to charge ratios are somewhat lower at ±3 V compared to the plots at ±1 V AC. This is obviously due to the presence of faradaic processes (i.e. electrolysis) that increase the measured current, but are not contributing to the actuation of IPMC.

6.2.2 Blocking force performance

Figure 6.13 presents the measured voltage, current, transported charge and corresponding blocking force responses in time for Pd-Pt IPMCs with different electrodes at 1 V DC input. As can be observed, the blocking force output of the IPMCs increases with increasing the impregnation time. The peak forces for the samples Pd(60), Pd(90), Pd(120) and Pd(150) are 2.8 mN, 3.8 mN, 6.2 mN and 8.6 mN, respectively. Thus, the maximum blocking force of Pd(150) in more than three times that of Pd(60). These results are in good correlation with the displacement measurements that also showed higher actuation performance for the samples prepared with longer impregnation period. It is interesting to note that the blocking force output of Pd-Pt IPMCs is noticeably higher compared to the Pt-IPMCs (Figure 5.17), while the displacement performances of the two types of samples are not that different. This can be related to the higher flexural moduli

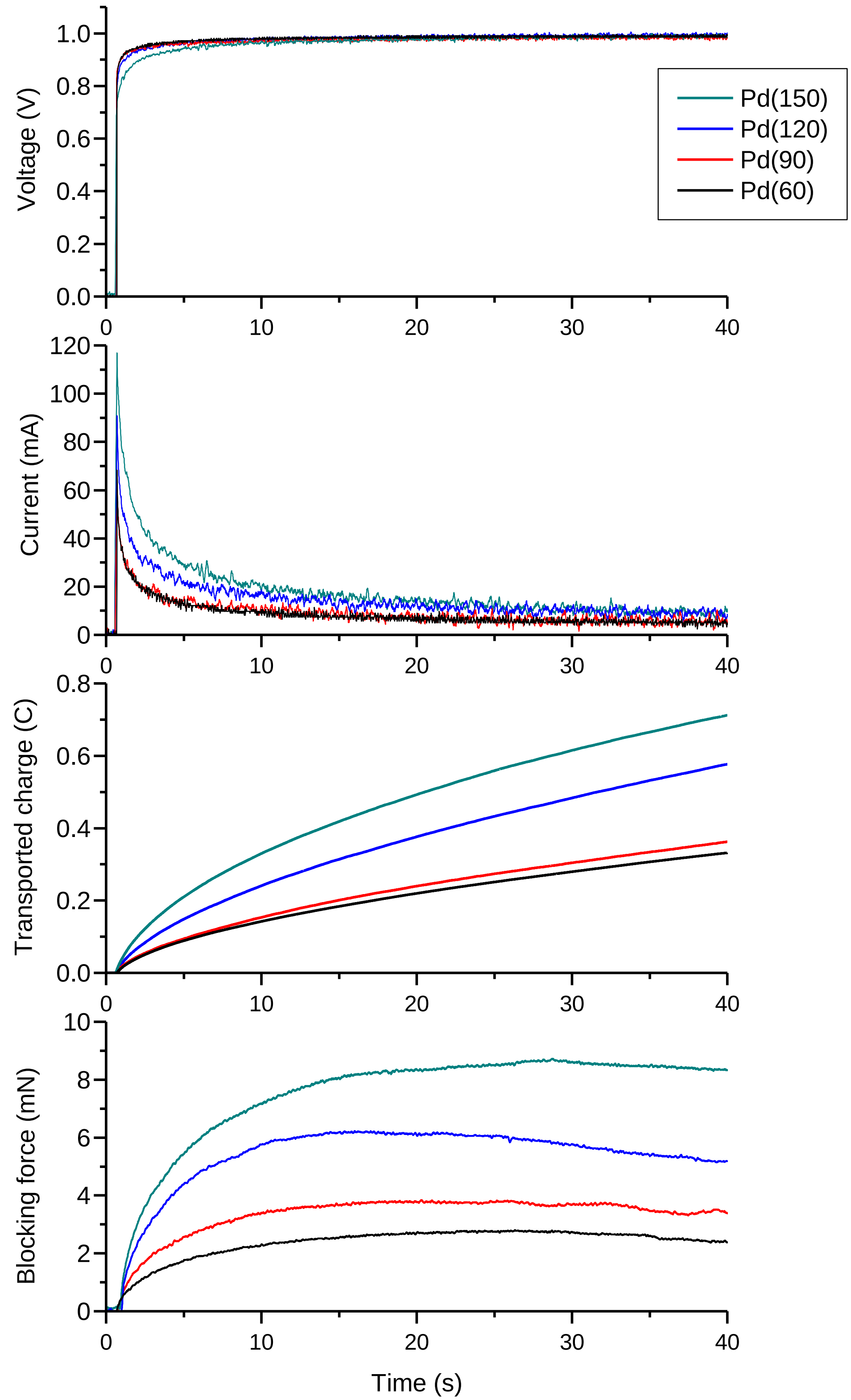

Figure 6.13: Voltage, current, transported charge and blocking force responses in time for Pd-Pt IPMCs with different electrodes measured at 1 V DC input.

of Pd-Pt IPMCs that may limit their maximum attainable deformation, but not as much the blocking force response, since no bending deformation is involved in case of these measurements.

The blocking force performance of the IPMCs was also evaluated at the higher operating voltages. Figure 6.14 shows the peak blocking forces of Pd-Pt IPMCs with different electrode surface structures as a function of impregnation time at 1, 2 and 3 V DC input. It can be seen that the peak force increases considerably with the impregnation time. This increase is more pronounced in case of higher input voltages (2–3 V). The increment in the peak force is most drastic from 90 min to 120 min impregnation time. Figure 6.15 presents the peak blocking force to the total transported charge ratio as a function of impregnation duration at the same input voltages (1–3 V). As can be seen,

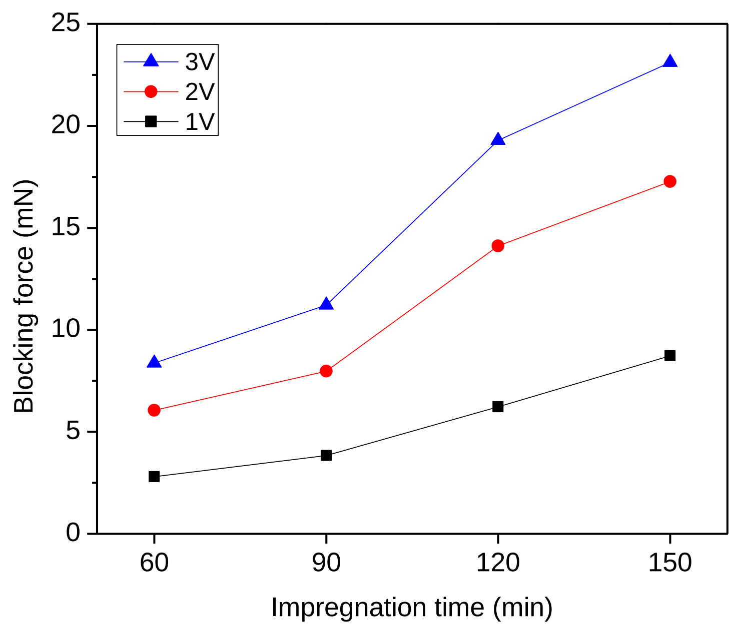

Figure 6.14: The peak blocking force vs. the impregnation time for Pd-Pt IPMCs, measured at 1, 2 and 3 V DC input.

the force to charge ratio increases also with the impregnation time, the higher ratio indicating more efficient transduction of IPMC. The increase up is to 120 min, further increment of the impregnation duration to 150 min decreases the ratio which, as in case of displacement measurements, can be explained by higher flexural stiffness of the IPMC samples prepared with longer impregnation time. Also, it can be noticed that the force to charge ratio is higher in case of 1 V compared to the measurements at 2–3 V DC, which can be expected due to the faradaic contribution at higher voltages that results in a higher current during the IPMC transduction. However, the electrochemical current only adds to the value of transported charge without contributing to the electromechanical output. The blocking force to transported charge ratios are overall somewhat higher compared to Pt-IPMCs (Figure 5.19), but not significantly.

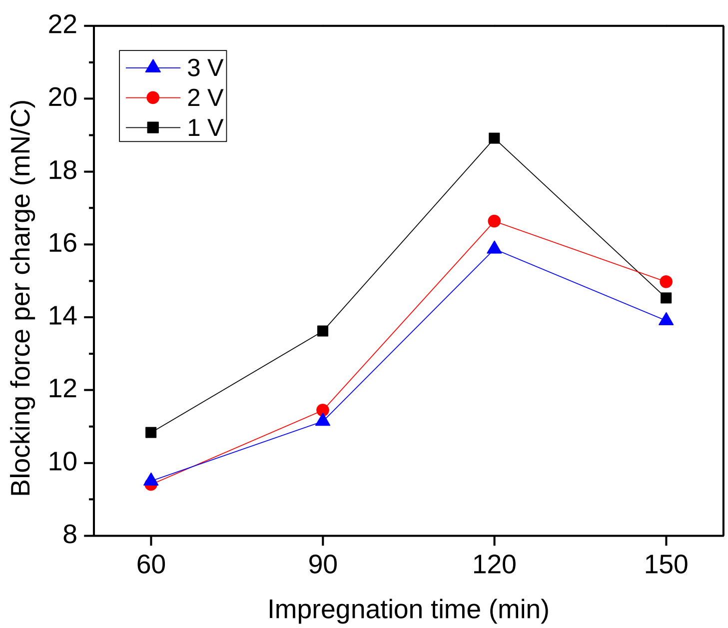

Figure 6.15: Peak blocking force to total transported charge ratio vs. the impregnation time for Pd-Pt IPMCs at 1, 2 and 3 V DC input.

6.3 Mechanoelectrical transduction

The mechanoelectrical transudction measurements were conducted in the frequency range of 1–10 Hz using a sinusoidal displacement with amplitude of 10 mm. Figure 6.16 shows the induced voltage of Pd-Pt IPMCs with different electrodes in response to imposed actuation at 1, 5 and 10 Hz. Noticeable changes in the voltage amplitude can be observed in case of different samples, the Pd(60) sample exhibiting the lowest and Pd(150) the highest peak voltage at all actuation frequencies. It can be noticed that Pd-Pt IPMCs display more than twice higher output voltage compared to Pt-IPMCs at the same experimental conditions (Figure 5.20). Also, the differences in the voltage responses in case of different samples are more apparent. This can be related to overall higher capacitance of Pd-Pt electrodes and rather drastic differences in the capacitances values in case of different samples, indicating corresponding differences in their interfacial surface areas. The highly dispersed porous Pd particles in the polymer matrix can result in a higher local volumetric strain effect (i.e. local changes in the anion concentration), leading to higher induced voltage. Despite, the voltage signal is still rather low – in the range of millivolts, which is in accordance with the theory presented in Chapter 3. Figure 6.17 presents the output voltage amplitude as a function of impregnation time. The overall trend shows a slight improvement in the voltage amplitude with increasing the impregnation time in Pd complex during the electroless plating. This data correlates with

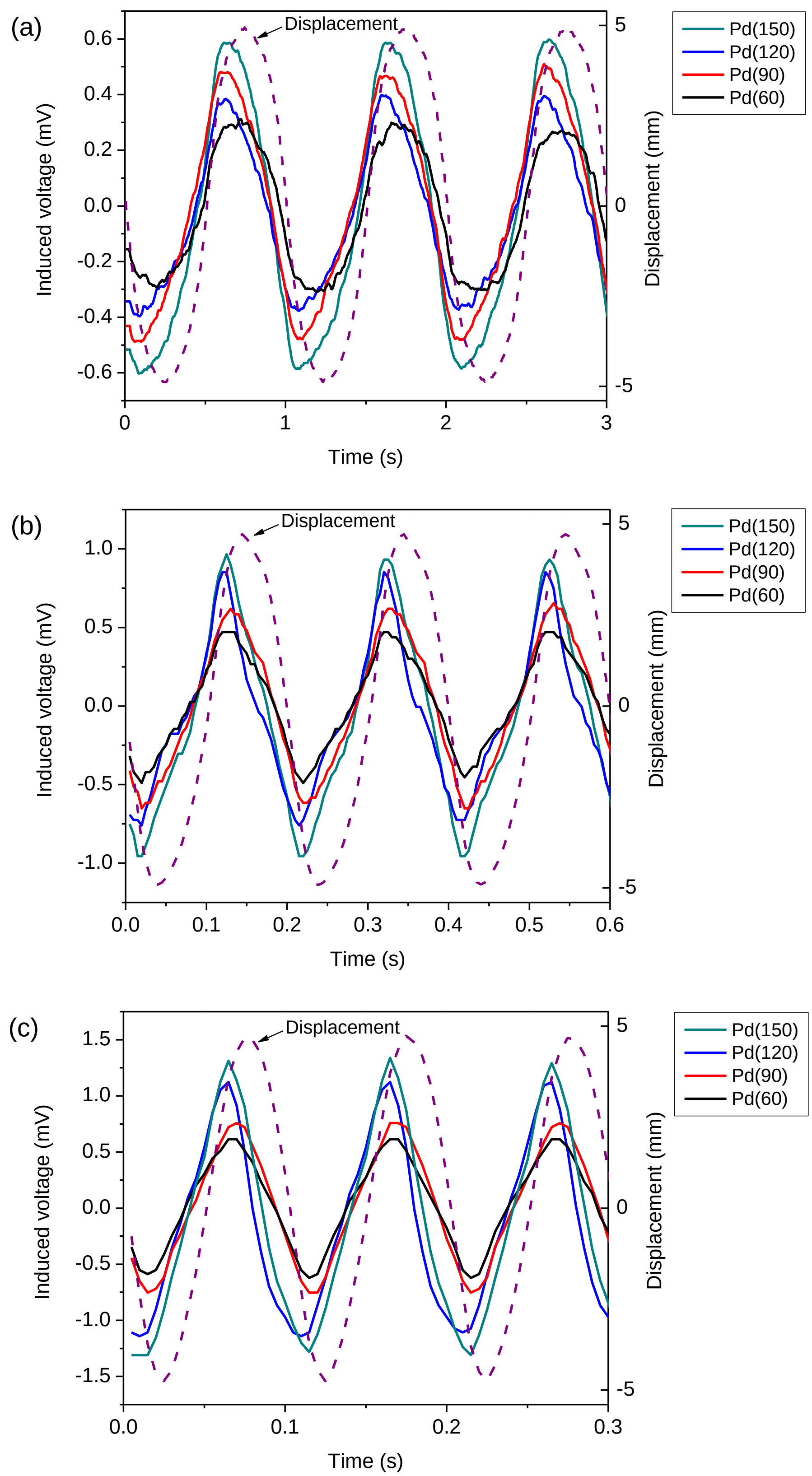

Figure 6.16: Induced voltage of Pd-Pt IPMCs at 1 Hz a), 5 Hz b) and 10 Hz c) actuation.

the electromehcanical transduction measurements, although, the overall effect of the electrode interfacial area on mechanoelectrical transduction is relatively low. The specific underlying reasons were discussed in Section 3.2 and 5.3.

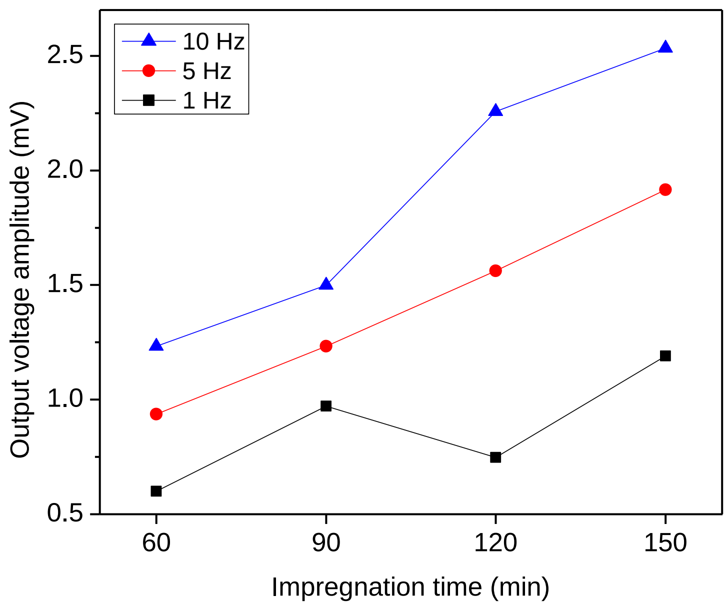

Figure 6.17: Induced voltage amplitude of Pd-Pt IPMCs vs. impregnation time under 1, 5 and 10 Hz imposed actuation.

6.4 Concluding remarks

Pd-Pt IPMCs with different electrode surface morphologies were prepared by controlling the impregnation time in Pd complex solution during the electroless plating process. It was observed that increasing the impregnation duration results in a higher content of palladium deposited in the vicinity of membrane surface, leading to a higher interfacial area of the electrodes. This was reflected in a considerable increase in the double-layer capacitance of IPMC. Extending the impregnation time and thereby increasing the dispersion of porous Pd particulates in the polymer matrix increased noticeably the total transported charge and the resulting displacement and blocking force output of IPMC. Increasing the impregnation duration from 60 min to 150 min improved the displacement amplitude more than three times (at 0.1 Hz, ±1 V AC square-wave). The corresponding improvement in the maximum blocking force output was also three-fold (at 1 V DC). These observations are in accordance with the finite element simulations reported earlier (Chapter 3, ref. [14]). The mechanoelectrical transduction measurements showed higher induced voltage in case of IPMCs prepared with longer impregnation time Pd complex soltion. However, compared to the electromechanical transduction, the effect of electrode surface morphology on the induced voltage was relatively low, which is in accordance with the theoretical prediction (see Chapter 3, ref. [14]). The presented results demonstrate that impregnation time in the electroless plating process of palladium has a significant impact on the charge dynamics and resulting electromechanical output of IPMC. Thus, with the proper control of this parameter the transduction performance of the material can be considerably enhanced.

Chapter 7

Conclusions and suggested future work

This dissertation investigated the effects of electrode surface morphology on the transduction of ionic polymer-metal composites (IPMCs) with Pt and Pd-Pt electrodes. To control and manipulate the surface structure of the mentioned electrodes, the key synthesis parameters were identified in the electroless plating process – that are the impregnation time (in case of Pd-Pt electrodes) and the number of impregnation-reduction cycles (in case of Pt electrodes). By controlling the mentioned parameters in the synthesis process, IPMCs with different electrode surface structures were fabricated. Other conditions and parameters were set at their optimum and kept constant. The changes in the electrode surface morphology and the resulting effects on the material's electromechanical, mechanoelectrical, electrochemical and mechanical characteristics were examined and analyzed. It was found that increasing the number of impregnation-reduction cycles under appropriate conditions leads to the formation of platinum nanoparticles with sharp tips and edges – called Pt nanothorn assemblies – at the polymer-electrode interface. These assemblies grew in size and developed tens of sharp tips radiating outward from the center of the assembly, increasing considerably the interfacial surface area and the double-layer capacitance of IPMC. The newly developed nanostructured Pt electrodes showed significant increase in the total transported charge during the actuation and notable improvement in the corresponding electromechanical output. Increment of the plating cycles from 1 to 7 increased the displacement performance more than 3 times (at 0.1 Hz, 3 V AC square-wave input). The peak blocking force improved more than 3 times at 3 V DC and more than 5 times at 1 V DC input. The ratios of peak strain to transported charge as well as the peak blocking force to transported charge were both considerably increased. The formation and growth of Pt nanothorn assemblies at the electrode interface also increased somewhat the induced voltage amplitude. However, compared to the electromehcanical transduction the effect of electrode surface structure on the induced voltage was relatively minor. The observed rather weak surface geometry effect is in accordance with the earlier theoretical prediction and can be explained by mechanoelectrical transduction being a local phenomenon that is mainly governed by a local volumetric strain induced changes in the anion concentration. Therefore, the surface charging is very low and the electrode surface structure has relatively minor effect in the mechanoelectrical transduction process.

In case of Pt-Pt IPMCs, the amount of porous palladium at the inner surface of the polymer membrane was controlled by varying the impregnation time in Pd complex solution during the electroless plating process. It was shown that increasing the impregnation duration leads to a higher content of palladium near the membrane surface, increasing considerably the double-layer capacitance of IPMC, and thus, the interfacial area of electrodes. Extending the impregnation time from 60 min to 150 min increased noticeably the total transported charge during the transduction and the corresponding electromechanical output. A three-fold increase in both displacement and peak blocking force was observed at 0.1 Hz ±1 V AC square-wave and 1 V DC input, respectively. Overall, the blocking force performance was somewhat higher compared to the Pt-IPMCs, while the displacement performances were rather similar. This is due to the higher flexural stiffness of Pd-Pt IPMCs that limits the bending actuation of the material. IPMCs prepared with longer impregnation time also showed somewhat higher induced voltage amplitude. As observed in case of Pt-IPMCs, the overall effect of the electrode surface morphology on the induced voltage was relatively low compared to the electromechanical transduction. However, the Pd-Pt electrodes showed nearly twice higher induced voltage amplitude compared the Pt-IPMCs, which can be related to the highly dispersed Pd particles in the polymer surface, resulting higher local volumetric strain effect, i.e. changes in the anion concentration.

The presented research demonstrates that with the appropriate control of the synthesis conditions, in particular, the impregnation time (Pd-Pt IPMCs) and the impregnation-reduction cycles (Pt-IPMCs), the transduction performance of IPMC material can be considerably enhanced. The developed synthesis techniques allow good control over the electrode surface structure, and even can be used to create more advanced surface design with Pt nanothorn assemblies. The designed IPMC electrodes with Pt nanothorn assemblies are first to be reported.

7.1 Suggested future work

The presented results revealed that the electrode surface structure can significantly affect the transduction performance of IPMC. The future work can include further investigation of Pt nanothorn assemblies with different sizes and shapes, and their corresponding effect on the transduction properties. The assemblies with smaller dimensions but more dense distribution could be more effective in terms of increasing the interfacial area of electrodes. By fine-tuning the synthesis parameters such as concentration of Pt complex solution, impregnation time, reduction conditions (temperature, concentrations) could lead to variations in the size and shape of the nanothorn assemblies or even result in formation of different geometries. For instance, besides the nanothorns, Pt nanoparticles with rod and leaf-like shapes have been created by electrodeposition method for applications in Raman spectroscopy. The present study demonstrates that by using the impregnation-reduction method with the appropriate set of synthesis conditions it is possible to create similar nanostructures to those obtained by electrodeposition method. Also, the effect of dispersive agents such as polyvinylpyrrolidone (PVP) could be explored in the synthesis process to control the dispersion of Pt nanoparticles.

The future study on Pd-Pt electrodes-based IPMCs can include investigating the effect of other synthesis parameters such as reduction temperature. Controlling the temperature could allow one to control the penetration depth and density of Pd particles in the polymer matrix. Here, the dispersive agents such as PVP can be also useful for controlling the dispersion of Pd particles. Also, the Pt top layer could be deposited by impregnation-reduction method prior to the deposition of Pd inner layer. Using an impregnation-reduction method for applying Pt top layer instead of chemical deposition from solution could result better electrode surface conductivity with less plating cycles and reduce the manufacturing time.

An interesting and relevant area of study would be also Au electrodes-based IPMCs. It has been shown that the electroless plating of gold can develop electrodes with fractal-like dendrites. Future study could involve investigating the effects of the fractals with different sizes and shapes on the transduction properties of Au-IPMCs, in particular the mechanoelectrical transduction that has been left completely untouched in case of this type of IPMCs.

References

[1] K. Oguro, Y. Kawami, and H. Takenaka, "Bending of an ion-conducting polymer film-electrode composite by an electric stimulus at low voltage," *Journal of Micromachine Society,* vol. 5, pp. 27–30, 1992.

[2] M. Shahinpoor and K. J. Kim, "Ionic polymer-metal composites: I. Fundamentals," *Smart Materials & Structures,* vol. 10, pp. 819-833, 2001.

[3] K. Asaka and K. Oguro, "Bending of polyelectrolyte membrane platinum composites by electric stimuli: Part II. Response kinetics," *Journal of Electroanalytical Chemistry,* vol. 480, pp. 186-198, 2000.

[4] S. Nemat-Nasser and J. Y. Li, "Electromechanical response of ionic polymer-metal composites," *Journal of Applied Physics,* vol. 87, pp. 3321-3331, 2000.

[5] D. Pugal, K. Jung, A. Aabloo, and K. J. Kim, "Ionic polymer–metal composite mechanoelectrical transduction: review and perspectives," *Polymer International,* vol. 59, pp. 279-289, 2010.

[6] Y. Bar-Cohen, *Electroactive polymer (EAP) actuators as artificial muscles : reality, potential, and challenges*, 2nd ed. Bellingham, Wash.: SPIE Press, 2004.

[7] M. Shahinpoor and K. J. Kim, "Ionic polymer-metal composites: IV. Industrial and medical applications," *Smart Materials & Structures,* vol. 14, pp. 197-214, 2005.

[8] Y. Bar-Cohen, "Biomimetics using electroactive polymers (EAP) as artificial muscles - A review," *Journal of Advanced Materials,* vol. 38, pp. 3-9, 2006.

[9] F. Carpi and E. Smela, editors, *Biomedical Applications of Electroactive Polymer Actuators*. Chichester, UK: John Wiley & Sons, Ltd, 2009.

[10] O. Sung-Weon Yeom and Il-Kwon, "A biomimetic jellyfish robot based on ionic polymer metal composite actuators," *Smart Materials and Structures,* vol. 18, pp. 085002, 2009.

[11] K. J. Kim, W. Yim, J. W. Paquette, and D. Kim, "Ionic Polymer-metal Composites for Underwater Operation," *Journal of Intelligent Material Systems and Structures*, vol. 18, pp. 123-131, 2007.

[12] R. Tiwari and K. J. Kim, "Disc-shaped IPMC for use in energy harvesting," in *Proc. SPIE 7289, Behavior and Mechanics of Multifunctional Materials and Composites* 2009, pp. 72891G.

[13] R. Tiwari and K. J. Kim, "Disc-shaped ionic polymer metal composites for use in mechano-electrical applications," *Smart Materials and Structures,* vol. 19, pp. 065016, 2010.

[14] D. Pugal, "Physics Based Model of Ionic Polymer-Metal Composite Electromechanical and Mechanoelectrical Transduction," Ph.D. Dissertation, University of Nevada, Reno, 2012.

[15] B. B. Mandelbrot, *The Fractal Geometry of Nature*: W. H. Freeman and Co., 1982.

[16] V. Palmre, S. J. Kim, and K. Kim, "Millimeter thick ionic polymer membrane-based IPMCs with bimetallic Pd-Pt electrodes," *Proceedings of the SPIE Smart Materials and Structures Conf.*, Vol. 7976, San Diego, California, USA, 2011, pp. 797615 (2011).

[17] S. M. Kim and K. J. Kim, "Palladium buffer-layered high performance ionic polymer-metal composites," *Smart Materials & Structures,* vol. 17, 2008.

[18] M. Shahinpoor, Y. Bar-Cohen, J. O. Simpson, and J. Smith, "Ionic polymer-metal composites (IPMCs) as biomimetic sensors, actuators and artificial muscles - a review," *Smart Materials & Structures,* vol. 7, pp. R15-R30, 1998.

[19] C. Bonomo, L. Fortuna, P. Giannone, and S. Graziani, "A method to characterize the deformation of an IPMC sensing membrane," *Sensors and Actuators A: Physical,* vol. 123–124, pp. 146-154, 2005.

[20] K. Farinholt and D. J. Leo, "Modeling of electromechanical charge sensing in ionic polymer transducers," *Mechanics of Materials,* vol. 36, pp. 421-433, 2004.

[21] C. Bonomo, C. D. Negro, L. Fortuna, and S. Graziani, "Characterization of IPMC strip sensorial properties: preliminary results," in *Circuits and Systems, 2003. ISCAS '03. Proceedings of the 2003 International Symposium on,* 2003, pp. IV-816-IV-819 vol. 4.

[22] P. J. James, T. J. McMaster, J. M. Newton, and M. J. Miles, "In situ rehydration of perfluorosulphonate ion-exchange membrane studied by AFM," *Polymer*, vol. 41, pp. 4223-4231, 2000.

[23] K. Yusaku, S. Tsuyoshi, T. Makoto, D. Masao, A. Kinji, S. Takayasu, *et al.*, "Sheet-Type Braille Displays by Integrating Organic Field-Effect Transistors and Polymeric Actuators," *Electron Devices, IEEE Transactions on*, vol. 54, pp. 202-209, 2007.

[24] L. Myung-Joon, J. Sung-Hee, L. Sukmin, M. Mu-seong, and M. Inhyuk, "Control of IPMC-based Artificial Muscle for Myoelectric Hand Prosthesis," in *Biomedical Robotics and Biomechatronics, 2006. BioRob 2006. The First IEEE/RAS-EMBS International Conference on*, 2006, pp. 1172-1177.

[25] C. Bonomo, P. Brunetto, L. Fortuna, P. Giannone, S. Graziani, and S. Strazzeri, "A Tactile Sensor for Biomedical Applications Based on IPMCs," *Sensors Journal, IEEE*, vol. 8, pp. 1486-1493, 2008.

[26] C. V. Riga, C. D. Bicknell, M. S. Hamady, and N. J. W. Cheshire, "Evaluation of robotic endovascular catheters for arch vessel cannulation," *Journal of Vascular Surgery*, vol. 54, pp. 799-809, 2011.

[27] S. J. Kim, D. Pugal, Y. Jun, J. Wong, K. J. Kim, and W. Yim, "A Rod-Shaped Ionic Polymer-Metal Composite for Use as an Active Catheter-Platform," in *ASME Smart Mater Adapt Struct Intell Syst*, 2010, pp. 145–151.

[28] S. J. Kim, D. Pugal, J. Wong, K. J. Kim, and Y. Woosoon, "A bio-inspired multi degree of freedom actuator based on a novel cylindrical ionic polymer-metal composite material," in *Advanced Robotics (ICAR), 2011 15th International Conference on*, 2011, pp. 435-440.

[29] S. A. Ruiz, B. Mead, H. Yun, W. Yim, and K. J. Kim, "Design optimization of rod shaped IPMC actuator," *Proceedings of the SPIE Smart Materials and Structures Conf.*, Vol. 8687, pp. 868722, 2013.

[30] Y. Bar-Cohen, *Biomimetics: biologically inspired technologies*. Boca Raton, FL: CRC Press, 2006.

[31] M. Aureli, V. Kopman, and M. Porfiri, "Free-Locomotion of Underwater Vehicles Actuated by Ionic Polymer Metal Composites," *Mechatronics, IEEE/ASME Transactions on*, vol. 15, pp. 603-614, 2010.

[32] G. Shuxiang, G. Yarning, L. Lingfei, and L. Sheng, "Underwater Swimming Micro Robot Using IPMC Actuator," in *Mechatronics and Automation, Proceedings of the 2006 IEEE International Conference on*, 2006, pp. 249-254.

[33] P. Byungkyu Kim and Deok-Ho Kim and Jaehoon Jung and Jong-Oh, "A biomimetic undulatory tadpole robot using ionic polymer–metal composite actuators," *Smart Materials and Structures*, vol. 14, pp. 1579, 2005.

[34] Z. Chen, T. I. Um, and H. Bart-Smith, "Bio-inspired robotic manta ray powered by ionic polymer–metal composite artificial muscles," *International Journal of Smart and Nano Materials,* vol. 3, pp. 296-308, 2012.

[35] K. Abdelnour, A. Stinchcombe, M. Porfiri, J. Zhang, and S. Childress, "Wireless Powering of Ionic Polymer Metal Composites Toward Hovering Microswimmers," *Mechatronics, IEEE/ASME Transactions on,* vol. 17, pp. 924-935, 2012.

[36] M. Yamakita, N. Kamamichi, T. Kozuki, K. Asaka, and L. Zhi-Wei, "A snake-like swimming robot using IPMC actuator and verification of doping effect," in *Intelligent Robots and Systems, 2005. (IROS 2005). 2005 IEEE/RSJ International Conference on*, 2005, pp. 2035-2040.

[37] G. Shuxiang, S. Liwei, and K. Asaka, "IPMC actuator-based an underwater microrobot with 8 legs," in *Mechatronics and Automation, 2008. ICMA 2008. IEEE International Conference on*, 2008, pp. 551-556.

[38] V. Palmre, J. J. Hubbard, M. Fleming, D. Pugal, S. Kim, K. J. Kim, *et al.*, "An IPMC-enabled bio-inspired bending/twisting fin for underwater applications," *Smart Materials and Structures*, vol. 22, p. 014003, 2013.

[39] J. J. Hubbard, M. Fleming, K. K. Leang, V. Palmre, D. Pugal, and K. J. Kim, "Characterization of Sectored-Electrode IPMC-Based Propulsors for Underwater Locomotion," *ASME Conference Proceedings*, vol. 2011, pp. 171-180, 2011.

[40] D. Pugal, K. J. Kim, K. K. Leang, and V. Palmre, "Modeling and designing IPMCs for twisting motion: electromechanical and mechanoelectrical transduction," *Proceedings of the SPIE Smart Materials and Structures Conf.*, Vol. 7976, pp. 79761S, 2011.

[41] K. J. Kim, D. Pugal, and K. K. Leang, "A Twistable Ionic Polymer-Metal Composite Artificial Muscle for Marine Applications," *Marine Technology Society Journal*, vol. 45, pp. 83-98, 2011.

[42] Z. Chen and X. Tan, "Monolithic fabrication of ionic polymer–metal composite actuators capable of complex deformation," *Sensors and Actuators A: Physical*, vol. 157, pp. 246-257, 2010.

[43] D. Dibakar Bandopadhya and Bishakh Bhattacharya and Ashish, "An active vibration control strategy for a flexible link using distributed ionic polymer metal composites," *Smart Materials and Structures*, vol. 16, pp. 617, 2007.

[44] R. Tiwari, K. J. Kim, and S. Kim, "Ionic Polymer-Metal Composite as Smart Velocity Sensors and Energy Harvesters," *Smart Structures & Systems*, vol. 4, pp. 549-563, 2008.

[45] D. Dogruer, R. Tiwari, and K. Kim, "Ionic polymer metal composites as energy harvesters," *Proceedings of the SPIE Smart Materials and Structures Conf.*, Vol. 6524, pp. 65241C, 2007.

[46] R. Tiwari and K. J. Kim, "Improved IPMC sensing by use of cation and through induced nano-to-micro scale surface cracks," *Proceedings of the SPIE Smart Materials and Structures Conf.*, Vol. 6932, pp. 69323H, 2008.

[47] J. K. Sangki Lee and Kwang, "Design of IPMC actuator-driven valve-less micropump and its flow rate estimation at low Reynolds numbers," *Smart Materials and Structures*, vol. 15, pp. 1103, 2006.

[48] T. T. Nguyen, N. S. Goo, V. K. Nguyen, Y. Yoo, and S. Park, "Design, fabrication, and experimental characterization of a flap valve IPMC micropump with a flexibly supported diaphragm," *Sensors and Actuators A: Physical*, vol. 141, pp. 640-648, 2008.

[49] K. J. Kim and M. Shahinpoor, "Ionic polymer-metal composites: II. Manufacturing techniques," *Smart Materials & Structures*, vol. 12, pp. 65-79, 2003.

[50] S. Nemat-Nasser, "Micromechanics of actuation of ionic polymer-metal composites," *Journal of Applied Physics*, vol. 92, pp. 2899-2915, 2002.

[51] B. J. Akle, M. D. Bennett, D. J. Leo, K. B. Wiles, and J. E. McGrath, "Direct assembly process: a novel fabrication technique for large strain ionic polymer transducers," *Journal of Materials Science*, vol. 42, pp. 7031-7041, 2007.

[52] B. J. Akle, "Characterization and Modeling of the Ionomer-Conductor Interface in Ionic Polymer Transducers" Ph.D. Dissertation, Virginia Polytechnic Institute and State University, 2005.

[53] T. Fukushima, K. Asaka, A. Kosaka, and T. Aida, "Fully plastic actuator through layer-by-layer casting with ionic-liquid-based bucky gel," *Angewandte Chemie-International Edition*, vol. 44, pp. 2410-2413, 2005.

[54] K. Mukai, K. Asaka, K. Kiyohara, T. Sugino, I. Takeuchi, T. Fukushima, *et al.*, "High performance fully plastic actuator based on ionic-liquid-based bucky gel," *Electrochimica Acta,* vol. 53, pp. 5555-5562, 2008.

[55] J. Wang, H. Chu, and Y. Li, "Why Single-Walled Carbon Nanotubes Can Be Dispersed in Imidazolium-Based Ionic Liquids," *ACS Nano,* vol. 2, pp. 2540-2546, 2008.

[56] J. Torop, V. Palmre, M. Arulepp, T. Sugino, K. Asaka, and A. Aabloo, "Flexible supercapacitor-like actuator with carbide-derived carbon electrodes," *Carbon,* vol. 49, pp. 3113-3119, 2011.

[57] N. Terasawa, N. Ono, K. Mukai, T. Koga, N. Higashi, and K. Asaka, "A multi-walled carbon nanotube/polymer actuator that surpasses the performance of a single-walled carbon nanotube/polymer actuator," *Carbon,* vol. 50, pp. 311-320, 2012.

[58] J. Torop, T. Sugino, K. Asaka, A. Jänes, E. Lust, and A. Aabloo, "Nanoporous carbide-derived carbon based actuators modified with gold foil: Prospect for fast response and low voltage applications," *Sensors and Actuators B: Chemical,* vol. 161, pp. 629-634, 2012.

[59] J. Torop, T. Sugino, K. Asaka, A. Jänes, E. Lust, M. Arulepp*, et al.*, "Low-voltage bending actuators from carbide-derived carbon improved with gold foil," *Proceedings of the SPIE Smart Materials and Structures Conf.*, Vol. 8340, pp. 834017, 2012.

[60] T. Sugino, K. Kiyohara, I. Takeuchi, K. Mukai, and K. Asaka, "Improving the actuating response of carbon nanotube/ionic liquid composites by the addition of conductive nanoparticles," *Carbon,* vol. 49, pp. 3560-3570, 2011.

[61] A. Punning, A. Kruusmaa, and A. Aabloo, "Surface resistance experiments with IPMC sensors and actuators," *Sensors and Actuators a-Physical,* vol. 133, pp. 200-209, 2007.

[62] N. Fujiwara, K. Asaka, Y. Nishimura, K. Oguro, and E. Torikai, "Preparation of Gold−Solid Polymer Electrolyte Composites As Electric Stimuli-Responsive Materials," *Chemistry of Materials,* vol. 12, pp. 1750-1754, 2000.

[63] K. Onishi, S. Sewa, K. Asaka, N. Fujiwara, and K. Oguro, "The effects of counter ions on characterization and performance of a solid polymer electrolyte actuator," *Electrochimica Acta,* vol. 46, pp. 1233-1241, 2001.

[64] U. Johanson, U. Mäeorg, V. Sammelselg, D. Brandell, A. Punning, M. Kruusmaa, *et al.*, "Electrode reactions in Cu-Pt coated ionic polymer actuators," *Sensors and Actuators B: Chemical,* vol. 131, pp. 340-346, 2008.

[65] U. Johanson, A. Punning, M. Kruusmaa, and A. Aabloo, "Self healing properties of Cu-Pt coated ionic polymer actuators," *Proceedings of the SPIE Smart Materials and Structures Conf.*, Vol. 6927, pp. 69271Y, 2008.

[66] C. K. Chung, P. K. Fung, Y. Z. Hong, M. S. Ju, C. C. K. Lin, and T. C. Wu, "A novel fabrication of ionic polymer-metal composites (IPMC) actuator with silver nano-powders," *Sensors and Actuators B: Chemical,* vol. 117, pp. 367-375, 2006.

[67] M. Siripong, S. Fredholm, Q. A. Nguyen, B. Shih, J. Itescu, and J. Stolk, "A cost-effective fabrication method for ionic polymer-metal composites," in *Electroresponsive Polymers and Their Applications*. vol. 889, V. Bharti, Y. BarCohen, Z. Y. Cheng, Q. Zhang, and J. Madden, Eds., ed Warrendale: Materials Research Society, 2006, pp. 139-144.

[68] B. J. Akle, M. D. Bennett, and D. J. Leo, "High-strain ionomeric-ionic liquid electroactive actuators," *Sensors and Actuators a-Physical,* vol. 126, pp. 173-181, 2006.

[69] B. J. Akle and D. J. Leo, "Single-Walled Carbon Nanotubes — Ionic Polymer Electroactive Hybrid Transducers," *Journal of Intelligent Material Systems and Structures,* vol. 19, pp. 905-915, 2008.

[70] N. Terasawa, N. Ono, K. Mukai, T. Koga, N. Higashi, and K. Asaka, "High performance polymer actuators based on multi-walled carbon nanotubes that surpass the performance of those containing single-walled carbon nanotubes: Effects of ionic liquid and composition," *Sensors and Actuators B: Chemical,* vol. 163, pp. 20-28, 2012.

[71] V. Palmre, D. Brandell, U. Maeorg, J. Torop, O. Volobujeva, A. Punning, *et al.*, "Nanoporous carbon-based electrodes for high strain ionomeric bending actuators," *Smart Materials & Structures*, vol. 18, 2009.

[72] V. Palmre, J. Torop, M. Arulepp, T. Sugino, K. Asaka, A. Jänes, *et al.*, "Impact of carbon nanotube additives on carbide-derived carbon-based electroactive polymer actuators," *Carbon,* vol. 50, pp. 4351-4358, 2012.

[73] V. Palmre, D. Brandell, U. Maeeorg, J. Torop, O. Volobujeva, A. Punning, *et al.*, "Ionic polymer metal composites with nanoporous carbon electrodes," in *Electroactive Polymer Actuators and Devices*. vol. 7642, Y. BarCohen, Ed., ed, 2010.

[74] V. Palmre, E. Lust, A. Jänes, M. Koel, A.-L. Peikolainen, J. Torop, *et al.*, "Electroactive polymer actuators with carbon aerogel electrodes," *Journal of Materials Chemistry*, vol. 21, pp. 2577-2583, 2011.

[75] F. Kaasik, J. Torop, A.-L. Peikolainen, M. Koel, and A. Aabloo, "Carbon aerogel based electrode material for EAP actuators," *Proceedings of the SPIE Smart Materials and Structures Conf.*, Vol. 7976, pp. 79760O, 2011.

[76] Y. Gogotsi, A. Nikitin, H. Ye, W. Zhou, J. E. Fischer, B. Yi, *et al.*, "Nanoporous carbide-derived carbon with tunable pore size," *Nat Mater,* vol. 2, pp. 591-594, 2003.

[77] B. Akle, S. Nawshin, and D. Leo, "Reliability of high strain ionomeric polymer transducers fabricated using the direct assembly process," *Smart Materials & Structures,* vol. 16, pp. S256-S261, 2007.

[78] W. Lu, R. Hartman, L. Qu, and L. Dai, "Nanocomposite Electrodes for High-Performance Supercapacitors," *The Journal of Physical Chemistry Letters,* vol. 2, pp. 655-660, 2011.

[79] A. Jänes and E. Lust, "Electrochemical characteristics of nanoporous carbide-derived carbon materials in various nonaqueous electrolyte solutions," *Journal of the Electrochemical Society,* vol. 153, pp. A113-A116, 2006.

[80] T. Wallmersperger, B. J. Akle, D. J. Leo, and B. Kröplin, "Electrochemical response in ionic polymer transducers: An experimental and theoretical study," *Composites Science and Technology,* vol. 68, pp. 1173-1180, 2008.

[81] D. Pugal, K. J. Kim, and A. Aabloo, "An explicit physics-based model of ionic polymer-metal composite actuators," *Journal of Applied Physics,* vol. 110, pp. 084904-9, 2011.

[82] I. Takeuchi, K. Asaka, K. Kiyohara, T. Sugino, N. Terasawa, K. Mukai, *et al.*, "Electromechanical behavior of fully plastic actuators based on bucky gel containing various internal ionic liquids," *Electrochimica Acta,* vol. 54, pp. 1762-1768, 2009.

[83] M. D. Bennett and D. J. Leo, "Ionic liquids as stable solvents for ionic polymer transducers," *Sensors and Actuators a-Physical,* vol. 115, pp. 79-90, 2004.

[84] T.-G. Noh, Y. Tak, J.-D. Nam, and H. Choi, "Electrochemical characterization of polymer actuator with large interfacial area," *Electrochimica Acta,* vol. 47, pp. 2341-2346, 2002.

[85] K. Onishi, S. Sewa, K. Asaka, N. Fujiwara, and K. Oguro, "Morphology of electrodes and bending response of the polymer electrolyte actuator," *Electrochimica Acta*, vol. 46, pp. 737-743, 2000.

[86] P. Matteo Aureli and Maurizio, "Effect of electrode surface roughness on the electrical impedance of ionic polymer–metal composites," *Smart Materials and Structures*, vol. 21, pp. 105030, 2012.

[87] D. Y. Lee, I.-S. Park, M.-H. Lee, K. J. Kim, and S. Heo, "Ionic polymer-metal composite bending actuator loaded with multi-walled carbon nanotubes," *Sensors and Actuators A: Physical*, vol. 133, pp. 117-127, 2007.

[88] Y. Jung, S. J. Kim, K. J. Kim, and D. Y. Lee, "Characteristics of ionic polymer–metal composite with chemically doped TiO_2 particles," *Smart Materials and Structures*, vol. 20, pp. 124004, 2011.

[89] V. Palmre, D. Pugal, K. K. Leang, and K. Kim, "The effects of electrode surface morphology on the actuation performance of IPMC," *Proceedings of the SPIE Smart Materials and Structures Conf.*, Vol. 8687, pp. 86870W, 2013.

[90] D. Pugal, K. J. Kim, A. Punning, H. Kasemagi, M. Kruusmaa, and A. Aabloo, "A self-oscillating ionic polymer-metal composite bending actuator," *Journal of Applied Physics*, vol. 103, pp. 084908-6, 2008.

[91] J. Park, V. Palmre, K. Kim, D. Shin, D. H. Kim, W. Yim, *et al.*, "A comparison study of ionic polymer-metal composites (IPMCs) fabricated with Nafion and other ion exchange membranes," *Proceedings of the SPIE Smart Materials and Structures Conf.*, Vol. 8687, pp. 868714, 2013.

[92] I. Takeuchi, K. Asaka, K. Kiyohara, T. Sugino, N. Terasawa, K. Mukai, *et al.*, "Electromechanical behavior of a fully plastic actuator based on dispersed nano-carbon/ionic-liquid-gel electrodes," *Carbon*, vol. 47, pp. 1373-1380, 2009.

[93] J. Torop, "Carbide-derived carbon-based electromechanical actuators," Ph.D. Dissertation, University of Tartu, Estonia, 2012.

[94] A. Chen and P. Holt-Hindle, "Platinum-Based Nanostructured Materials: Synthesis, Properties, and Applications," *Chemical Reviews*, vol. 110, pp. 3767-3804, 2010.

[95] N. Tian, Z.-Y. Zhou, S.-G. Sun, L. Cui, B. Ren, and Z.-Q. Tian, "Electrochemical preparation of platinum nanothorn assemblies with high surface enhanced Raman scattering activity," *Chemical Communications*, vol. 0, pp. 4090-4092, 2006.

[96] A. A. Kelly and K. M. Knowles, *Crystallography and Crystal Defects*, 2nd ed.: Jon Wiley & Sons, Ltd, 2012.

[97] *Characterization and Failure Analysis of Plastics*: ASM International, 2003.

[98] H. Wang and L. Pilon, "Reply to comments on "Intrinsic limitations of impedance measurements in determining electric double layer capacitances" by H. Wang, L. Pilon [Electrochimica Acta 63 (2012) 55]," *Electrochimica Acta,* vol. 76, pp. 529-531, 2012.

[99] A. J. Bard and L. R. Faulkner, *Electrochemical methods: Fundamentals and Applications*, 2nd ed.: Wiley, 2000.

[100] H. Wang and L. Pilon, "Intrinsic limitations of impedance measurements in determining electric double layer capacitances," *Electrochimica Acta,* vol. 63, pp. 55-63, 2012.

[101] D. Kim and K. J. Kim, "Experimental Investigation on Electrochemical Properties of Ionic Polymer–Metal Composite," *Journal of Intelligent Material Systems and Structures,* vol. 17, pp. 449-454, 2006.

[102] D. Kim and K. J. Kim, "Electrochemistry of ionic polymer-metal composite," *Proceedings of the SPIE Smart Materials and Structures Conf.*, Vol. 5759, pp. 464-469, 2005.

[103] M. Porfiri, "Charge dynamics in ionic polymer metal composites," *Journal of Applied Physics,* vol. 104, pp. 104915-10, 2008.

[104] Y. Liu, R. Zhao, M. Ghaffari, J. Lin, S. Liu, H. Cebeci, *et al.*, "Equivalent circuit modeling of ionomer and ionic polymer conductive network composite actuators containing ionic liquids," *Sensors and Actuators A: Physical,* vol. 181, pp. 70-76, 2012.

[105] R. Kötz and M. Carlen, "Principles and applications of electrochemical capacitors," *Electrochimica Acta,* vol. 45, pp. 2483-2498, 2000.

[106] L. Jiao and J. R. Regalbuto, "The synthesis of highly dispersed noble and base metals on silica via strong electrostatic adsorption: I. Amorphous silica," *Journal of Catalysis,* vol. 260, pp. 329-341, 2008.

[107] N. K. Nag, "A Study on the Formation of Palladium Hydride in a Carbon-Supported Palladium Catalyst," *The Journal of Physical Chemistry B,* vol. 105, pp. 5945-5949, 2001.

[108] D. Kim, K. J. Kim, J.-d. Nam, and V. Palmre, "Electro-chemical operation of ionic polymer-metal composites," *Sensors and Actuators B-Chemical*, vol. 155, pp. 106-113, 2011.

[109] J. M. Gere, *Mechanics of Materials*, 5th ed. Pacific Grove: Brooks/Cole, 2001.

[110] J. Torop, M. Arulepp, J. Leis, A. Punning, U. Johanson, V. Palmre, *et al.*, "Nanoporous Carbide-Derived Carbon Material-Based Linear Actuators," *Materials*, vol. 3, pp. 9-25, 2010.

Appendix A

Efficiency calculations

The efficiency of conversion of electrical input into mechanical output in case of IPMCs with different electrodes was evaluated according to the method reported by Kim *et al.* [108]. The electromechanical energy conversion efficiency (η) is expressed as

$$\eta = \frac{\text{Power output}\,\textit{(mechanical)}}{\text{Power input}\,\textit{(electrical)}} \cdot 100\% = \frac{P_{out}}{P_{in}} \cdot 100\%, \tag{1}$$

The electrical power input was calculated using Joule's Law as $P_{in} = VI$. The strain-energy density (u) in J/m^3 is defined as [109]

$$u = \frac{Y\varepsilon_b^2}{2}, \tag{2}$$

where Y is the Young's modulus and ε_b is the bending strain of IPMC. The mechanical power output (P_{out}) can be calculated as

$$P_{out} = \frac{(u_f - u_i)V_m}{t} = \frac{Y\varepsilon_b^2 V_m}{2t}, \tag{3}$$

where u_f and u_i are the final and initial strain-energy density, and V_m is the volume of IPMC. Therefore, the efficiency becomes

$$\eta = \frac{Y\varepsilon_b^2 V_m}{2VIt} \cdot 100\%. \tag{5}$$

Figure A.1 shows the efficiencies of Pt-IPMCs with different electrode surface structures as a function of plating cycles at ±3 V AC square-wave input at different frequencies (0.05–1 Hz). It can be seen that increasing the plating cycles and thereby creating the nanothorn assemblies leads to higher transduction efficiency of IPMC. The overall improvement in the efficiency is 7–8 times. The efficiency values range from 0.01–0.1% and are comparable to other similar types of actuators [110]. Also, it can be noticed that the efficiency decreases after 7 platings, which can be related to the increasing flexural modulus that starts to limit the actuation. This trend was also observed in case of displacement and blocking force measurements, discussed in Chapter 5.

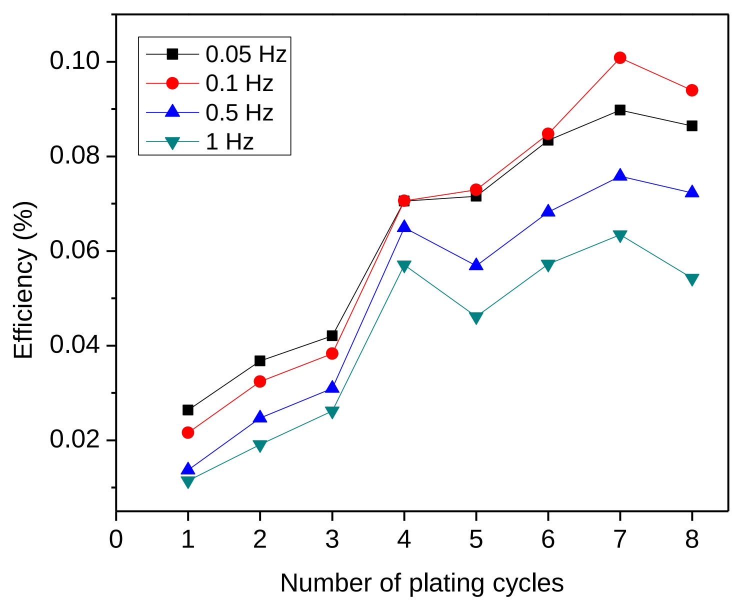

Figure A.1: Efficiency of Pt-IPMCs versus plating cycles at ±3 V AC square-wave input.

Appendix B

Remarks on measurement uncertainty

The accuracy/uncertainty range of the measurement equipment given by manufacturer is listed in Table B.1. This list only includes some key components of the system. The measurement setups also contain other units such as signal generators, controllers, power supplies, signal amplifiers, which makes the exact evaluation of the overall accuracy of the system difficult. However, based on the consecutive repeated measurements and observed signal-to-noise ratios, the error from the apparatus is estimated to be less than 5%. The main source of uncertainty in the experiments is from variations in the properties of IPMCs on sample-by-sample basis and execution of the measurements. The latter can include errors from placement of the samples in the setups, and variations in the initial shape, contact clamping pressure, room temperature etc. Not all IPMC samples prepared in this study were perfectly flat, but somewhat curved, which changes the effective length and actuation dynamics in the measurements. However, based on the measurements with three sets of samples, the experimental error determined from the standard deviation was within 15%, which is considered acceptable in case of this type of soft polymeric materials [74].

Table B.1: Accuracy/uncertainty range of the measurement equipment.

Equipment	Resolution/ uncertainty range
Laser displacement sensor/ optoNCDT 1401, Micro-Epsilon	0.01…0.02 % FSO (Full scale output) Measuring range: 5–200 mm
Blocking force load cell/GSO-30, Transducer Techniques	Accuracy: 0.05% of range Range: 30 g
Potentiostat/ (PGZ 402) VoltaLab 80, Radiometer analytical	Resolution: 0.003% of range Accuracy: ±0.2% of range Range: 1 A
Universal testing machine/Instron 5565	0.5 % of reading down to 1/250 of load cell capacity

Appendix C

Related publications

Journal papers on IPMC design, characterization and related activities:

- J. J. Hubbard, M. Fleming, **V. Palmre**, D. Pugal, K. J. Kim, K. K. Leang, "Monolithic IPMC Fins for Propulsion and Maneuvering in Bio-Inspired Underwater Robotics," *Journal of Oceanic Engineering*, 2013 (In press);

- **V. Palmre**, J. J. Hubbard, M. Fleming, D. Pugal, S. Kim, K. J. Kim, K. K. Leang, "An IPMC-enabled bio-inspired bending/twisting fin for underwater applications," *Smart Materials and Structures*, 22, 014003, 2013;

- D. Kim, K. J. Kim, J.-d. Nam, **V. Palmre**, "Electro-chemical operation of ionic polymer-metal composites," *Sensors and Actuators B-Chemical*, 155, 106-13, 2011;

Conference papers on IPMC design, characterization and related activities:

- M. A. Tsugawa, K. K. Leang, **V. Palmre**, and K. J. Kim, 'Sectored tube-shaped ionic polymer-metal composite actuator with integrated sensor," Proceedings of the ASME 2013 Conference on Smart Materials, Adaptive Structures and Intelligent Systems (SMASIS), Oct. 2013;

- **V. Palmre**, D. Pugal, K. K. Leang, K. J. Kim, "The effects of electrode surface morphology on the actuation performance of IPMC," Proceedings of the SPIE Smart Materials and Structures Conf., Vol. 8687, 86870W, April 2013;

- J. Park, **V. Palmre**, K. Kim, D. Shin, D. H. Kim, W. Yim, C. Bae, "A comparison study of ionic polymer-metal composites (IPMCs) fabricated with Nafion and other ion exchange membranes," Proceedings of the SPIE Smart Materials and Structures Conf., Vol. 8687, 868714, April 2013;

- **V. Palmre**, D. Pugal, K. J. Kim, “Characterization of longitudinal tensile force of millimeter thick IPMCs,” Proceedings of the SPIE Smart Materials and Structures Conf., Vol. 8340, 83402L, April 2012;

- D. Pugal, K. J. Kim**, V. Palmre**, K. K. Leang, A. Aabloo, “Physics based electromechanical model of IPMC considering various underlying currents,” Proceedings of the SPIE Smart Materials and Structures Conf., Vol. 8340, 83400P, March 2012;

- **V. Palmre**, S. J. Kim, K. Kim, “Millimeter thick ionic polymer membrane-based IPMCs with bimetallic Pd-Pt electrodes,” Proceedings of the SPIE Smart Materials and Structures Conf., Vol. 7976, 797615, March 2011;

- D. Pugal, K. J. Kim, K. K. Leang, **V. Palmre**, Modeling and designing IPMCs for twisting transduction, Proceedings of the SPIE Smart Materials and Structures Conf., Vol. 7976, 79761S, March 2011;

- J. J. Hubbard, M. Fleming, K. K. Leang, **V. Palmre**, D. Pugal, K. J. Kim, “Characterization of Sectored-Electrode IPMC-Based Propulsors for Underwater Locomotion,” Proceedings of the ASME 2011 Conference on Smart Materials, Adaptive Structures and Intelligent Systems (SMASIS), Sept. 2011;

- K. Cheng, E. Yang, C. Lee, Z. Ricks, **V. Palmre,** K. J. Kim, “Fine-tuned polymer nano-composite coatings for use in geothermal plants," Proceedings of the ASME 2011 Conference on Smart Materials, Adaptive Structures and Intelligent Systems (SMASIS), Sept. 2011;